



OSLO METROPOLITAN UNIVERSITY
STORBYUNIVERSITETET

Department of Civil Engineering and Energy Technology
Institutt for Bygg- og energiteknikk
Energi og miljø i bygg
Postadresse: Postboks 4 St. Olavs plass, 0130 Oslo
Besøksadresse: Pilestredet 35, Oslo

CANDIDATE NR.

895

AVAILABILITY

Open

Telefon 67 23 50 00

www.oslomet.no

MASTER'S THESIS

TITLE	DATE
The possibility of reducing power peaks through a temporary reduction in central heating system power - simulations in IDA ICE	2023-05-25
	PAGES/APPENDICES
	72/18
AUTHOR	SUPERVISOR
Albin Zahiti	Mehrdad Rabani

SUMMARY

In response to the growing trend of electrification in society, this thesis investigates the utilization of temporary shutdowns in central heating systems to reduce power consumption during peak periods while maintaining thermal comfort. A comprehensive literature review reveals promising results from previous studies in this field. Simulations were conducted using IDA ICE 4.8, employing various strategies and considering the water volume in the distribution network as a heat storage medium. The simulations demonstrate the potential that temporary shutdowns have by significantly decreasing peak power consumption for up to three consecutive hours without compromising thermal comfort, particularly in Passive House models. In summary, this research underscores the feasibility of implementing temporary shutdowns in central heating systems as an effective strategy for managing peak power demands.

KEYWORDS

Power Peak Reduction

Central Heating System

IDA ICE

Preface

This thesis is the final work in the two-year engineering Master's degree programme *Energy and Environment in Buildings* at Oslo Metropolitan University (OsloMet).

I would like to acknowledge the guidance I received throughout the semester from Mehrdad Rabani, who served as my main supervisor, and Habtamu Bayera Madessa, who served as co-supervisor. Their insightful contributions have been invaluable.

Also, I would like to express my gratitude to Ida Bryn and Ørnulf Kristiansen from Multiconsult, both for suggesting the topic and for their willingness to devote time from their otherwise busy schedules for meetings and clarifications on the subject. Their participation has played a pivotal role in shaping this thesis.

Lastly, I would like to thank my fellow students, who have been excellent discussion partners and overall motivators throughout the entire duration working on this thesis.

- *Albin Zahiti, 25.05.2023*

Abstract

In recent times there has been a trend of electrification worldwide, as large parts of the world move away from the use of fossil fuels. This shift is of significant importance, particularly within the building sector, which accounts for a significant portion of the electricity consumption. Furthermore, this highlights the importance of implementing strategies to avoid power peaks, which put immense strain on the electrical grid. Several different strategies have been proposed and analyzed by other researchers thus far, with the intention of reducing and/or shifting such power peaks, in order to better manage the available power without necessitating grid expansion solely for the accommodation of said peaks.

This thesis examined the possibility of utilizing temporary shutdowns in available power in the central heating system of an office building to reduce power consumption during these peaks, while simultaneously maintaining thermal comfort for the occupants. A literature review showed promising results from earlier simulations and experiments, which had examined several aspects of the subject at hand, including the thermal capacity of different constructions and dedicated thermal energy storage solutions, as well as several different control strategies for different systems. In addition to the literature review, multiple simulations employing different strategies were run in IDA ICE 4.8, for both a TEK17- and Passive House-worthy building envelope. Furthermore, the total water volume of the distribution pipes was considered as a heat storage medium. Custom controllers were developed using available IDA ICE tools, in order to adjust the temperature setpoints and operation schedules of different components, and their signals were logged to verify that they operated as expected.

The results indicate that there is a lot of potential in these temporary shutdowns with regard to reduction of power consumption during periods of high demand. Among the most promising findings was the fact that the heating power in the central heating system could be shut off completely for up to three hours during a morning peak period without sacrificing thermal comfort. As expected, the Passive House model showed better performance than the TEK17 model in all simulations. The simulations also highlight the potential of considering the water volume in the distribution network as short-term heat storage with regard to water-borne space heating systems.

Sammen drag

I en tid når verden beveger seg vekk fra fossile brensler til fordel for elektrisk energi, er det blitt betydelig viktigere å sikre tilstrekkelig elektrisitet til oppvarmingsformål og samtidig unngå en ellers unødvendig utbygging av strømmettet som kun har som hensikt å håndtere tidsbegrensede effekttopper. Dette er av særlig betydning for byggebransjen, som står for en stor andel av det totale forbruket av elektrisk energi. En rekke strategier for å redusere og/eller forskyve effekttopper er blitt foreslått og analysert tidligere, med hensikt å effektivisere utnyttelsen av den tilgjengelige effekten, uten å nødvendiggjøre ytterligere utbygging av strømmettet utelukkende for håndtering av disse toppene.

Denne masteroppgaven utforsker muligheten for midlertidige kutt i tilgjengelig effekt i energisentralen til et kontorbygg, med hensikt å redusere effekttopper i perioder med høy belastning, uten at det går på bekostning av brukernes termiske komfort. En litteraturgjennomgang av tidligere simuleringer og eksperimenter, som blant annet har undersøkt varmekapasiteten i ulike konstruksjoner og dedikerte varmelagringsteknologier, så vel som ulike kontrollstrategier for ulike teknologier, viste lovende resultater. I tillegg til litteraturgjennomgangen er det gjennomført en rekke simuleringer med ulike strategier i IDA ICE 4.8 for både en TEK17- og en Passivhus-verdig klimaskjerm. Samtidig er det totale vannvolumet i rørnett for systemet betraktet som et varmelagringsmedium. Skreddersydde kontroller for tilpasning av temperatursettpunkt og driftsplan for ulike komponenter er utviklet i programmet ved bruk av eksisterende verktøy i IDA ICE, og deres signaler er loggført for å verifisere at de opererer som forventet.

Resultatene tilsier at det er stort potensiale i midlertidige effektkutt med hensyn til reduksjon av forbruk i perioder med høyt effektbehov. Et av de viktigste funnene er muligheten for å slå av oppvarming i energisentralen i opptil tre timer samtidig som termisk komfort opprettholdes. Som forventet presterer Passivhus-modellen bedre enn TEK17-modellen i samtlige simuleringer. Simuleringene framhever også potensialet for å utnytte vannvolumet i rørnett til midlertidig varmelagring i forbindelse med vannbårne oppvarmingssystemer.

Nomenclature

\dot{m}	Mass flow rate [kg/s]	HotTank	Stratified hot water tank representing total water volume in all heating circuits
\dot{Q}	Heat transfer rate [W]	HP	Heat Pump
c_p	Specific heat capacity [J/(kg*K)]	ICA	Inner Control Algorithm
m	mass [kg]	IDA ICE	IDA Indoor Climate and Energy
Q	Sensible heat stored [J]	Met	Metabolic rate
AHU	Air Handling Unit	MPC	Model Predictive Control
ASHP	Air-Source Heat Pump	PCM	Phase Change Material
CHS	Central Heating System	PH	Passive House
Clo	Insulation value of clothing	Plant	Central heating system model in IDA ICE
COP	Coefficient of Performance	PMV	Predicted Mean Vote
DH	District Heating	PPD	Predicted Percentage of Dissatisfied
DHN	District Heating Network	PV	Photovoltaics
DHS	District Heating System	RH	Relative Humidity
DHW	Domestic Hot Water	TABS	Thermally Activated Building Systems
DR	Demand Response	TEK17	Norwegian regulations on technical requirements for construction works
DSM	Demand-Side Management	TES	Thermal Energy Storage
DUT_v	Design temperature for the winter season	WSHP	Water-Source Heat Pump
E-MPC	Economic Model Predictive Control	ΔT	Difference between two temperatures
ESBO	Early Stage Building Optimization		
GSHP	Ground-Source Heat Pump		
HEP	Hourly Electricity Price		

Contents

1	Introduction	1
1.1	Objective	2
1.2	Prerequisites and Limitations	2
2	Theory	3
2.1	Thermal Comfort	3
2.2	Varying Heat Demand	5
2.3	Existing solutions/technologies	5
2.3.1	Electric heating	6
2.3.2	Oil and Gas	6
2.3.3	Biofuel	6
2.3.4	Solar Energy	6
2.3.5	Heat Pumps	7
2.3.6	District Heating	8
2.3.7	Thermally Activated Building Systems (TABS)	9
2.4	Hybrid Heating Systems	9
2.5	Power Peaks and Methods of Reduction	10
2.5.1	Thermal Energy Storage	10
2.5.2	Flexibility	11
2.6	Simulation Software	12
2.6.1	SIMIEN	12
2.6.2	TRNSYS	12
2.6.3	EnergyPlus	12
2.6.4	IDA ICE	12
3	Literature Review	13
3.1	Thermal Inertia and Heat Capacity	13
3.2	TES	14
3.3	Control Strategies	14
3.4	Research Gap	17
4	Method	18
4.1	Case Study	18
4.2	Input Data	19
4.2.1	Climate Data	19
4.2.2	Zones	20
4.2.3	Windows	21
4.2.4	TEK17 Case	22
4.2.5	Passive House Case	22
4.3	Plant	23
4.4	Ventilation	26
4.5	Zone Heating	28

4.6	Simulations	29
4.6.1	Simulation Overview	29
4.6.2	Simulation 1	30
4.6.3	Simulation 2	31
4.6.4	Simulation 3	32
4.6.5	Simulation 4	33
4.6.6	Simulation 5	34
4.7	Logged Data	34
5	Results & Discussion	36
5.1	Simulation 1	36
5.2	Simulation 2	46
5.3	Simulation 3	52
5.4	Simulation 4	58
5.5	Simulation 5	65
6	Conclusion	72
6.1	Suggestions for Further Research	72
	Appendix	80
A	IDA ICE Climate for Blindern	80
B	Thermal Bridge inputs	81
C	Occupancy Schedules	83
D	Lighting Schedules	84
E	TEK17 & Passive House Window Details	85
F	Materials for TEK17 External Walls	86
G	Materials for TEK17 Slab Towards Ground	87
H	Materials for Passive House External Walls	88
I	Materials for Passive House Slab Towards Ground	89
J	Heating Load Simulations	90
K	Boiler Data	92
L	HotTank Data	93
M	Controller Setpoints for Open Landscape	94
N	Main Temperatures & PPD for Open Landscape Zone	94

O AHU Temperatures & Mechanical Inflows for Open Landscape Zone	95
P Signals & Boiler Output (17.-18. January)	97
Q Supply & Return + HotTank Temperatures (16.-20. January)	107
R Mass Flow Rates (16.-22. January)	111

1 Introduction

In recent times, there has been an increasing focus on reducing the impact that human activities have on the environment. The Paris Agreement from 2015 is a distinct example, as it is a legally binding treaty that aims to limit global warming to less than 2°C compared to pre-industrial levels [1]. The European Union has adopted The European Climate Law, whose goal is to reduce the net greenhouse gas emissions in the union by no less than 55% by 2030, compared to 1990 levels [2], with Norway also adopting the goal in the second half of 2022 [3]. Locally, the Norwegian government has also been aiming for more sustainable development in general through what it calls "The Green Shift" (Norwegian: *"Det grønne skiftet"*), which requires, among several goals and measures, increased use of renewable energy and low-polluting technologies [4]. One result of this policy is the ban on the use of mineral oils as a heat source for buildings, which has been in effect since the beginning of 2020 [5].

Generally, a trend of electrification can be observed, especially in the building sector - a development that could put electrical grids in a precarious situation with regard to their capacity [6]. For example, in 2020 the British government presented a ten point plan, in which the installation of 600 000 heat pumps (HPs) per year by 2028 is one of the concrete actions meant to achieve "greener buildings" [7]. Furthermore, Norway already has a high and ever growing share of electricity in the total energy use compared to other countries - a development being fueled by the reduced use of fossil fuels [6, 8]. Such efforts will inevitably increase the electricity demand, putting a higher strain on the electrical grid.

Simultaneously, the electrical grid also has to keep up with the increasing demand caused by the ever growing global population. While efforts to improve the efficiency may dampen the pace at which the electrical demand increases, it is estimated that the overall energy demand in buildings will increase by 3.4 TWh in Norway alone, by the year 2050, due to the increase in total building area [9].

Norway is a country where a large part of space heating is based on electrical energy, which, when evaluated in conjunction with the cold climate and population growth, emphasized the need for the reduction of power peaks for heating. In 2022, The Energy Commission (Norwegian: *Energikommisjonen*) was appointed by the Norwegian Ministry of Petroleum and Energy to survey the energy demand and resulting need for increased capacity for the electrical grid in the years leading up to 2030. The resulting report, published in February 2023, pointed out three main categories of measures that could be enacted on the consumer side. The first category consists of measures that yield a permanent reduction in heat demand during cold seasons, such as improving the building envelope or utilizing alternative heating sources, such as district heating (DH), HPs, and biofuels. The second category focuses on varying between different energy carriers in the heating systems, for example through seasonal storing of thermal energy in energy wells. The third category, which is also the most relevant solution with regard to this thesis, deals with more short term flexibility, such as temporarily turning off the power for water-borne heating systems without a noticeable drop in temperature among the occupants, or heating large volumes of water in hot water tanks during hours with lower overall power consumption. [8]

The current Norwegian regulations on technical requirements for construction works (TEK17) §14-4 require that buildings with a heated gross internal area of more than 1,000 m² must facilitate the use of "energy-flexible" heating systems, while also covering 60% of the building's net heating demand [10]. In this context, "energy-flexible" refers to the possibility of utilizing different energy sources for heating, with water-borne heating systems being the preferred type [11]. The term "flexibility" could also refer to how the production and consumption of electricity could be adapted to reduce power peaks (see Section 2.5.2) [6, 12].

This Master's thesis seeks to examine potential solutions and methods that could reduce heating-related power consumption in office buildings over short periods, so-called "power peaks", further reducing the strain on heat distributing systems, such as DH and/or the electrical grid. The background for this thesis was the limited research on the potential for using the existing water volume in the distribution pipe systems between the central heating system (CHS) and the space being heated as a heat storage medium itself, as well as typical building practices in Norway.

1.1 Objective

The objective of this Master's thesis is divided into two parts:

1. A literature review of the possibility for and effects of power peak reduction and shifting for heating systems, supported by a preceding chapter detailing the theory behind several aspects regarding space heating - from heat sources to the thermal comfort of occupants.
2. A simulation-based study analyzing the possibility of reducing the power supplied to water-borne heating systems, and the resulting effects on indoor temperature and thermal comfort through the use of IDA Indoor Climate and Energy (IDA ICE), while also exploring the possibility of utilizing the heat capacity of the water volume in the piping system for heat storage.

1.2 Prerequisites and Limitations

The work that went into this thesis, which consisted of gathering and processing information, developing the IDA ICE models, and simulating the different scenarios, was subject to several challenges, prerequisites, and limitations.

Utilizing IDA ICE itself has been a notably laborious process, as learning to use this software, with its vast selection of components, inputs and general simulation possibilities, constitutes an extensive task. Most of the time spent on the software was concentrated on ensuring that the models that were used, were fit for the intended tasks. Nonetheless, relying exclusively on a software doesn't guarantee realistic outputs, even if the software is as renowned and capable as IDA ICE. Ideally, measurements or other experimental data should have been used to verify the results from the simulations. However, since this was not possible given the short time frame of the thesis work, this is left as an opportunity for future research regarding the subject. Additionally, the modelling conducted in IDA ICE is based on several assumptions, such as occupant behavior, while excluding objects that would otherwise affect the heat capacity and thermal inertia of the construction, such as furniture. The focus on simulating the water volume of the piping network itself is a source of uncertainty, as the tank model that was used was not intended for such applications. The plant model itself was also a limitation, as making small changes in existing components often resulted in simulation errors.

The development of the model in IDA ICE, as well as the aforementioned conditions, shifted the focus of the thesis throughout the semester. While it was initially intended for a hybrid heating system to be examined for potential power peak reducing abilities, hiccups along the way resulted in the simulations being focused on the use of a singular heating source, while the theory and literature review sections also address the possibility of using hybrid heating systems. Further assumptions, limitations, and other conditions worth mentioning are listed in the sections where they apply.

2 Theory

In Norway the heating systems for a building are developed based on the design temperature for the winter season (Norwegian: *Dimensjonerende utelufttemperatur vinter*, DUT_v), which is defined as the lowest three day average outdoor air temperature for the given location between 1971 and 2000 [13]. Given that this temperature can be between $-7\text{ }^{\circ}\text{C}$, near the coast, and $-42\text{ }^{\circ}\text{C}$, in colder inland areas [13], it is important that the chosen heating system is capable of supplying sufficient heat even in these extreme cases.

2.1 Thermal Comfort

The main goal when supplying heat to a space is to achieve and maintain thermal comfort for as many occupants as possible [14]. NS-EN ISO 7730:2005 defines the term "thermal comfort" as a state of experienced satisfaction regarding the thermal surroundings [15]. Figure 1 shows the minimal requirements for surface temperatures, indoor air temperature, air velocity and thermal asymmetry in order to achieve a satisfactory thermal comfort according to NS-EN ISO 7730 [15].

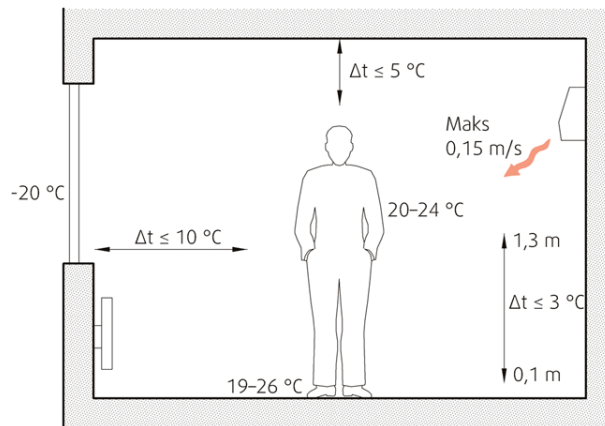


Figure 1: Minimal requirements given by surface temperatures, indoor air temperature, air velocity and thermal asymmetry according to NS-EN ISO 7730 [15]

NS-EN ISO 7730:2005 also presents the terms Predicted Mean Vote (PMV) and Predicted Percentage of Dissatisfied (PPD) [15]. The PMV index is a numerical scale used to explain the thermal sensation among a group of occupants, and is calculated using data such as clothing, relative humidity (RH) and mean radiative temperature. Ideally, it should match the mean value obtained from occupants' rating of the thermal sensation they experience on a seven-point scale from -3 to 3 , with the former being cold, and the latter being hot. The closer the mean values is to the neutral 0 , the higher the number of occupants who experience thermal comfort. PPD is a prediction of the percentage of people in a group that are expected to be dissatisfied with the local thermal situation given a specific metabolic rate (Met) and insulation level of clothing (Clo) [15, 16, 17]. Figure 2 presents PPD graphically as a function of PMV.

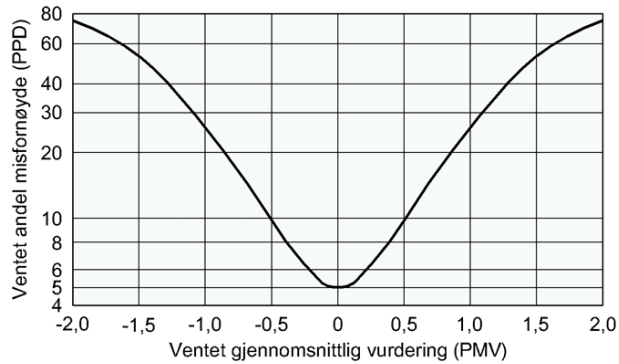


Figure 2: PPD as a function of PMV [17]

NS-EN 16798-1:2019 presents four categories (I-IV) for indoor environmental quality, with I being bound by the highest expectations, and IV the lowest. For a TEK17 building, category II is the most relevant. Default temperature ranges are given for different building types and categories. For offices and other similar spaces in category II, the temperature range for the heating season is 20-24 °C, and 23-26 °C for the cooling season. For mechanically heated and cooled buildings in category II, PPD is expected to be lower than 10 % and PMV is to remain within a +/- 0,5 point range of the neutral value of zero. [18]

To account for the many factors that affect the thermal conditions in a room, it is common to refer to the operative temperature, rather than the air temperature, when considering such ranges. The operative temperature is a function of several factors, including air temperature, air velocity, radiation asymmetry, Clo, Met, among other factors [17]. Figure 3 is a graph that shows the optimal operative temperature given a specific Met and Clo. However, it has also been observed that men and women experience thermal comfort differently, with optimal thermal comfort varying with up to 3 °C between the genders, according to a review by E. Haselsteiner [19]. Considering that the Figure 3 is based on data related to men, what men experience as optimal operative temperature, women may experience as too cold.

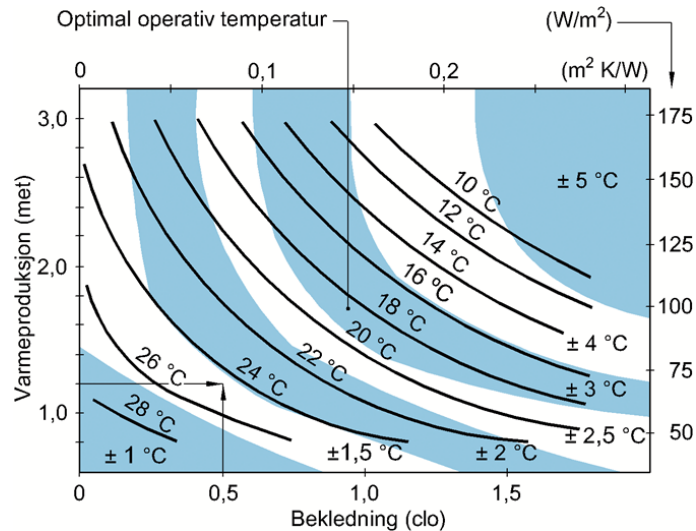


Figure 3: Optimal operative temperature given a specific Met and Clo [17]

2.2 Varying Heat Demand

The demand for space heating in a building will vary throughout the year, from no space heating demand in the summer to potentially reaching design capacity of the heating system in the winter (see Figure 4 A), as is the case in Norway, which historically has relied heavily on electric heating [8]. This is mainly due to the fluctuating outdoor temperature [20]. Variations in electricity consumption, both on a daily and an annual basis, reflect the same demand, as can be seen in Figure 4 B [21]. Furthermore, daily variation will also occur, and will differ between building types based on the usage pattern. Increased heating demand during the day can be expensive for the end users, and potentially cause more pollution due to the use of fossil fuels [20].

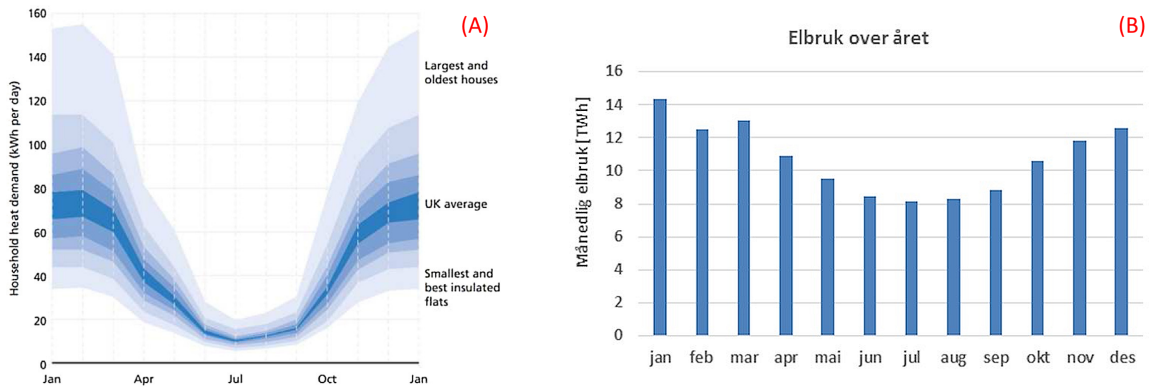


Figure 4: (A) Heat demand variation in the UK during a typical year for different residential constructions [22]. (B) Monthly electricity consumption [TWh] over a year [21]

2.3 Existing solutions/technologies

There are many sources and solutions to choose from when planning for space heating, and the choice of technologies is generally the result of local availability, the intended use of the heated space, as well as several other considerations, such as technical and financial ones [23].

Some heat sources are electricity, oil or gas, biofuel, solar energy, and energy extracted from air, wind, or water through the use of HPs [11, 23]. Water as a source can be found in underground boreholes, lakes, rivers, or the sea [24].

It is important to note that all solutions have their advantages and disadvantages. One aspect that can make a solution more favorable compared to other solutions is whether the energy source is a primary or secondary source. This is in part due to the potential pollution of the sources. Primary sources come directly from natural resources, such as crude oil or coal, whereas secondary sources are products derived from either primary sources or other secondary sources, and covers sources such as electricity and gasoline to mention a few [25].

One important factor is the percentage of the total heat demand for a building that each technology can cover. This depends primarily on three factors, according to a report by Erichsen & Horgen from 2011 [26]:

- What demands the delivered heat is meant to cover, e.g. space heating, ventilation and/or domestic hot water (DHW)

- How many points of delivery and/or water-borne systems for heating that are available in the building.
- The possibilities and limitations that the infrastructure results in, both technically and architectonically.

2.3.1 Electric heating

Although electricity is required to power several components when using other heating technologies, in this section, the main focus is on the use of electricity for space and ventilation heating. Electricity is a widely available source, and investment costs for equipment is usually lower than the other sources mentioned in this section [24]. Electricity can be used for direct heating of air using for example panel heaters, or fan assisted heating coils in ventilation systems [27]. Alternatively, electricity can be used for space or air heating indirectly by first heating up a medium, such as water, through the use of a heating coil in a boiler, and distributing the heat using pipes and different units. Such solutions include radiators, underfloor heating systems, and air heaters in ventilation systems, to mention a few [27]. Electricity is also used for direct heating of water for distribution through DH networks [27]. Electricity can cover 100 % of the heating demand for both space heating and DHW [28]. Some downsides of relying on electricity is that it is often produced using non-renewable sources and is usually more expensive in periods of high demand [24].

2.3.2 Oil and Gas

Oil and gas boilers work very similarly to each other in that they burn either oil or gas to heat water, which is then used for the intended heating purposes [29]. Both types of boilers are expected to cover at least 80% of both space heating and DHW [28]. Boilers of this kind are associated with high levels of pollution, as every liter of oil expended releases 2,7 kg CO₂ into the atmosphere [30]. Following the Norwegian ban on mineral oils as heating sources, such boilers are not as common in Norway as they are abroad [5], yet they are still present if retrofitted to run on biofuels..

2.3.3 Biofuel

Biofuel can either be solids, such as wood, pellets, briquettes, or sawdust, or liquids, such as bio-oil or biogas [24, 27]. A biofuel boiler functions similar to oil and gas boilers, and is expected to cover the entire energy demand for both space heating and DHW, and is therefore well suited as a top load [24, 28, 31]. In Norway, ENOVA will support the acquisition of a biofuel boiler with up to 10 000 NOK, since biofuels are considered as renewable sources [32]. Older oil boilers can also be modified to run on bio oils, making the switch to a renewable source easier [31].

2.3.4 Solar Energy

On a clear day, the solar irradiance on the earth's surface can be up to 1000 W/m² at solar noon [33]. This means that there is considerable potential for space heating using solar power, which is a free source, and can result in a near carbon neutral solution [26]. Furthermore, solar collectors are often expandable systems, enabling the connection of several modules into larger arrays, and can therefore potentially cover a large heating demand [34]. This solution also yields more energy per m² compared to photovoltaic (PV) panels [34].

Despite the many benefits of utilizing solar power, there are several disadvantages that must be considered. With the solar irradiation being highest at the equator, it will decrease the further north or south one moves [34]. Hence, the orientation of the solar collectors is crucial to secure stable heat production. In addition,

weather and seasonal conditions also affect the heat production [34]. A cloudy sky will reflect parts of the solar radiation back into space, while the winter season farther from the equator results in shorter periods of irradiation from the sun - both factors that reduce the heat production of the solar collectors [33]. The maximum energy coverage for space heating is difficult to determine when using solar heat, as the solar irradiation is unpredictable, but it is estimated to be around 15-30% [26, 28, 34]. For DHW it is expected to cover 40-50% of the energy demand [31].

2.3.5 Heat Pumps

HPs are able to extract energy from several heat sources with relatively low temperature, such as air and water, and increase the temperature through the use of a compressor, before supplying it to the desired location [11, 23, 27]. Despite utilizing a high-exergy energy carrier, in the form of electricity, to run the compressor, the majority of the heat that is supplied by the heat pump is extracted from the low temperature source. This means that HPs deliver more energy, in the form of heat, to the end user than the amount of electric energy used to run the HP [8]. Hence, HPs have a high Coefficient of Performance (COP), which gives the ratio of useful power produced (heat in kW) to electric power supplied (in kW) to the compressor [35].

Air-Source Heat Pumps

Outdoor air is an easily accessible energy source, which means that installing an air-source HP (ASHP) is easier than the other heat pump technologies, since it requires less intervention in the surroundings of the installation location compared to water- and ground-source HPs (GSHPs). This also results in the lowest investment cost, making it the most popular choice of HPs [8, 23]. ASHPs can be used to heat up either inside air, so-called air-to-air HPs (A2A-HP), or water for hydronic heating systems, so-called air-to-water HPs (A2W-HP). An A2A-HP is assumed to be able to cover up to 40% of the required energy demand for space heating [28].

Despite being broadly available, outdoor air is also affected by high temperature fluctuations both with the change of seasons over a year, as well as daily fluctuations, with the lowest temperatures being inversely correlated to the demand for heating indoors [23]. Luckily, there are HPs that are specifically designed for the cold Nordic climate, and that can operate even in temperatures as low as $-25\text{ }^{\circ}\text{C}$ [36].

Water-Source Heat Pumps

In this thesis, a separation between Water-Source HPs (WSHPs) and GSHPs has been made, even though GSHPs could use water as their source of heat.

WSHPs can extract heat from either sea water or underground water sources. Both of these sources have their limitations, though, as their availability depends on location and hydrological conditions. Sea water is available as a source for buildings located near the coast, while groundwater is typically available in areas where the ground conditions are sandy or contain a lot of gravel, or in close proximity to rivers. [23]

Sea water does not experience temperature variations as extreme as outdoor air, with the temperature range along the Norwegian coast being between a minimum of $3\text{-}5\text{ }^{\circ}\text{C}$ and a maximum of $9\text{-}14\text{ }^{\circ}\text{C}$ [37]. The groundwater temperature is approximately $1\text{-}2\text{ }^{\circ}\text{C}$ higher than the mean yearly temperature [38], with the latter being $6,3\text{ }^{\circ}\text{C}$ for Oslo [39]. SINTEF Byggforsk's detail number 552.403 also lists a similar temperature range for groundwater, at about $2\text{-}8\text{ }^{\circ}\text{C}$, a relatively constant temperature throughout the year [37]. WSHPs can cover up to around 80 % of the annual energy demand for both space heating and DHW [28].

Ground-Source Heat Pumps

Ground-source HPs (GSHP), also called geothermal HPs, extract thermal energy from geothermal energy wells, which can be up to 300 m deep [23, 37]. The technology takes advantage of the relatively constant underground temperature, which is higher than the outdoor air temperature in the winter, and lower in the summer [40].

The use of this technology requires a sufficient number of wells tailored to the demand for thermal energy, as well as an optimal distance between each well [23]. There are several benefits to using GSHPs. Despite a higher cost of investment when compared to ASHPs, GSHPs generate less noise, have a longer lifespan, require significantly less maintenance, and are not affected by the outdoor temperature fluctuations [41]. Similarly to WSHPs, GSHPs can cover up to 80 % of both space heating and DHW demand annually [28].

Figure 5 shows a diagram of different configurations of a GSHP based on the selected source.

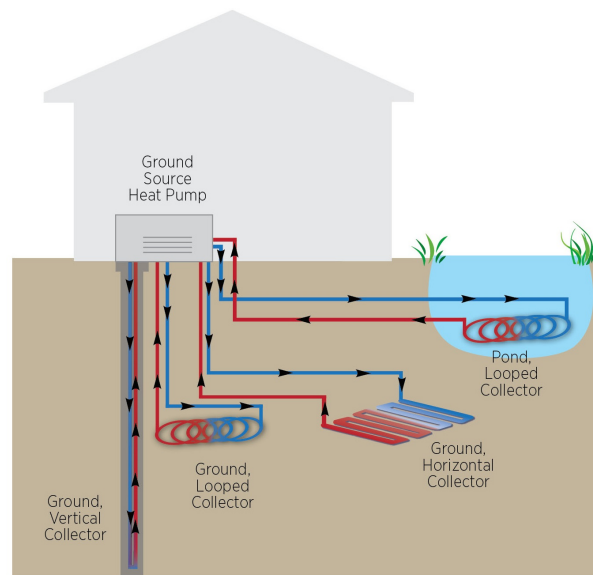


Figure 5: Schematic showing different sources for GSHPs [42]

2.3.6 District Heating

DH is a favorable way of supplying heat to buildings, as there are several energy sources that can be used to generate the heat. One of the most relevant sources, with regard to the reduction of greenhouse gas emissions, is surplus heat from different industries and processes [43, 34]. Among these processes, the most common source is the incineration of waste [6, 43]. Other sources include bio fuels, HPs, and off-peak electricity [6, 43, 44].

There are several advantages and benefits to using DH compared to other technologies. Both the size and scope of DH networks (DHNs) results in an economic advantage, while the environmental impact of DHNs remains relatively low compared to fossil fuels and electricity-based heating [45]. For the end users, investing in a heat exchanger to connect to the DH is far less costly than investing in a heat pump system. This is because the HP systems contain high tech components, and require more advanced control systems in addition to the work that is required locally when facilitating the installation of water- or ground-source HPs [23]. The wide

selection of potential energy sources not only functions as a safeguard for the security of supply, but also makes the shift away from primary energy sources possible [45]. This means that high exergy electricity that would otherwise be converted to heat directly, now can be used in other sectors more efficiently [46]. Furthermore, DH is able to cover 100 % of the annual heat demand for both space heating and DHW [28].

Nonetheless, there are times when the main sources used in the heat generation facilities are insufficient to cover the power peaks, which means that the DH plants must use other sources to meet the demand [6]. Often such peak loads consist of boilers operating on fossil fuels or electricity [47].

2.3.7 Thermally Activated Building Systems (TABS)

Thermally Activated Building Systems (TABS) are used to control the indoor temperature by using water-borne heating/cooling systems integrated into building mass, such as ceilings and floors [48]. Although TABS are not heating sources themselves, their characteristic low temperature difference between water temperature and desired room temperature makes them particularly useful with regard to energy saving, as low-temperature, low-exergy heating and cooling systems [48, 49]. Not only are they very easily combined with numerous energy sources, such as GSHPs [48], but they also help reduce power peaks by using the building structure they are embedded within as TES, hence providing significant thermal flexibility [50].

2.4 Hybrid Heating Systems

Although many current heating technologies constitute significant improvements compared to their predecessors, they do not always cover the entire heat demand [51]. Heating technologies, and in particular those relying on renewable energy, have an optimal point of operation, which is decided by several factors, among which are the heating demand and sufficiently high source temperature [26]. As stated in Section 2.3.4, solar energy can cover at most 30 % of the space heating demand, is susceptible to fluctuating heat production caused by obstructions to the solar irradiation, and yields the least heat when it is needed the most - in the heating season. Such a solution would need to be paired with another technology to fully cover the heating demand. It could, for example, be paired with a HP, either working in parallel as either base or top load, or in series, where the solar collectors function as the primary heat source for the HP [52]. Combinations of solar collectors and electric boilers are not only found in CHSs, but also in larger applications, such as sources for DH [53]. Figure 6 shows a principle drawing of such a configuration for application with a DHN.

A hybrid heating system will not only ensure more reliable heating, even on the coldest days, but can also be fitted with smart controllers that switch between the sources based on the demand and available energy [51]. Such solutions can also ensure optimal operation of the system regardless of load size [26].

Cost can also be a strong motivator for installing a hybrid heating system. A dual-source HP that combines an ASHP and a GSHP may not be as efficient as a GSHP itself, but is more efficient than the ASHP on its own, and has lower investment costs than the GSHP [40].

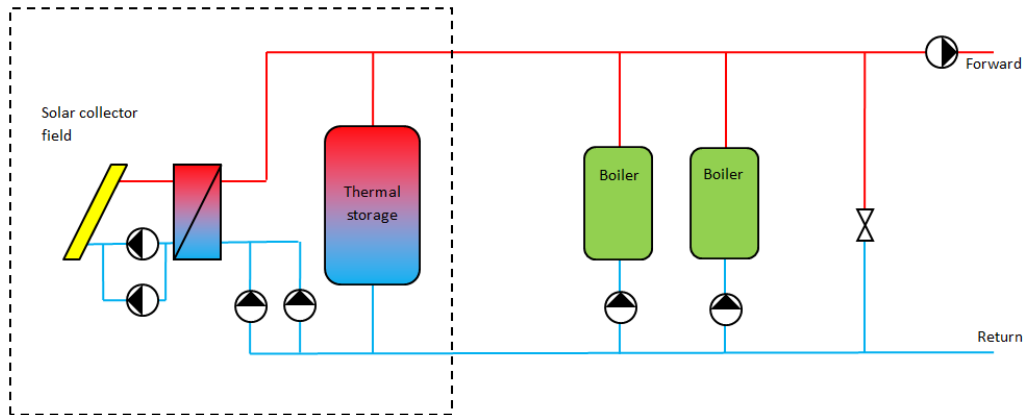


Figure 6: Principle drawing of combination of solar collector and boilers [53]

2.5 Power Peaks and Methods of Reduction

Power peaks occur as a result of high simultaneous electricity consumption from industrial and/or commercial power consumers [54]. Power peaks generally occur in the morning hours (07:00-11:00) and in the afternoon (17:00-19:00) during weekdays in the winter season [6]. Since the grid and power production must be able to handle power peaks, and with the ever increasing power consumption, reducing such peaks is crucial to ensure stable supply of electricity [6].

There are many ways of reducing power peaks. Two of the most common methods are peak shaving, also known as "load shedding", and load shifting. Peak shaving implies reducing the consumption for a short period of time to avoid a would-be power peak, while load shifting implies shifting the consumption from one period to another [54]. While the former reduces the total energy consumption, the latter only shifts the consumption, without necessarily reducing the total consumption. One example of peak shedding related to heating is reducing or turning off the space heating before a peak in power consumption or electricity price occurs. Since electric heating is considered a high-inertia load, the effects of turning it off will not be noticed immediately, which can save energy without compromising the thermal comfort, especially in well-insulated buildings [6]. The term Demand-Side Management (DSM) refers to the modification of the pattern of electricity consumption on the consumer side, and is often used for long-term solutions aiming to avoid power peaks by, for example, reducing the need for new or bigger heating systems that would increase the power demand [55, 56]. The application of DSM appears to be more common with regard to the electricity grid, but can also be applied to a DH system (DHS) [57]. Another term related to DSM is Demand Response (DR), which is more focused on short-term reduction of power peaks, which includes peak shedding or load shifting the energy use to off-peak periods [58].

2.5.1 Thermal Energy Storage

To avoid high cost and minimize the installed power for a heating or cooling system, different types of Thermal Energy Storage (TES) are often utilized [59]. TES is beneficial for taking advantage of periods with low electricity prices or a surplus of produced energy from sources such as solar, in order to generate and store heat that can be used when the energy prices are higher or there is less available energy from the source [12]. One simple form of TES are buffer tanks, which can either be used exclusively for storing heat produced by other

technologies, or produce heat itself, as is the case with water boilers [26]. The use of large-scale TES tanks is also widespread in DHNs [43]. The building mass could also be considered as a form of TES, especially in buildings with high thermal inertia [60]. The use of Phase Change Materials (PCMs) as heat storage, whereby thermal energy is stored by taking advantage of the latent heat required to facilitate phase transitions, also appears to be a promising option for future constructions [61]. Apart from PCMs, the aforementioned technologies store energy in the form of sensible heat, where the stored energy entails an increase in temperature of the medium the heat is stored in [62]. Equation 1 describes how the amount of sensible heat stored (Q [J]) is a function of the material's mass (m [kg]), specific heat capacity (c_p [J/(kg*K)]), and change in temperature between final and initial state (ΔT [K]). Figure 7 shows how temperature and phase of materials such as water and PCMs change with increasing heat. The horizontal parts of the graph show where latent heat is absorbed by the material, e.g. PCMs, to facilitate the phase change. The parts of the graph where an increase in temperature can be observed as a result of increasing heat symbolize sensible heat, which is used in traditional hot water tank storage.

$$Q = mc_p\Delta T \quad (1)$$

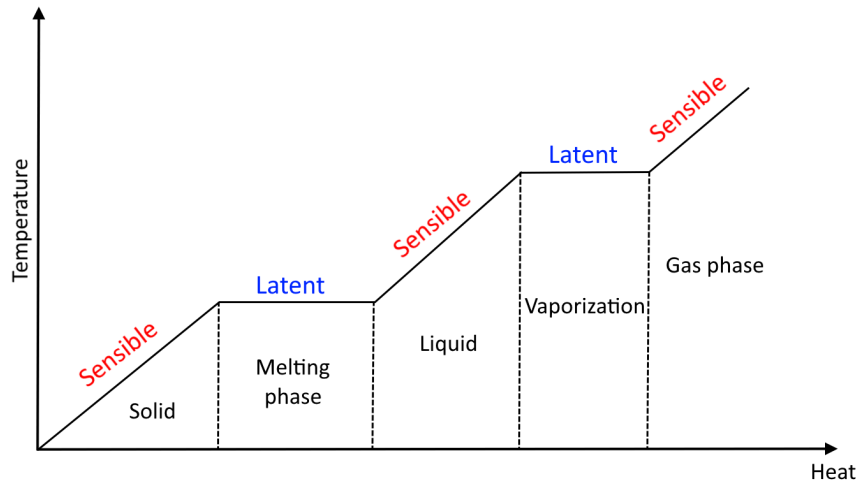


Figure 7: Heating process from solid to gas with sensible and latent heat behavior

2.5.2 Flexibility

The term "Flexibility" is often used in regard to power peak reduction to describe how different technologies and control strategies enable flexible production and consumption of electrical energy [6, 12]. When moving from older, more easily regulated technologies, such as gas boilers, to "green" technologies, such as HPs, which rely heavily on outside factors that can not be controlled, the control strategy of operation, as well as combination of technologies, is important to ensure flexibility [63]. DH also constitutes a source of flexibility, particularly in Norway, given the relatively recent ban on mineral oils for heating [5, 6]. This comes both from the use of multiple sources for the production of heat for in DH systems, and the frequent use of large-scale buffer tanks [43]. The term "flexibility" is, however, widely used in other contexts as well, such as the previously mentioned use by the Norwegian regulations on technical requirements for construction works (TEK17).

2.6 Simulation Software

There are many different types of simulation software that are used to model heating technologies and the regulation of said technologies. This section lists some of the most common software, and explains why IDA ICE 4.8 was chosen.

2.6.1 SIMIEN

SIMIEN is the leading software when it comes to energy calculations in Norway. The first version of the software was made available in 2008, and the software is updated regularly to keep up with the newest Norwegian regulations and standards.[64] The newest software conducts checks against TEK17 and SN-NSPEK 3031:2021 [65].

2.6.2 TRNSYS

TRNSYS is a tool used for simulating transient systems. Not only does it allow for simulations regarding the performance of both electrical and thermal energy systems, but also enables analyses of other dynamic systems, such as traffic flows or biological processes. [66]

2.6.3 EnergyPlus

EnergyPlus is a free, open-source software used for building energy simulations. The development of the software is funded by The United States Department of Energy, making the software relevant and popular in the U.S. [67]

2.6.4 IDA ICE

IDA Indoor Climate and Energy (IDA ICE) is a complex simulation program made by Swedish developer EQUA Simulation AB that enables modelling of building structures, as well as their systems and controllers [68]. IDA ICE has been validated according to several standards, including EN 15255:2007, EN 15265:2007, EN 13791, and ANSI/ASHRAE 140-2004 [69].

The software provides several pre-made systems for heating and cooling, such as GSHPs, electric boilers and chiller etc. Simultaneously, it allows for customization of the components making up the existing systems in the software, which allows for new systems to be simulated as well. One example of a custom heating system in IDA ICE was conducted in 2012 by Graziano Salvalai [70], who implemented a simplified GSHP model, and validated it using experimental data. There is also an example of an exhaust air HP for residential applications made available on EQUA's website [71].

3 Literature Review

This chapter is the result of a review process of a selection of articles related to the subject of reduction and shifting of power peaks. It is meant to supplement the information presented in Section 2 with examples of where the mentioned strategies have been applied, either through experiments or simulations. Both power peaks with regard to the electrical grid and thermal supplies, such as DH, are discussed in the studies that are presented.

3.1 Thermal Inertia and Heat Capacity

As stated earlier, thermal characteristics of constructions and heating systems play an important role in maintaining thermal comfort indoors. Several studies have investigated the importance of such attributes in different building types and climates.

Airaksinen and Vuolle [72] achieved up to 62 % reduction in consumed energy when going from a standard Finnish building code construction to a low energy construction, while the peak energy demand was reduced by 34 %. Hayati et al. [73] examined an existing, DH-connected multifamily building in Sweden by using IDA ICE and measured data, in order to examine the possible use of the building's thermal inertia for load shaving during power peaks. A temperature decay test was conducted and the results showed, on average for the entire building, that a 61% reduction in supplied energy would only yield a 0.3°C reduction in temperature over a 5 hour period.

Heier et al. [74] simulated the addition of thermal mass to the construction as a measure for reducing both heating and cooling peaks. They recommend that the thermal mass be placed on the inside of the building, and, if PCMs are to be incorporated in order to increase the total thermal mass, their phase change temperature should be close to that of the heating setpoint. Both PCMs and concrete achieved similar improvements, but PCMs were preferred, as their higher latent heat storage capabilities require a significantly lower thickness to achieve the same reduction of power peaks and energy consumption.

Not all power reductions are intentionally performed to save energy, however, and sometimes high power demand could exceed the electrical grid's capacity, leading to an unintended shutdown of the heating systems. Such a scenario was examined by Fransson et al. [75], using both field measurements and simulations in IDA ICE, for both a single-family dwelling, and a multi-family dwelling. For both dwelling types, the drop in temperature was low, even 8 hours after the power outage. For a mean outdoor temperature of 6.3 °C, the most prominent drop was only 3 °C. This study only took into account the thermal inertia of the relatively old 1950s and 1960s building structures themselves.

E. Guelpa [76] analyzed the impact that the thermal capacities of components found in a District Heating Network (DHN), i.e. all components from supplier to end user, potentially have on heating demand peaks. A night shutdown was initiated to determine the importance of the thermal capacities during the reheating phase in the morning. For the DHN in Turin, Italy, the combined heat capacity of the heating circuits among the end users was estimated to be equal to that of the distribution lines between the main transport network and different customers. Most of the energy required in the morning hours (0.33 GWh) went to heating the the components in the DHN, with the remaining (0.07 GWh) being used to heat the actual buildings connected to the DHN. This highlights the importance of proper management of the thermal masses in the DHN, while also touching on the possibility of exploiting the thermal capacity of the water content present in the DHN for thermal peak reduction.

3.2 TES

An analysis published by Thermal Storage UK [12] estimated that by increasing the use of smart thermal storage, the United Kingdom could reduce the peak electricity demand by a whole 1.6 GW on the coldest winter day by 2030. Further benefits are reduced greenhouse gas emissions and more flexibility from renewable sources.

A paper published by Hirschev et al. [77] looked into trends regarding the potential reduction of energy and power demand that could be achieved with a HP-TES combination. Several temperature arrangements maintaining two fixed temperature bodies (TES and thermal sink) and one varying temperature (thermal source) were considered for this combined system. The highest energy savings potential for both heating and cooling operation was achieved when the temperature of the TES is close to that of the thermal sink, whereas the highest peak demand reduction favors a higher TES temperature than sink temperature during heating operation, as this allows for direct heat flow from the former to the latter according to the second law of thermodynamics, ergo reducing the necessary operational duration of the HP, or even eliminating the need for the HP to be operational altogether.

Further mentions of thermal inertia, heat capacity, or the use of TES or similar technologies are listed alongside the other findings from articles in the following section of the literature review. This because most articles found regarding these themes tend to examine their impact in conjunction with other measures that are more in focus, i.e. the chosen control strategies.

3.3 Control Strategies

Regardless of which heating system, technology, or building type that is considered, ensuring that the heating is regulated optimally is crucial to achieve maximum energy efficiency, avoid power peaks, and maintain thermal comfort. There are countless methods and strategies for regulating heating supply that have been investigated, and some of them are presented in this section.

In 2020, Benakopoulos et al. [78] conducted tests in and simulations of a Danish office building, and found that switching from a more traditional continuous high-temperature heating operation to either a night-setback, or continuous low-temperature heating operation, cost savings of 23.1 and 18.6 %, respectively, as well as energy savings of around 11 % for both solutions, could be achieved. The most relevant finding, however, is the fact that a low-temperature system will eliminate the need for a rapid reheating phase in the morning - a common source of power peaks.

Foteinaki et al. found that preheating of spaces can facilitate an effective load shifting, with a morning peak load reduction of up to 87 % through DR when heating is supplied by DH [79]. Basciotti and Schmidt [80] developed a database consisting of the reheating duration for different building standards and climatic conditions relevant to a DHN through the use of TRNSYS and measurements for validation. This data was consequently used to shift power peaks by optimizing a DSM strategy, which resulted in a reduction of power peaks of up to 35 % over the course of a day. Simultaneously, the energy production for the DHN was increased by approximately 2 %.

Measurements and IDA ICE simulations conducted by Hajian et al. [81] in 2022 showed that implementing a dynamic heating control could yield a 8.9 % reduction in maximum power consumption related to space heating, compared to a conventional heating control in a Finnish apartment block connected to a DHN. Ala-

Kotila et al. [82] performed field tests of a DR system installed in Finnish student apartment buildings that already used a dynamic weather forecast control, and were connected to a DHN. After implementing the DR system, the peak load reduction was reported to be on average 14-15%. Energy consumption and greenhouse gas emissions were consequently cut by 11% and 9%, respectively.

Arteconi et al. [83] analyzed the implementation of DSM for existing TABS in a commercial building. They found that TABS offer flexibility and make peak shaving relatively easy to achieve without sacrificing thermal comfort, in part due to the lack of design changes needed. Despite both maintaining a comfortable indoor climate (19-26°C) and cost savings, no significant overall energy reductions were achieved. Arteconi et al. [84] also tested a DSM strategy consisting of switching off a ASHP + TES system during a 3-hour peak in Northern-Ireland, in order to flatten an afternoon load curve. The results showed that the HP could be turned off for up to 3 hours while maintaining the indoor temperature above 19°C at nearly all times, and above 20°C for 86% of the time. This entails that a TES system is included for lower-inertia distribution systems (e.g. radiators), as the inclusion of a water-based TES required the HP to top up the energy in the tank during off-peak hours. However, for higher-inertia systems (e.g. underfloor heating), performance was much more promising, even without a TES system. Consequently, including a TES unit yielded a slight increase in energy consumption, which was deemed acceptable due to economic incentives related to off-peak use, as well as the use of "green" energy in the form of an ASHP.

A similar setup to that of Arteconi et al. [84], consisting of an ASHP + TES + PV, was tested by Tarragona et al. [85]. The study was based on EnergyPlus simulations for 17 different climate zones in the U.S., Canada, and Saudi Arabia, and used a control strategy consisting of a Model Predictive Controller (MPC) combined with an Inner Control Algorithm (ICA) to operate the heating system. This led to a reduction in on-peak energy purchase of approximately 90% in nearly all the climate zones. Furthermore, the addition of a TES system was also an important factor in enabling optimal utilization of the electricity generated on-site for the purpose of heating.

Alimohammadisagvand et al. [86] investigated the possibility of using knowledge of the Hourly Electricity Price (HEP) for load shifting through DR, and found that the control strategy that modified the set point for the indoor temperature based on a comparison between the current HEP and previous HEPs was the most effective at minimizing the delivered energy and cost of electrical heating. This control strategy yielded a reduction of 3.1% and 9.6% in maximum total delivered energy and cost, respectively, compared to regulating according to a constant set point for indoor temperature. One aspect worth mentioning in particular is the attention that was paid to maintaining thermal comfort through the monitoring of parameters other than just indoor air temperature, such as RH and air velocity.

Baetn et al. [87] proposed a MPC strategy for an ASHP that considered the energy cost for the end user, the environmental impact of the energy consumption, and potential expansions required due to high consumption, to develop an optimal strategy. It showed that the resulting cost and consumption varies a lot based on which of the three aforementioned factors that is weighted the most. For example, with a lower environmental impact weight, the cost becomes more important, which in turn leads to increased off-peak heat generation and storage. Generally, however, the peak production is reduced, especially with the addition of a hot water tank, which only results in minor increased costs for the end user. Additionally, the thermal storage capabilities of the building mass, underfloor heating system, and space heating buffer tank are also acknowledged.

Knudsen et al. [88] reported an experiment based on a novel, DH-based Economic Model Predictive Control

(E-MPC) scheme, which was applied to water radiators in a well-insulated single-family building. This control used data from a heating meter, sensors, and weather data from the internet to develop a linear black box model, which proved to be useful in shifting the energy use from high to low demand periods. This shift was achieved without deviating from an acceptable thermal comfort during the variable setpoint data collection stage, which meant that the application of the model could consequently be performed in zones that were occupied.

Amato et al. [89] also conducted tests in an occupied single-family house in Denmark by mimicking the operation of an E-MPC scheme aiming to shift loads by increasing the setpoint of radiators from 20 °C to 22 °C in the hours preceding the high-price peak around 5 o'clock in the morning. The additional heat added in the boost periods, which were 1, 3, and 5 hours, was intended to be stored in the thermal mass of the building. As can be seen in the first row of Figure 8, the temperature decay after shutdown during the peak period was proportional to the duration of the heat boost period, at around 1.5, 3.5, and 6 h for the boost periods of 1, 3, and 5 h, respectively. The second row of Figure 8 shows how the supply and return temperature of the DH is impacted by the scheme.

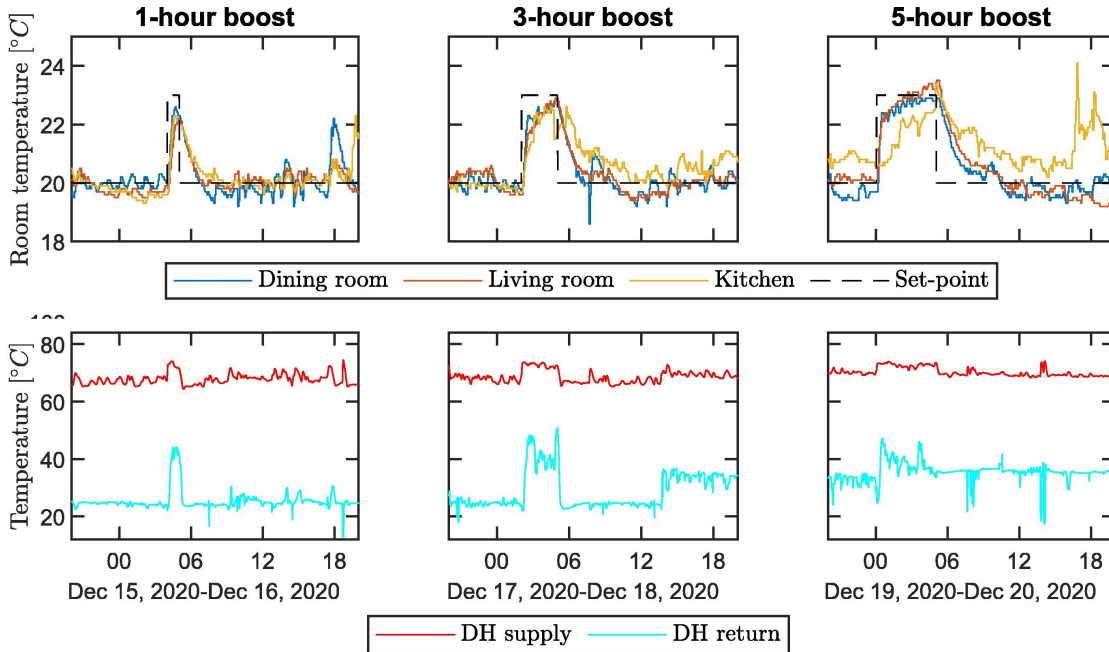


Figure 8: Data from experiment 1. First row: Temperature setpoints and room temperatures. Second row: DH supply and return temperatures. [89]

Not all strategies intended to reduce electric power peaks yield exclusively positive results, however, as shown by Li et al. [90]. In a hybrid system located in China, which consists of sewage-source centrifugal HPs and gas boilers, the latter are used to avoid power peaks in low temperature conditions, when the HPs experience a low COP. Naturally, this leads to increased CO₂ emissions, which is undesirable.

3.4 Research Gap

While there are a lot of approaches to reducing power peaks in space heating systems, there are also some potential solutions that have not been explored sufficiently. Some sources [47, 76] have at the very least mentioned the possibility for utilizing the water volume in piping networks as storage for thermal heat. However, most of those are related to DHNs rather than water volumes of pipes within buildings. Furthermore, research regarding the topics of power peak reduction and shifting considering Norwegian building codes don't occur nearly as often as other countries. These gaps in research, combined with promising results from Nordic countries in general [81, 82, 88, 89], were the main motivation for this thesis and the work that was done in IDA ICE, which is further described in Section 4.

4 Method

4.1 Case Study

In order to ensure a realistic case relevant to Norwegian standards, the properties of the main IDA ICE model were designed to conform to the building envelope requirements given by TEK17 for an office building. For the improved building envelope case, the construction was altered in accordance with the Passive House (PH) standard for non-residential buildings (NS 3701:2012 [91]). The models consisted of three different rooms with varying total area, window area, intended use, and occupation schedules resembling realistic usage patterns for an office building. Figure 9 shows the 3D view of the building in IDA ICE, including the names of the three rooms. The model shows the outline of all the radiators that have been placed under the windows in the rooms, in order to prevent cold draughts from the cooled window surfaces.

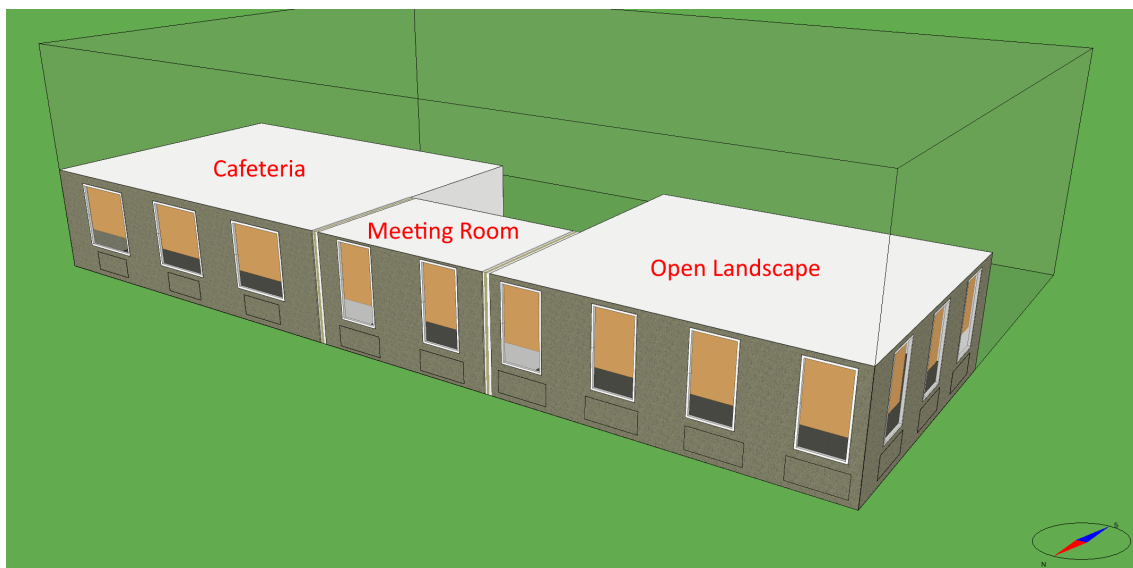


Figure 9: 3D view of construction that was evaluated in IDA ICE

As can be seen in Figure 9, the main facade of the building is oriented towards north and is located on the bottom floor - both adjustments made to increase the potential heat loss, in order to analyze the worst case scenario regarding heat loss. Given the high number of simulations and logged data (see Section 4.6), it was decided to prioritize the Open Landscape zone when it came to reviewing the simulation results. This is justified by the fact that in most office buildings, it is the open landscapes and offices that are occupied first in the morning, as there are typically no meetings in the first few hours, and the cafeteria is usually frequented more around lunch time. Furthermore, the building envelopes for all zones are designed using the same input data, while the open landscape is the room with the largest number of windows, making it an interesting area of focus. It is also worth mentioning that the handling and presentation of the results becomes significantly more manageable, in particular with regard to the time allocated for this thesis, and clear by focusing on one zone than it would be if all the zones were to be evaluated.

4.2 Input Data

Table 1 shows the most relevant requirements for the TEK17 and PH constructions that were used in the models for this thesis. The actual values used for the TEK17 and PH cases are listed in Section 4.2.4 and Section 4.2.5, respectively, in addition to appendixes referenced in said sections.

Table 1: Requirements from TEK17 and Passivehouse standard (NS 3701:2012) for office buildings

Parameter	TEK17 value	Source	Passivehouse Value	Source	Unit of measurement
U-value External Wall	$\leq 0,22$	TEK17 §14-3	0,10 - 0,12	NS 3701:2012	W/(m ² K)
U-value Floor	$\leq 0,18$		0,08	Tabell B.1*	W/(m ² K)
U-value Windows & Doors	$\leq 1,2$		$\leq 0,8$	NS 3701:2012	W/(m ² K)
n50	$\leq 1,5$		$\leq 0,60$		h ⁻¹
Thermal Bridges	$\leq 0,05$	TEK17 §14-2	$\leq 0,03$	Tabell 9	W/(m ² K)
Efficiency of Heat Exchanger (AHU)	≥ 80		≥ 80		%
Average Lighting Power (During Operation)	8	NS 3031:2014	4	NS 3701:2012 Tabell 8	W/m ²
<i>*Table B.1 in NS 3701:2012 lists examples of U-values</i>					

In contrast to standard practices in some other countries, the Norwegian requirements given in TEK17 require the thermal bridge value to be applied per m² of floor area, rather than per surface area. The input method for IDA ICE taking this into account is shown in Appendix B.

4.2.1 Climate Data

In order to test a realistic scenario that is known to the involved parties of this thesis, the location and climate were set to Blindern - Oslo, Norway, and a .PRN climate file for this location was imported into IDA ICE. The file contains data such as air temperature, RH, and solar irradiance. The most important factor, the outdoor air temperature, is visualized in Figure 10 (a), for January 16th through 20th. The lowest temperature for the selected week occurs at the same time as the design power demand from the heating load simulation for the TEK17 baseline case, which is around 7:00 on January 17th. Figure 10 (b) shows the outdoor air temperatures over the course of the year according to the climate file. The climate file was obtained using a software called "EPW-Gen" [92], which was created by P.G. Schild, and is not publicly available. The location input data for IDA ICE with regard to climate is available in Figure 70 in Appendix A.

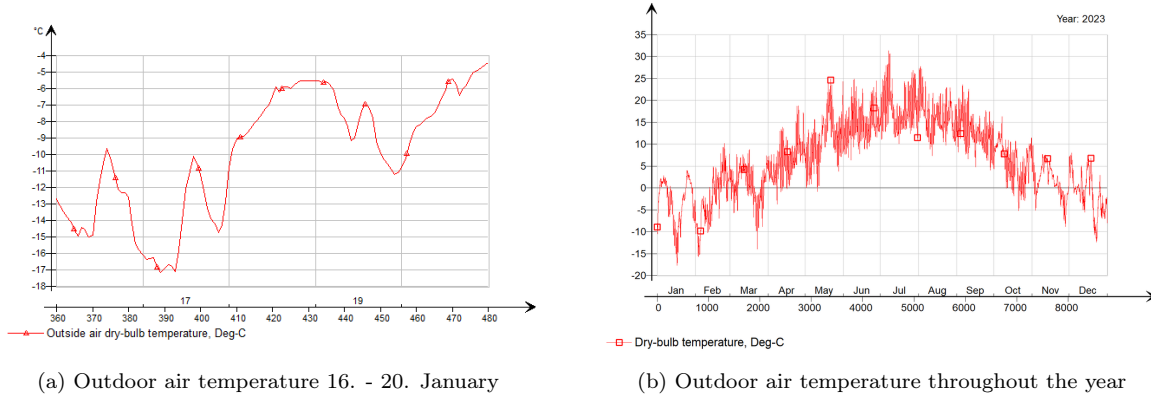


Figure 10: Climate data for IDA ICE model

4.2.2 Zones

A realistic model requires rooms with accurate intended use and usage patterns. As Figure 9 shows, there are three different zones in the building. The first room (north-west) is an open landscape, the middle room is a meeting room, and the last room (north-east) is the serving area, which is assumed to be heated in the same way as the other two zones, and therefore does not require any special design for heating. The latter room is similar in construction to the open landscape, albeit with fewer windows and a different usage pattern.

Figures 11 and 12 show the general input details for the three zones of the TEK17 and PH cases, respectively. It is worth pointing out that the value for lights in the TEK17 case was set to 6 W/(m²), rather than the max requirement of 8 W/(m²) given in NS 3031:2014, while internal loads due to equipment were disregarded. Both of these assumptions came as a result of high initial internal heat loads, which yielded unrealistic conditions in the zones.

Name	Group	Floor height, m	Room height, m	Floor area, m ²	Heat setp, °C	Cool setp, °C	AHU	System	Supply air, L/(s.m ²)	Return air, L/(s.m ²)	Occup., no./m ²	Lights, W/m ²	Lights, kWh/m ²	Equipme nt, W/m ²	Equipme nt, kWh/m ²	Ext win. area, m ²
Cafeteria		0.0	2.7	66.72	21.0	26.0	Air Ha...	VAV, te...	2.0	2.0	0.3179	6.0	12.48	0.0	0.0	8.326
Meeting Room		0.0	2.7	15.24	21.0	26.0	Air Ha...	VAV, te...	2.0	2.0	0.318	6.0	12.48	0.0	0.0	3.8
Open Landscape		0.0	2.7	55.76	21.0	26.0	Air Ha...	VAV, te...	2.0	2.0	0.11	6.0	14.04	0.0	0.0	12.6
Total/m²									2.0	2.0	0.2337	6.0	13.11	0.0	0.0	9.556

Figure 11: General info regarding the three zones for TEK17 case

Name	Group	Floor height, m	Room height, m	Floor area, m ²	Heat setp, °C	Cool setp, °C	AHU	System	Supply air, L/(s.m ²)	Return air, L/(s.m ²)	Occup., no./m ²	Lights, W/m ²	Lights, kWh/m ²	Equipme nt, W/m ²	Equipme nt, kWh/m ²	Ext win. area, m ²
Cafeteria		0.0	2.7	66.72	21.0	26.0	Air Ha...	VAV, te...	2.0	2.0	0.3179	4.0	8.32	0.0	0.0	8.326
Meeting Room		0.0	2.7	15.24	21.0	26.0	Air Ha...	VAV, te...	2.0	2.0	0.318	4.0	8.32	0.0	0.0	3.8
Open Landscape		0.0	2.7	55.76	21.0	26.0	Air Ha...	VAV, te...	2.0	2.0	0.11	4.0	9.36	0.0	0.0	12.6
Total/m²									2.0	2.0	0.2337	4.0	8.741	0.0	0.0	9.556

Figure 12: General info regarding the three zones for PH case

Figure 13 shows the occupation (left) and lighting (right) schedules for the Open Landscape zone. Further data regarding the occupancy and lighting schedules for the other zones can be found in Appendix C and Appendix D, respectively. It should be noted that the occupancy schedule for the meeting room (see Appendix C) does

not reflect the comment made in section 4.1 regarding the lower occupancy in the morning hours for said room. Nonetheless, considering the focus on the Open Landscape, the results should not be affected considerably by this error, even though all the zones are connected to the same heating system.

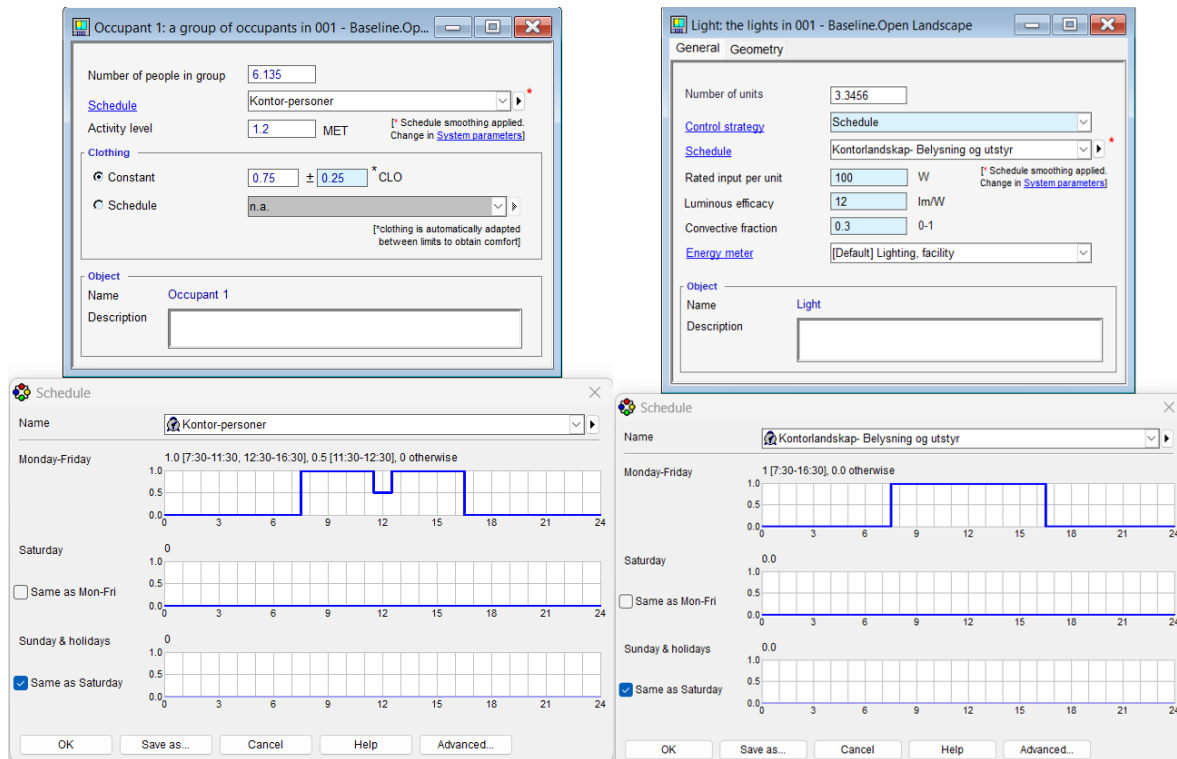


Figure 13: Occupation (left) and lighting (right) data for the open landscape zone

4.2.3 Windows

For windows, the construction consisted of the three-pane glass windows. The selected windows were based on an existing construction in IDA ICE, albeit with reduced air gap between the panes in order to increase the total U-value of panes & frame to $1.1 \text{ W}/(\text{m}^2\text{K})$. The windows used in the PH case were adapted to the stricter requirements by altering the TEK17 windows to have a larger distance between the individual panes, from 10 mm to 18 mm, and the U-value of the frame was changed from $2.0 \text{ W}/(\text{m}^2\text{K})$ to $1.5 \text{ W}/(\text{m}^2\text{K})$. The g-value for the windows in both cases was 0.6. Further data for all the windows in both the TEK17 and PH case is made available in Appendix E.

4.2.4 TEK17 Case

The TEK17 case was designed to match the TEK17 building envelope requirements presented in Table 1. Figure 14 shows the input materials that were used for the external walls and the floor towards the ground. Only external surfaces differ between the TEK17 and PH cases, with the internal surfaces remaining unchanged from default. For further data regarding the properties of the materials, see Appendix F and Appendix G.

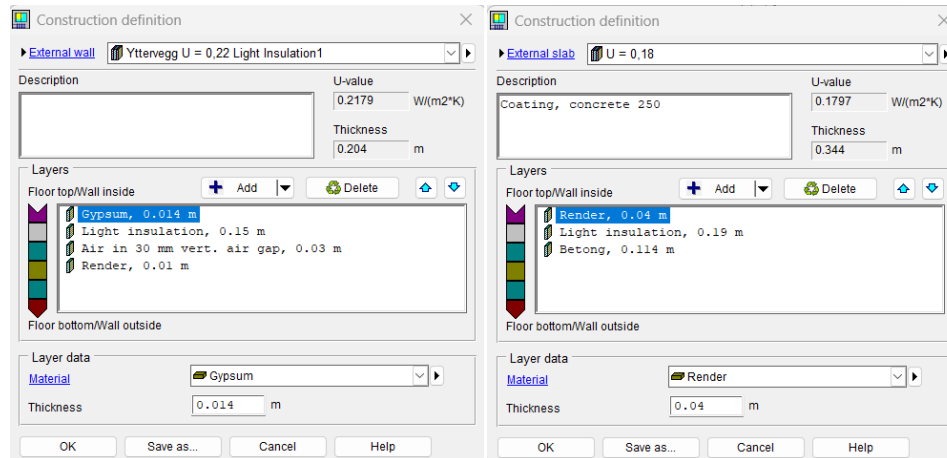


Figure 14: General construction of external walls (left) and floors towards the ground (right) for TEK17 case

4.2.5 Passive House Case

Similarly to the TEK17 case, a PH simulation model was also developed. This was done by improving specific features of the TEK17 case, so that they would match the values given in the PH standard NS 3701:2012 [91]. Figure 15 lists the input materials that were used for the external walls and the floor towards the ground in this case. Further data can be seen in Appendix H and Appendix I.

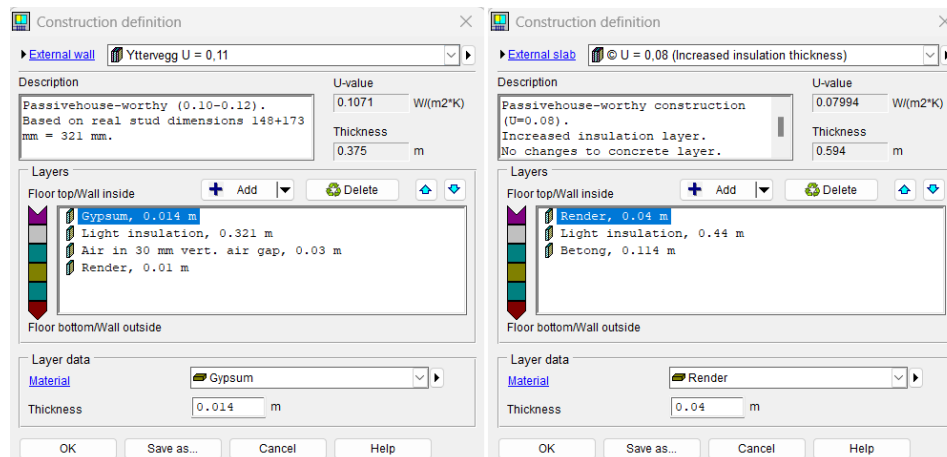


Figure 15: General construction of external walls (left) and floors towards the ground (right) for the PH case

4.3 Plant

Instead of using the plant model that is selected by default in IDA ICE, the Early Stage Building Optimization (ESBO) plant was chosen to replace it, as shown in Figure 16. The ESBO plant made it possible to adjust an existing, stratified hot water tank ("HotTank" - see (D) in Figure 16) to make it closer represent the water volume in the heating circuit. The greyed out parts of the plant are parts of the cooling and DHW systems which were not investigated in this thesis, but could not be removed from the plant, as their absence would cause problems with the simulations.

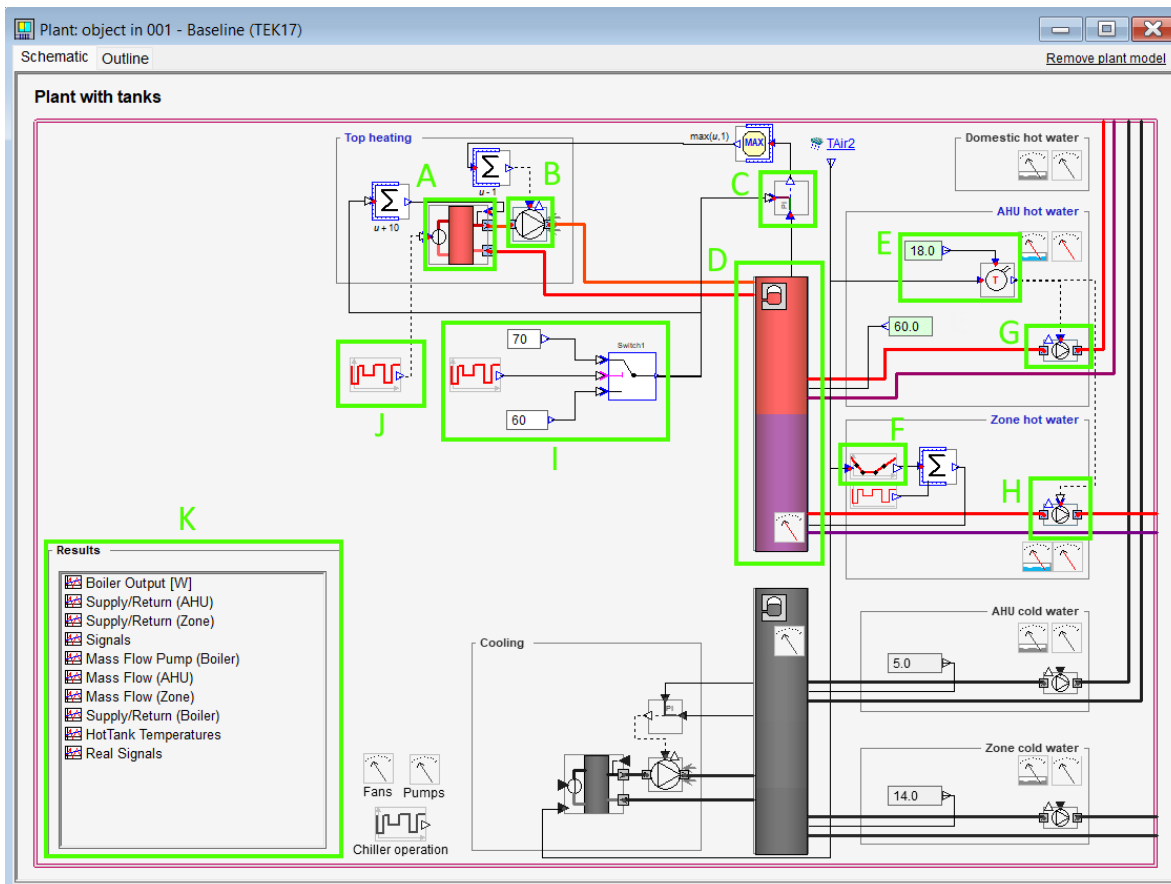


Figure 16: ESBO plant: (A) = Boiler, (B) = Boiler pump, (C) = PI controller for boiler pump, (D) = HotTank representing water volume in pipes, (E) = Thermostat controlling AHU & zone pumps, (F) = P-controller with linear segments, (G) = AHU circuit pump, (H) = Zone heating circuit pump, (I) = Setpoint control for boiler & PI controller, (J) = Schedule for boiler operation, (K) = Output files for logging values

The boiler (A) was designed based on a heating load simulation which was conducted using an "endless" (99,999 kW) power supply to find the necessary maximum heating demand given the data from the baseline TEK17-worthy building. Based on this simulation, the boiler was given a value of 3.836 kW. Later, after some values related to the building envelope were corrected, it was discovered that the real design value was 3,636 kW. Since most simulations were already completed at the point when this was discovered, and given that the difference between the actual value and the initial value only was around 5 %, a decision was made to keep the initial value.

The distributions of total max power for zone heating and Air Handling Unit (AHU) for both the initial (a) and actual (b) values are available in Figure 17, while the the heating load simulations are available in Appendix J. Note that the change between Figure 17 (a) and Figure 17 (b) lies in the zone heating, whose reduction in maximum power demand can be attributed to the aforementioned adjustments made to the building envelope.

All input data for the boiler is available in Appendix K. For Simulation 5 (see Section 4.6.6), which utilized a DH instead of an electric boiler, the boiler power was increased to 100 kW, so that the system could extract the necessary power depending on the strategy and setpoints being used. The boiler output can be adjusted between 0 kW and its maximum available capacity through three modes, which can be seen in the parameter section of Appendix K. The first mode is $\text{MODE} = 0$, where the boiler is shut off completely, the second is $\text{MODE} = 1$, where the boiler varies the supplied power between the " $\text{MODE} = 0$ " setting of 0 kW and the maximum given boiler capacity, depending on the demand, and the last is $\text{MODE} = 2$, where the boiler is forced to operate at maximum available power as long as this signal is maintained. For the simulations included in this thesis, only modes 0 and 1 were used as inputs for the boiler, with the potential utilization of $\text{MODE} = 2$ being left for the software to control.

Building		
Systems energy		
	Max., kW	Time
■ Zone heating	2.024	
■ AHU heating	1.812	
■ Dom. hot water	0.0	
Total	3.836	17 Jan 06:05

(a) Initial design value (3,8 kW)

Building		
Systems energy		
	Max., kW	Time
■ Zone heating	1.819	
■ AHU heating	1.817	
■ Dom. hot water	0.0	
Total	3.636	17 Jan 06:04

(b) Actual design value (3,6 kW)

Figure 17: Design values for boiler distributed between zone heating and AHU

The boiler pump (B) is what keeps the circuit between boiler and HotTank running, and is controlled by the PI controller (C). The boiler delivers a higher supply temperature than the setpoint of the HotTank (D), which is the result of an "ADDER" block that is present in the plant by default. Earlier attempts at running simulations with this block removed resulted in errors, and directly connecting the setpoint signal to the boiler was therefore disregarded as an approach. An attempt was also made to replace the main pump with a simple pump in order to better control the flow. This strategy also resulted in simulation errors, and it was therefore decided to keep this aspect of the plant unchanged from the default ESBO plant. The PI controller regulates the pump based on the difference between a setpoint temperature and the measured temperature of

the HotTank. The HotTank setpoint is by default determined by the highest temperature requested of the tank, which in this case is 60 °C, as this is the supply temperature for both the AHU and the zone heating. In this thesis, however, a new setpoint controller (I) was created using a schedule and switch block in the ESBO plant. The new controller enables preheating of the HotTank, as further described in Section 4.6, by increasing the setpoint from the default temperature of 60 °C to, for example, 70 °C.

The HotTank itself is reduced in volume, from the default 1 m³ to 0,2148 m³. This volume was determined using a ratio of water volume of heating system to area of floor of 1,56 L/m². The ratio was obtained using unpublished data from an existing hospital building in Norway, which in and of itself constitutes a potential source of error, as hospitals and offices are designed and operated differently. Nevertheless, the value made it clear that 1 m³ was too large of a volume, which makes sense when considering the fact that the stratified tank was intended to be a storage tank, and not what it was used for in this thesis. To further adapt the HotTank to this thesis, the stratification was limited to only 2 layers, as opposed to the default value of 8 layers. This was done to ensure that the hotter top layer represent the supply temperature of the water for both the AHU & zone heating, and the colder lower layer represent the mean return temperature for these circuits. Further parameters for the HotTank are available in Appendix L. There were some problems with adjusting the height of inlets and outlets connected to the HotTank, which in turn will affect the results. Since the inlet and outlet for the boiler circuit are very close to each other, even though the outlet going back to the boiler should be at the bottom, the boiler will not be supplied with the coldest water from the bottom layer of the HotTank.

The thermostat (E) keeps the AHU pump (G) and zone heating pump (H) running as long as the outdoor temperature is lower than 18 °C. The proportional controller (F) is supposed to enable outdoor temperature compensation, but has been altered to supply 60 °C at all outdoor temperatures. In addition to the boiler, the zone heating pump can also be controlled by the boiler operation schedule (J) in those simulations where such a measure is required. This is possible because both the boiler operation schedule and the thermostat yield either 0 or 1 as output values, which is what both the AHU pump and zone pump require.

The data presented in the results section (see Section 5) was logged using output files that are available in IDA ICE. The output files enable the logging of several variables, such as supply and return temperatures, in the same file and graph for easier comparison and analysis.

4.4 Ventilation

The maximum supply and return air volumes of $2.0 \text{ L}/(\text{s}\cdot\text{m}^2)$, which can be seen in Figure 11 and Figure 12, were determined based on values from TEK17 and the Norwegian authorities for labor inspection (Norwegian: *Arbeidstilsynet*). TEK17 §13-3 requires $26 \text{ m}^3/\text{h}$ of clean air per person for public buildings and office buildings [93]. Arbeidstilsynet recommends allocating 6 m^2 of floor space per person [94]. This information yields a value of $4.42 \text{ m}^3/(\text{h}\cdot\text{m}^2)$ of clean air for ventilation of emissions from the occupants' activity, and equals $1.3 \text{ L}/(\text{s}\cdot\text{m}^2)$. For emissions from materials, TEK17 requires ventilation rates of 0.7 and $2.5 \text{ m}^3/(\text{h}\cdot\text{m}^2)$ outside of and during time of use, respectively [93]. The latter equates to $0.7 \text{ L}/(\text{s}\cdot\text{m}^2)$, which is the same that Arbeidstilsynet lists for low-emitting materials [94]. Hence, the ventilation flow rate is determined to be minimum $0.7 \text{ L}/(\text{s}\cdot\text{m}^2)$ during periods without occupant presence, and a maximum of $(1.3 + 0.7) \text{ L}/(\text{s}\cdot\text{m}^2) = 2.0 \text{ L}/(\text{s}\cdot\text{m}^2)$ when the Temperature + CO_2 control strategy requires more air to ventilate for CO_2 pollution or cool the room, the latter of which is irrelevant for this thesis. Using $0.7 \text{ L}/(\text{s}\cdot\text{m}^2)$ as a minimum ventilation rate also means that all building materials in the building are assumed to be low-emitting. Appendix M shows relevant setpoints for the Open Landscape zone.

The default AHU in IDA ICE was slightly modified to enable varying supply temperature, as can be seen in Figure 18. Instead of a traditional switch between a constant, scheduled, or outdoor temperature-compensating control, a new scheduled setpoint control (A) was added, which enabled the switch between two different temperatures by using a "Schedule" block. The AHU was set to supply $19 \text{ }^\circ\text{C}$ by default, which in practice meant setting the setpoint of the controller to $18 \text{ }^\circ\text{C}$, since the fan by default heats the supply air by another $1 \text{ }^\circ\text{C}$. The fan operation schedule (B) enables manipulation of the supply and extraction fans, (C) & (G,) respectively, but was not altered in this thesis. The "Air side effectiveness" of the cooling coil (D) was set to zero, in order to turn it off, since heating was the main focus. The same input for the heating coil (E) was set to 1. The effectiveness of the heat exchanger (F) was set to 0.8 by default, and was kept at this value, as it is the minimum requirement of both TEK17 and the PH standard (see Table 1).

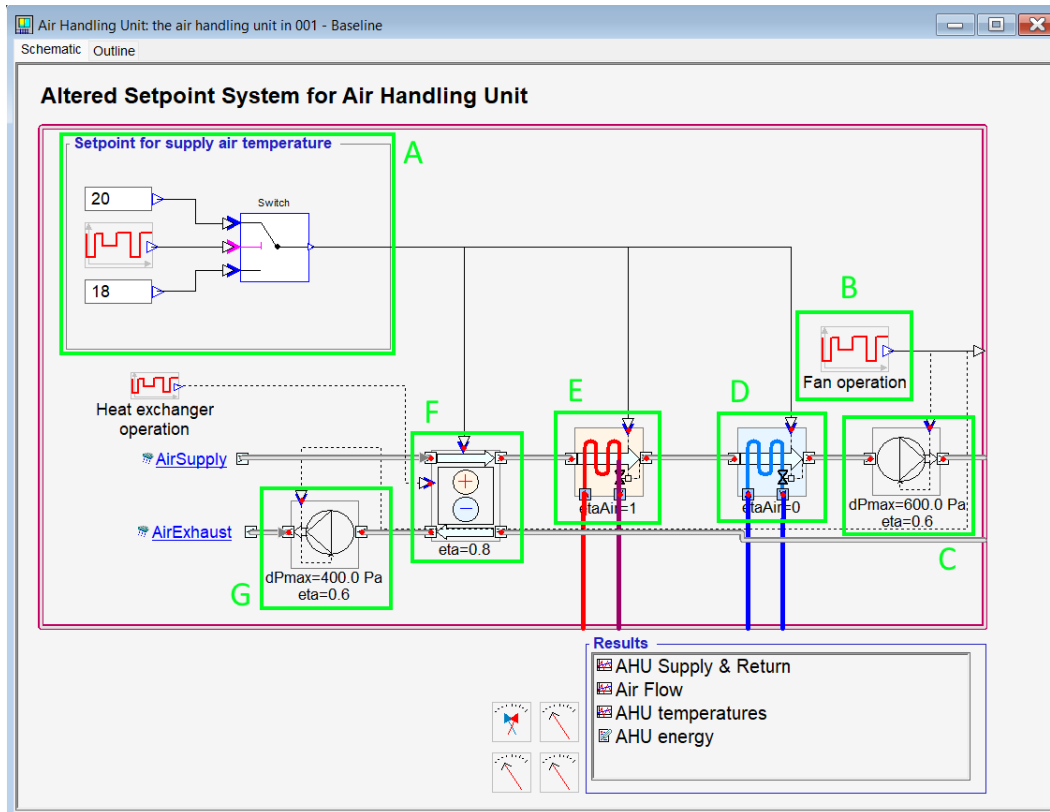


Figure 18: Air Handling Unit (AHU) modified to enable switch between two different supply temperatures. Note that the supply temperature is the chosen temperature plus 1 °C, which is added by the supply fan (C).

A = Setpoint control for supplied air temperature, B = Schedule for operation of supply fan (C) and extraction fan (G), D = Cooling coil, E = Heating coil, F = Heat exchanger.

4.5 Zone Heating

Zone heating is performed through the use of radiators, which are a common solution for office buildings. They are placed strategically under the windows to prevent cold draughts. In Figure 19 the input data for the radiators in the Open Landscape zone can be seen. The design power of 132.49 W is the same for all seven radiators in the zone, four of which belong to the same facade and are shown in Figure 19. The sum of all seven radiators is 927.4 W, which is the max required room unit power according to the heating load simulation (see Figure 82 in Appendix J). The supply and return temperatures at maximum power are set to 60 and 40 °C, respectively. Preliminary simulations showed that the radiators do not necessarily operate according to these setpoints, but further results are discussed in Section 5. The radiators are not only installed to counteract the heat losses through transmission and infiltration, but also ventilation, since the supply air temperature is set to 19 °C, which is lower than the heating setpoint of 21 °C.

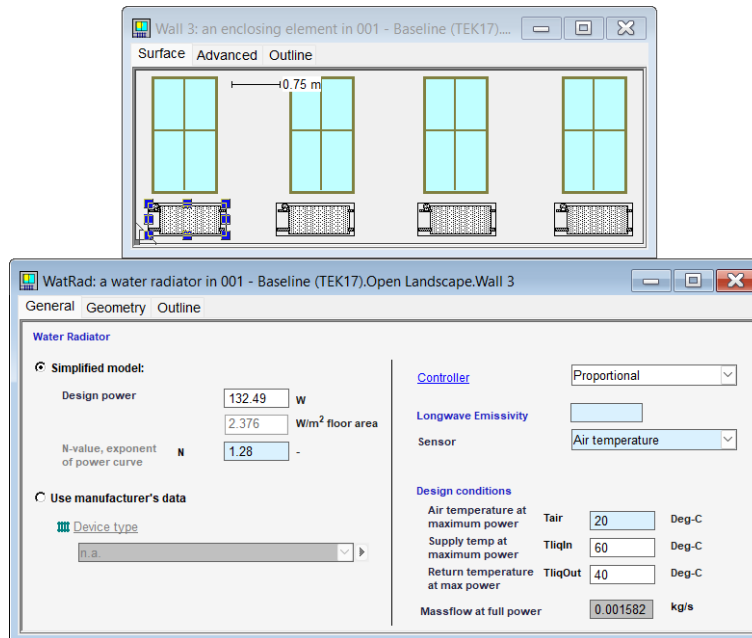


Figure 19: Input data for radiators in Open Landscape

4.6 Simulations

4.6.1 Simulation Overview

The changes made between each simulation in IDA ICE, for both TEK17 and PH cases, are listed below. As stated earlier, the construction of the cases remained unchanged with regard to the steps below. The first four simulations are conducted with an electric boiler (limited power of 3.836 kW), while Simulation 5 is conducted with DH (power of boiler set to 100 kW). The two case models are referred to with their primary identifiers TEK17 and PH for TEK17 and PH worthy building envelopes, respectively, while the simulation is specified by the suffix SX, where X is the number of the simulation (e.g. TEK17-S3). The simulations are described in further detail in their respective sections over the following pages.

- **Simulation 1: Reference simulation**

The plant was generated according to the previously stated input data, and simulations were run to gather data regarding the heating process of the baseline building.

- **Simulation 2: Temporary shutdown of boiler**

The effects of only turning off the boiler in the plant for 3 hours in the period between 6:00 and 9:00 in the morning, without changing any other aspects of the heating, were investigated.

- **Simulation 3: Temporary shutdown of boiler + Preheating of HotTank (70 °C)**

Preheating of HotTank was evaluated between 3:00 and 6:00 in the morning as a means of load shifting away from 3 hour peak period (6:00-9:00), during which the boiler would be turned off.

- **Simulation 4: Temporary shutdown of boiler & zone pump + Preheating of HotTank (70 °C) + Increased setpoint for supply air during shutdown**

An attempt to redirect all the accumulated thermal energy in the HotTank to the AHU during the shutdown period (6:00-9:00), while the AHU supply air setpoint is increased to match the setpoint for the zone heating (21 °C).

- **Simulation 5: District Heating enabled. Temporary shutdown of boiler & zone pump + preheating of HotTank (70, 80 & 90 °C) + Increased setpoint for supply air during shutdown & preheating phase**

Similar to Simulation 4, albeit with preheating of air and more power available through a connection to a DHN.

4.6.2 Simulation 1

After having designed the TEK17 and PH buildings and adapted the ESBO plant to the theme of the thesis, reference simulations were run to establish a baseline for the two cases through the "custom simulation" option in IDA ICE. Apart from the data given in Table 1 for TEK17 and PH, all aspects of the two cases were identical. This also includes the mistake in utilizing the initial design value of 3,836 kW for the boiler in the ESBO plant, which should not be a significant problem for this simulation, since both the TEK17 and PH cases should only use the required power during operation. For the TEK17 case this power is around 3.6 kW, as previously stated.

In this simulation, the schedule for boiler operation (A in Figure 20) was set to the existing "Always On" schedule that is available in IDA ICE (see Figure 21 a), which would output a constant value of 1 to the boiler, ensuring that the boiler would operate under MODE 1 - "normal regime" (see Section 4.3) for all days in the simulation. The boiler operates in this mode by default, but the schedule was added from the beginning to ensure that all connections between components remain unchanged between simulations.

The schedule in the custom HotTank setpoint controller (B in Figure 20) was set to the existing "Always Off" schedule (see Figure 21 b), which yields a constant output of 0, which would prioritize the lower input of the switch (C in Figure 20) in the controller, hence maintaining a constant setpoint of 60 °C for the PI controller and 70 °C for the boiler throughout the simulation period. Given that both the AHU and zone heating request a supply temperature of 60 °C from the HotTank, the HotTank would use this value as the setpoint for the top layer by default. This setpoint would also be connected to the ADDER block of the boiler setpoint and the PI controller by default. Although the same setpoint was used in Simulation 1, the default connections to the ADDER block and PI controller were replaced in favor of the aforementioned custom controller for the same reason as for the boiler operation schedule.

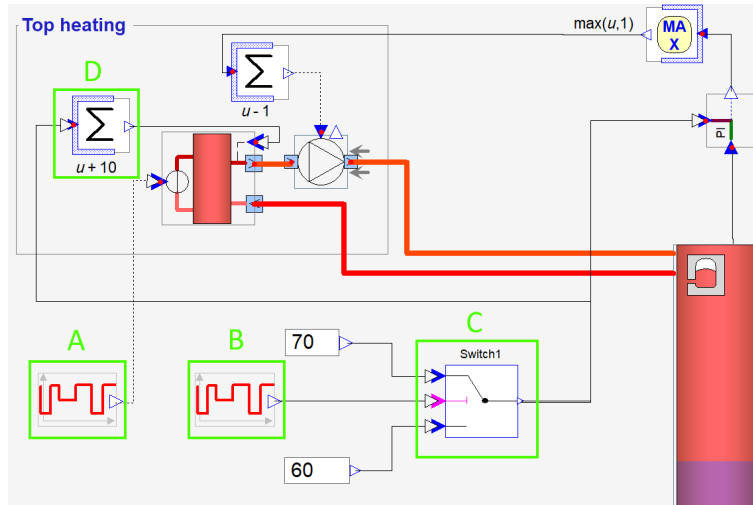


Figure 20: Connection of schedules and setpoints in ESBO plant for Simulation 1

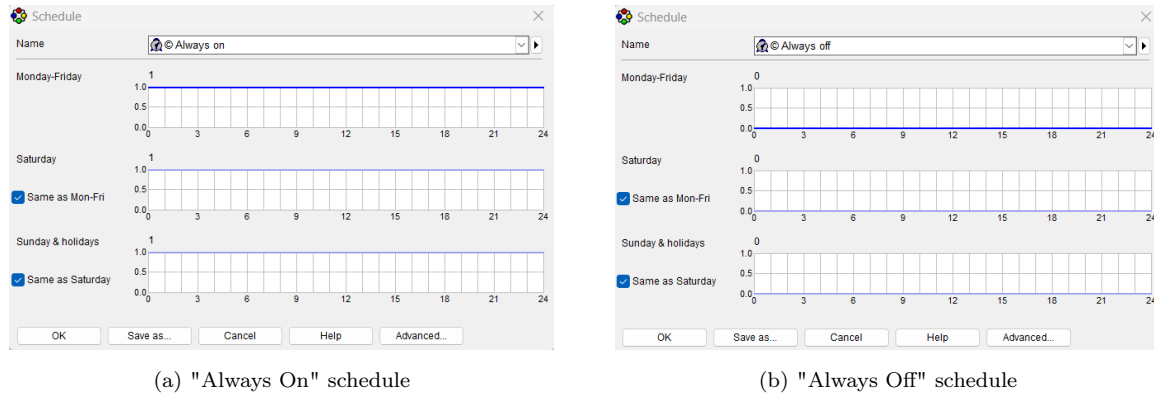


Figure 21: Existing schedules in IDA ICE

4.6.3 Simulation 2

Simulation 2 was performed to find out whether thermal comfort could be maintained throughout a 3 hour period in the morning, during which the boiler would be forced to shut down completely while the AHU and zone heating would continue to operate with the heat that was left in the HotTank. The idea was for the hot water in the HotTank, symbolizing the water volume in the piping network, to be used to maintain the heat supply to the AHU heating and radiators. The three hour period between 6:00 and 9:00 was selected based on several factors. In addition to the trends in electricity spot price and the article by Arteconi et al. [84], which showed promising results for the same duration, the minimal temperature from the climate file, and consequently the maximum power demand for the thesis, occurred during this period on January 17th. The price shown in Figure 22 is the actual electricity spot price [NOK/kWh] for South-East Norway (NO1) on January 17th 2023 according to the Norwegian Consumer Council (Norwegian: *Forbrukerrådet*) [95]. Clearly, the chosen period constitutes a typical morning power peak, with another peak occurring around 17:00.

Figure 22: Spot price for South-East Norway (NO1) 17th January 2023 according to the Norwegian Consumer Council

The boiler was shut down by changing the schedule for boiler operation (A in Figure 20) from "Always On" to the custom schedule shown in Figure 23. Note that the shutdown does not apply to weekends, as energy prices tend to be lower. Furthermore, it is not necessary to maintain the same level of thermal comfort on the weekends, given the absence of occupants in the office, thereby making an analysis for these two days redundant.

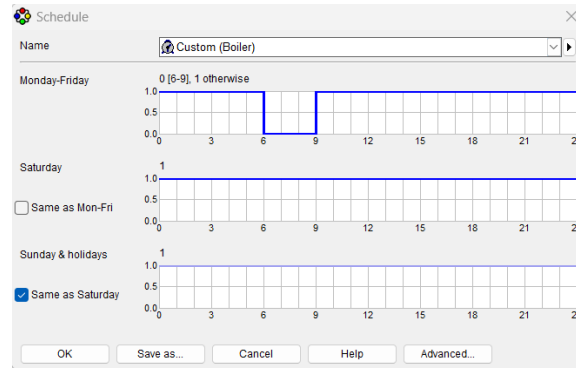


Figure 23: Schedule that shuts off boiler operation between 6:00 and 9:00

4.6.4 Simulation 3

Simulation 3 consisted of preheating the HotTank during the three hours (3:00-6:00) preceding the shutdown period (6:00-9:00). The idea was to create a surplus of energy with regard to the heating load simulation during these three hours, so that the AHU and zone heating circuits have more heat to extract during the shutdown period. In IDA ICE this was performed by increasing the temperature setpoint for the custom boiler and PI controller by 10 °C. For a realistic storage tank, the top layer temperature could be raised even higher, with the supply temperature to the AHU and zone being adjusted through regulation of the water flow rate or a three-way valve. However, in a piping network that does not consider a storage tank, the heat that is supplied by the heating technology will be the supply temperature for the entire main distribution circuit, increasing the risk of a high return temperature. With regard to the secondary circuits for the AHU and zone heating, the delivered power could be flow rate-regulated to negate the high return temperature on the primary circuit. Nonetheless, any evaluations regarding the simulations in this thesis must be done according to the response from the software.

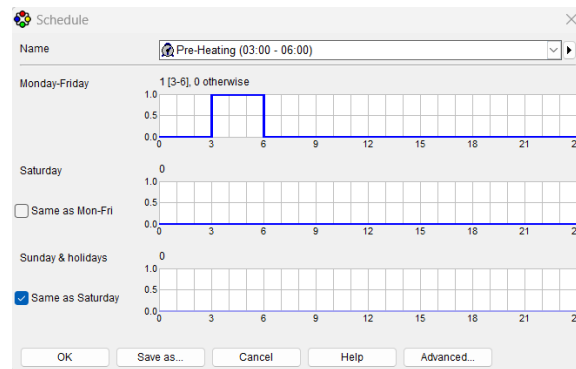


Figure 24: Schedule that increases setpoint between 3:00 and 6:00

4.6.5 Simulation 4

For simulation 4, in addition to the boiler, the pump for the zone heating was also shut off, while the temperature setpoint for the supply air was increased from 19 to 21 °C for the shutdown period. The idea was to redirect all the available energy from the HotTank to the ventilation air in an attempt to maintain thermal comfort. Initially, this was based on the assumption that it would take less energy to heat the air directly via the heating coil in the AHU than if the radiators were to be used, as they require more heat to heat up the radiator itself before they begin to heat up the space. While this would be accurate for a reheating phase after for example a night setback schedule, for this thesis that would not be the case. Nonetheless, it is interesting to see what results can be achieved in the entire heating system when allowing the radiators to radiate whatever energy is left at the beginning of the shutdown, while simultaneously prioritizing the supply air for the entire shutdown period. The zone heating circuit was shut off by connecting the schedule for the boiler operation to the zone heating pump, as shown with a green line in Figure 25.

The schedule that was part of the custom AHU setpoint control presented in Figure 18 under Section 4.4 was modified similarly to the one shown in Figure 24, but with the increased setpoint between 6:00 and 9:00 rather than 3:00 and 6:00, as can be seen in Figure 26 (a).

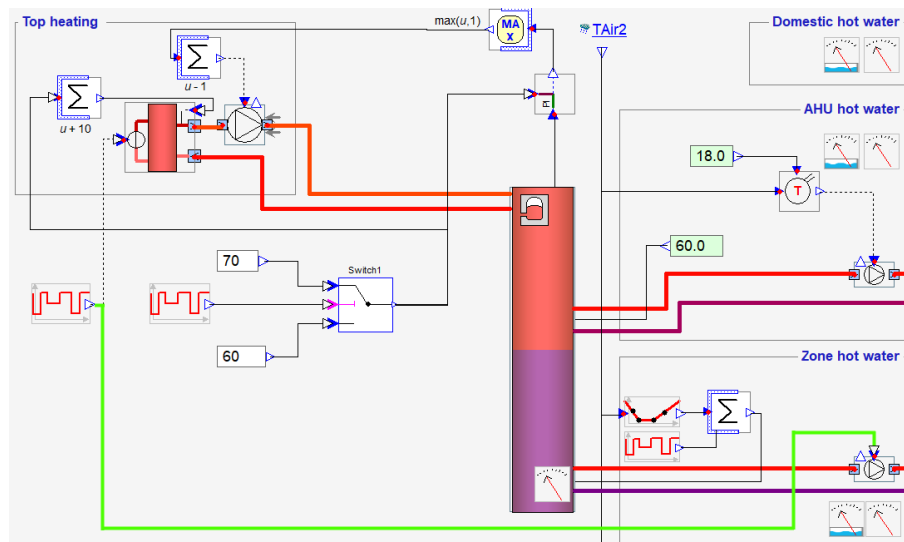


Figure 25: Energy plant showing connection (green line) between boiler operation schedule and zone pump

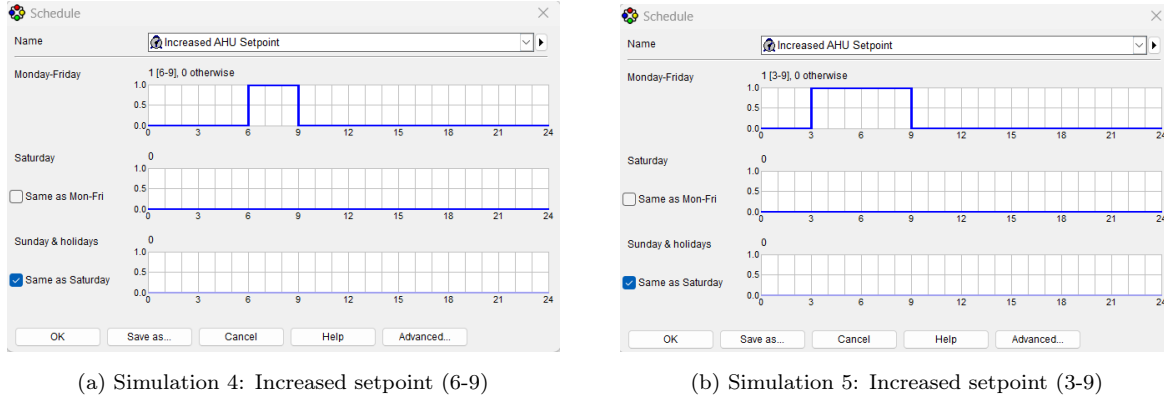


Figure 26: Schedules for increased supply air temperature setpoint for AHU

4.6.6 Simulation 5

Simulation 5 is similar to Simulation 4, albeit with a connection to a DHN supplying the heating power, and a longer duration of increased setpoint for supply air, from 6:00-9:00 to 3:00 to 9:00. The increase in setpoint temperature for the supply air was performed by altering the schedule in the custom AHU setpoint control to cover all six hours from 3:00 to 9:00, as can be seen in Figure 26 (b). The switch from electric boiler to DH was done by increasing the boiler's available power from 3.836 kW to 100 kW. The idea was to test several setpoint temperatures for the preheating of the HotTank, which could only be achieved with a higher power available. The temperatures that were investigated in detail were 70, 80, and 90 °C. Additionally, data for the boiler power consumption from an additional simulation with 100 °C was also included, but no further data was extracted, as there was not enough time available to further analyze this run to the same extent as the aforementioned simulations. For this reason it was also decided to only run the TEK17 case, as its less insulated building envelope was expected to give more prominent results than the PH case. The three main simulation runs are named 5A, 5B, and 5C to distinguish between their respective HotTank temperature setpoints of 70, 80, and 90 °C. Using the different preheating temperatures would make it possible to see how much power each of them requires, both for the preheating and in the reheating stage after the shutdown period.

4.7 Logged Data

In order to best present the results of the simulations, and lay a good foundation for the discussion of said results, a selection of output data from was logged as output graphs from IDA ICE. As the main focus is on maintaining thermal comfort in the selected zone, the main temperatures (mean air and operative temperatures) were logged alongside PPD. For this data, Monday-Friday (January 16th-20th) were the most interesting days, as these are the only days that the different simulations affected, and also the only days with occupants present. The supply air temperature and inflow of ventilation were also logged for the same days as the main temperatures. This data is mostly interesting with regard to Simulation 4 and Simulation 5, where air supply temperatures were altered. The energy balance in the room was logged for two days only, January 17th and 18th, as these two days represent the coldest day and a relatively normal January day, respectively, and because including more days would make it difficult to see the changes before, during and after shutdown periods for each day. The energy balance data for each simulation is available in the subsection corresponding to the

simulation under Section 5. Regarding the altered setpoints and schedules, and the response from IDA ICE to all the changes made, four sets of data were logged, with their main purpose being to verify the effect of the operations conducted in each simulation. The first set consisted of the signals to the boiler, the zone pump, and the AHU pump, as well as the MODE of the boiler as a comparison between the input from the schedule and the boiler's response. The second set simply shows the temperature setpoint for the boiler and PI controller. The third is the heating power output of the boiler, and the last shows the temperature setpoint of the supply air. Since one of the areas of focus in this thesis is the effect of the different simulation strategies on the entire system, four aspects were logged. These were the supply and return temperatures related to the three circuits; the boiler, AHU, and zone, in addition to the two layer temperatures in the HotTank. The last set of data are the mass flow rates of the main pump, AHU pump, and zone pump.

5 Results & Discussion

5.1 Simulation 1

Simulation 1 generally yields expected results, considering that these simulations were run using the design values from the heating load simulation. As can be seen in Figure 27, the operative temperature remains above 21 °C most of the time for the last three days, when the outdoor temperature never falls below -11 °C. For the two first days, however, the temperature falls down to 20.5 °C in the morning hours, which is also the coldest period for both days according to the data from the climate file (see Section 4.2.1). This discrepancy between the resulting temperature and the initial setpoint temperature of 21 °C could be due to some tolerance level in the model, but remains unknown for the time being. Naturally this is a point that would be worth looking into in the future, and in retrospect, it would also have been interesting to log data related to the individual radiators, to analyze whether they perform as expected.

The PPD remains below 8 % all week, with the last three days staying below 7 %. Although the operative temperature is not always above 21 °C, the PPD indicates that the indoor climate is sufficiently comfortable with regard to the thermal criteria.

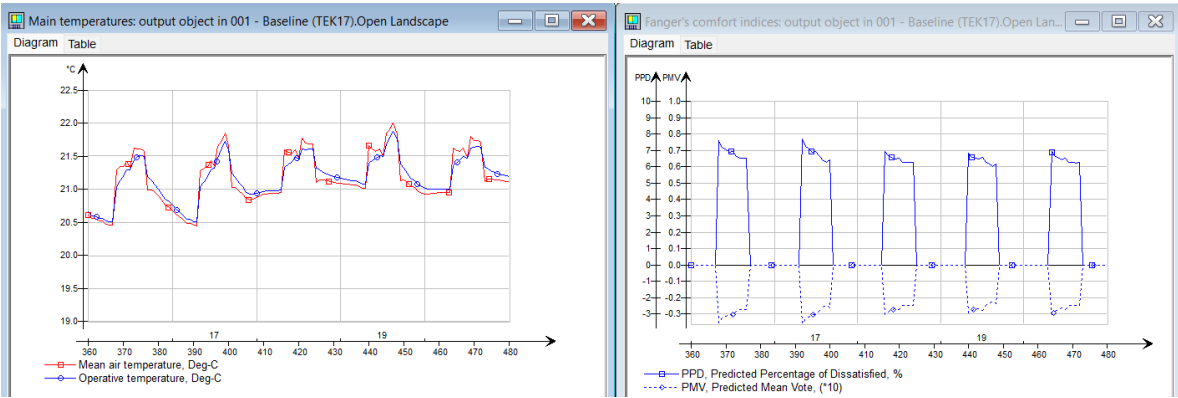


Figure 27: Main temperatures (left) and PPD (right) for TEK17 case after Simulation 1

For PH-S1 (see Figure 28), both main air temperature and operative temperature stay above 21 °C throughout the week, with the PPD staying at around 6 %, and never exceeding 7 %. The enhanced performance, in comparison to TEK17-S1, primarily stems from the improved building envelope. Although the boiler capacity remains unchanged from TEK17-S1, meaning that it is oversized with regard to the PH building envelope, it should not be fully utilized during the normal operation regime in PH-S1. It is assumed that this holds true, given that the heating system should only consume as much heat as is necessary, which is expected to be less than TEK17-S1. However, it is important to note that these simulations lack a real case building for direct comparison, and further simulations involving operational changes may introduce some margin of error in this aspect.

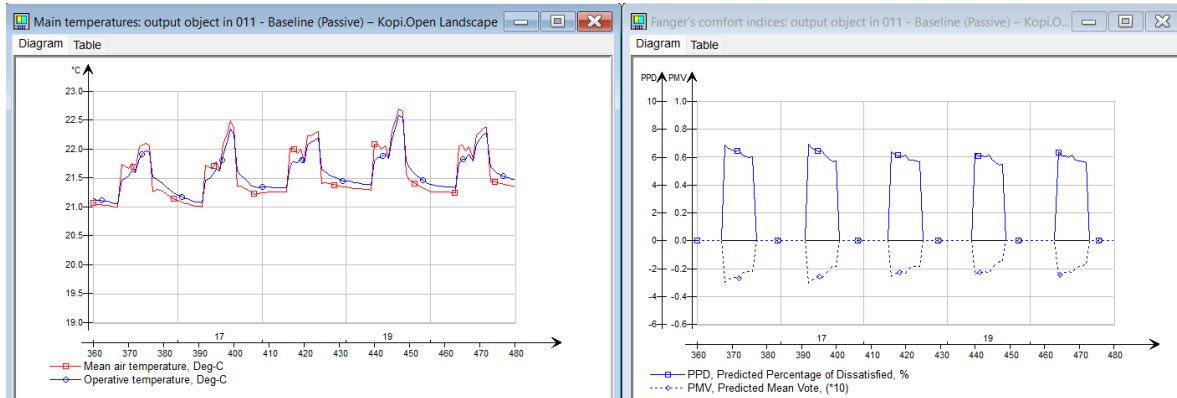
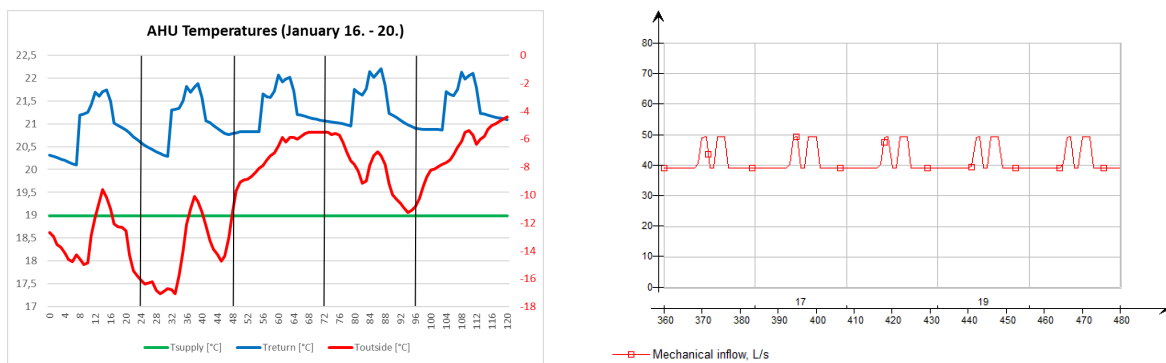


Figure 28: Main temperatures (left) and PPD (right) for PH case after Simulation 1

Figure 29 (a) shows the supply (green) and return (blue) air dry-bulb temperatures as well as outdoor mean air temperature (red) for the AHU in TEK17-S1, while Figure 29 (b) shows the mechanical inflow of air. It is clear that the supply air temperature remains at the design value of 19 °C, while the return temperature is the same as the mean air temperature in the zone. The inflow is adjusted between the setpoints of 0.7 and 2.0 L/(s*m²), and yields a pattern similar to that of the occupancy in the zone, highlighting the effect of using the Temperature + CO₂ control previously described in Section 4.4. The resulting minimum air flow rate is the minimum setpoint of 0.7 L/(s*m²) multiplied by the room area of 55.76 m², which yields an air flow rate of 39 L/s. The maximum flowrate stays at around 50 L/s, rather than the maximum possible value of 112 L/s.

For Simulation 2, Simulation 3, and PH-S1, the graphs described in the previous paragraph yield the same values for mechanical inflow, as well as supply and outdoor mean air temperature, with the return air temperature being the only varying value between cases. The latter output can be seen in the main temperature graph for the respective cases, while the graphs for AHU supply and return air temperatures and inflow are available in Appendix O. The outdoor temperature is only included in Figure 29 (a). For simulations that yield different results than the aforementioned, the graphs will be discussed in their respective sections.



(a) Supply & return temperatures for AHU, and outdoor mean air temperature

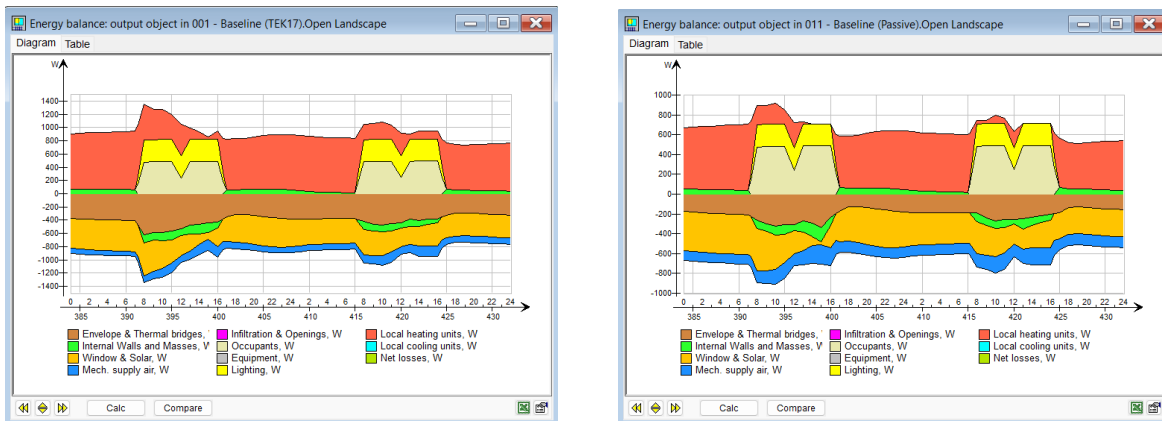
(b) Mechanical ventilation inflow in L/s

Figure 29: AHU temperatures

The energy balances for Simulation 1 over the dates of January 17th and 18th can be seen in Figure 30 for both TEK17-S1 (a) and PH-S1 (b). One of the most noticeable aspects in these graphs is the heating contribution resulting from the internal loads, i.e. occupants (beige) and lighting (yellow). These two loads follow their respective schedules, giving them their distinctive shape. The increased heat loss during the occupied hours can also be attributed to the increased difference in temperature, or energy, between the indoor and the outdoor spaces. This is in line with the second law of thermodynamics, which states that heat naturally flows from a point of high energy to a point of lower energy in a spontaneous attempt to achieve a thermal balance.

It should be noted that through their contribution of thermal energy to the space, the occupants are themselves being cooled down, emphasizing the importance of the local heating units (radiators, red) to maintain thermal comfort. The radiators provide the majority of the heat outside of working hours of occupants and lighting, while also contributing significantly in the early hours of January 17th for both cases. Because of the improved building envelope of PH-S1, the supplied heat from the radiators is lower than TEK17-S1 in general, peaking at just over 700 W before occupants arrive in the morning of January 17th, compared to around 900 W for the same period in TEK17-S1. Their supplied heat is lower on 18. January, as expected, and even goes down to zero in the afternoon of 18. January for PH-S1.

Regarding the heat losses that lead to an increased heating demand, the main culprits are the building envelope and the windows, both during and outside hours of occupant presence. The supply air, which is 3 °C below the heating setpoint of the zone, is also contributing to cooling down the space, although to a lesser extent than the heat lost through the aforementioned pathways of heat loss. During the occupied period, the internal walls and masses (green) absorb heat, which is then released outside of the occupied period.



(a) TEK17 case

(b) PH case

Figure 30: Energy balance from Simulation 1 for TEK17 case (a) and PH case (b)

Figure 31 shows control signals, setpoints, and boiler output from Simulation 1 for TEK17-S1. For further simulations, only the boiler output will be discussed, as the signal outputs and setpoints are included exclusively to verify that the changes made to the boiler and controllers in the plant and AHU result in a change in response from the HVAC systems. The remaining figures containing these graphs can be found in Appendix P.

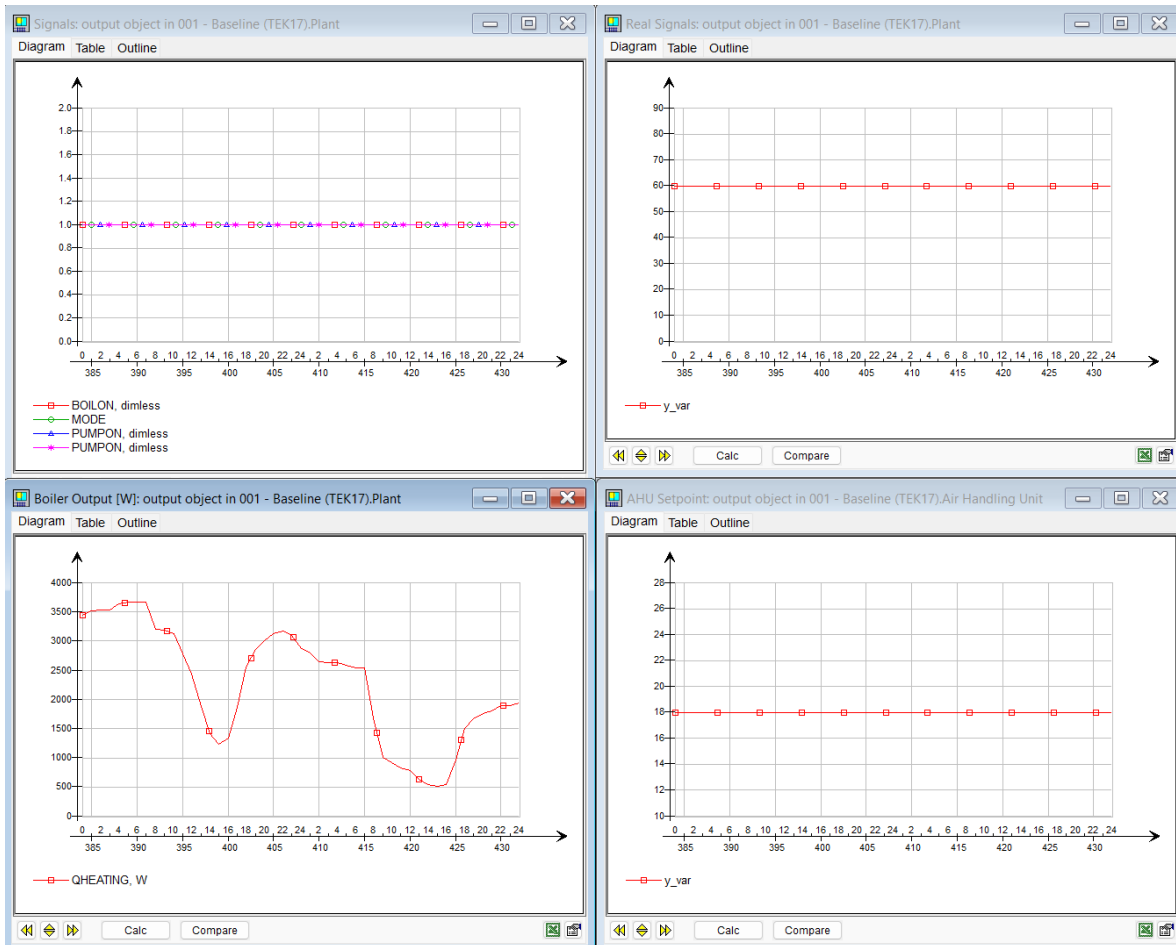


Figure 31: Signals and boiler output during January 17th & 18th from Simulation 1 for TEK17 case. From left to right, top to bottom: Control signals (Boiler + AHU & zone pumps) [-], Setpoint of boiler and PI controller [$^{\circ}\text{C}$], Boiler output [W], AHU controller SP [$^{\circ}\text{C}$] (Note that this is 1°C lower than resulting setpoint due to 1°C increase over supply fan).

The graph in the upper left corner shows the signal from the boiler operation schedule ("BOILON", red), the responding "MODE" of the boiler (green), the operation signal of the AHU pump ("PUMPON", blue), and the operation signal of the zone pump ("PUMPON", pink). Since none of the default signals have been changed for these components, they remain at a steady value of 1, indicating that the pumps are on and that the boiler is operating according to a "normal regime". From top to bottom of the right column, the setpoint temperatures for the boiler + PI controller and the AHU supply air, respectively, can be seen. These also remain unchanged, as there have not been made any changes in the reference simulation. The bottom left graph shows the boiler output in [W], and visualizes the difference in heating demand resulting from the varying outdoor temperature and occupant presence. The peak of just above 3.6 kW in the morning of January 17th is in line with the actual heating load simulation (see Section 4.3), and the decrease of around 1 kW in power demand for the same hour the following day further highlights daily variations in temperature. The dip in power output is the result of decreased demand during the hours that the occupants are present and lights are on, which is also the period with increasing outdoor air temperature (see Section 4.2.1), further reducing the heating demand.

Figure 32 shows the boiler output for PH-S1. While similar in the output pattern, the values for this case are lower than TEK17-S1. The power peak on the morning of January 17th sits just below 3.2 kW, and the minimum point on the afternoon of 18. January is as low as 300 W for this case, compared to just above 500 W for TEK17-S1. As previously assumed, the full capacity of the boiler is not utilized for the PH either, given the normal operation of the heating system.

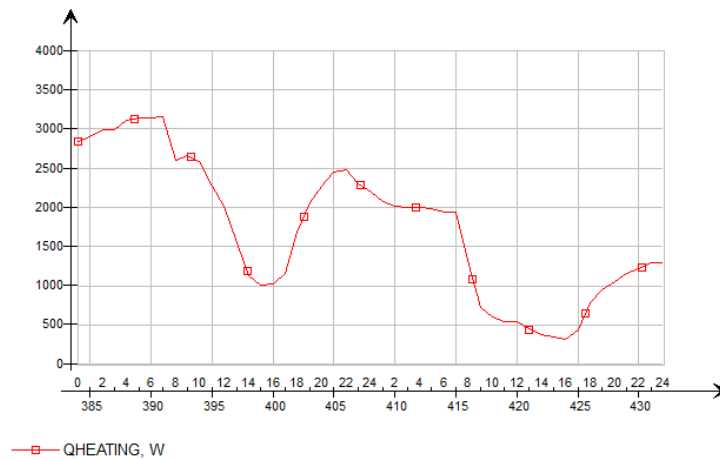


Figure 32: Boiler output [W] from Simulation 1 for PH case

Figure 33 contains data for the supply and return temperatures for the water-borne heating system, as well as the temperature of the two layers in the HotTank for TEK17-S1.

The upper left graph shows the supply (green) and return (red) temperatures from and to the boiler, respectively. The effect of the "ADDER" block that was described in Section 4.3 can also be seen, as the boiler maintains a constant supply temperature of 70 °C to the HotTank. The return temperature, however, varies throughout the day, with a peak in the afternoon. The return temperature being this high is worthy of critique, as the boiler circuit ideally should be supplied with a lower return temperature from the bottom of the HotTank, the same way the return temperature in a realistic circuit should be significantly lower. Simulation errors after attempting to change the height of the return pipe connection to the HotTank, as well as lacking information on how the connections operate, left no choice but to leave the connections unchanged for the simulations.

The graph in the top right corner shows the temperature in the HotTank. The green line is the top layer, and the red line is the bottom layer. The bottom layer temperature remains between 30 and 40 °C throughout the entire period, while the top layer fluctuates a lot more, between around 55 to 67 °C. The increase during the day could be caused by the reduced heating demand that results from the presence of internal loads, which allows the temperature in the tank to get closer to the setpoint of 60 °C. The temperature does, however, increase to above 60 °C for at least a short period every day. It is not unthinkable that the temperature is between 60 and 70 °C due to these values being the setpoints of the HotTank and supply from boiler, respectively. Nonetheless, this raises some questions regarding the actual operation of the default IDA ICE design of the boiler + main pump + PI controller combination. Despite this, one aspect of this thesis surrounds the changes in the heating system as different simulations are run, which means that there is still valuable information to be obtained from comparing the different simulations, despite the many shortcomings of IDA ICE and the available information surrounding the software.

The bottom left graph shows the supply (green) and return (red) temperatures of the AHU circuit. This circuit shows the most stable temperature difference between supply and return, with the return being a constant 20 °C lower than the supply. This corresponds to the settings of the heating coil in the AHU, which is set to ensure a temperature drop of 20 °C for the heating liquid by default. The colder first two days require more heat to maintain a stable supply air temperature of 19 °C, hence the drop in temperature in the morning hours on these days. For the following three days the temperatures are relatively stable around design values.

The last graph, in the bottom right corner, shows the supply and return temperatures of the zone heating circuit connected to the radiators. The supply temperature (green) follows the same values as the supply temperature of the AHU circuit. The return temperature, however, decreases during the day, when there are occupants present. Initially, this appears very odd, considering that the radiators give off less heat when there are occupants present. However, this must be viewed in connection to the mass flow rate of the circuit, as described later in this section.

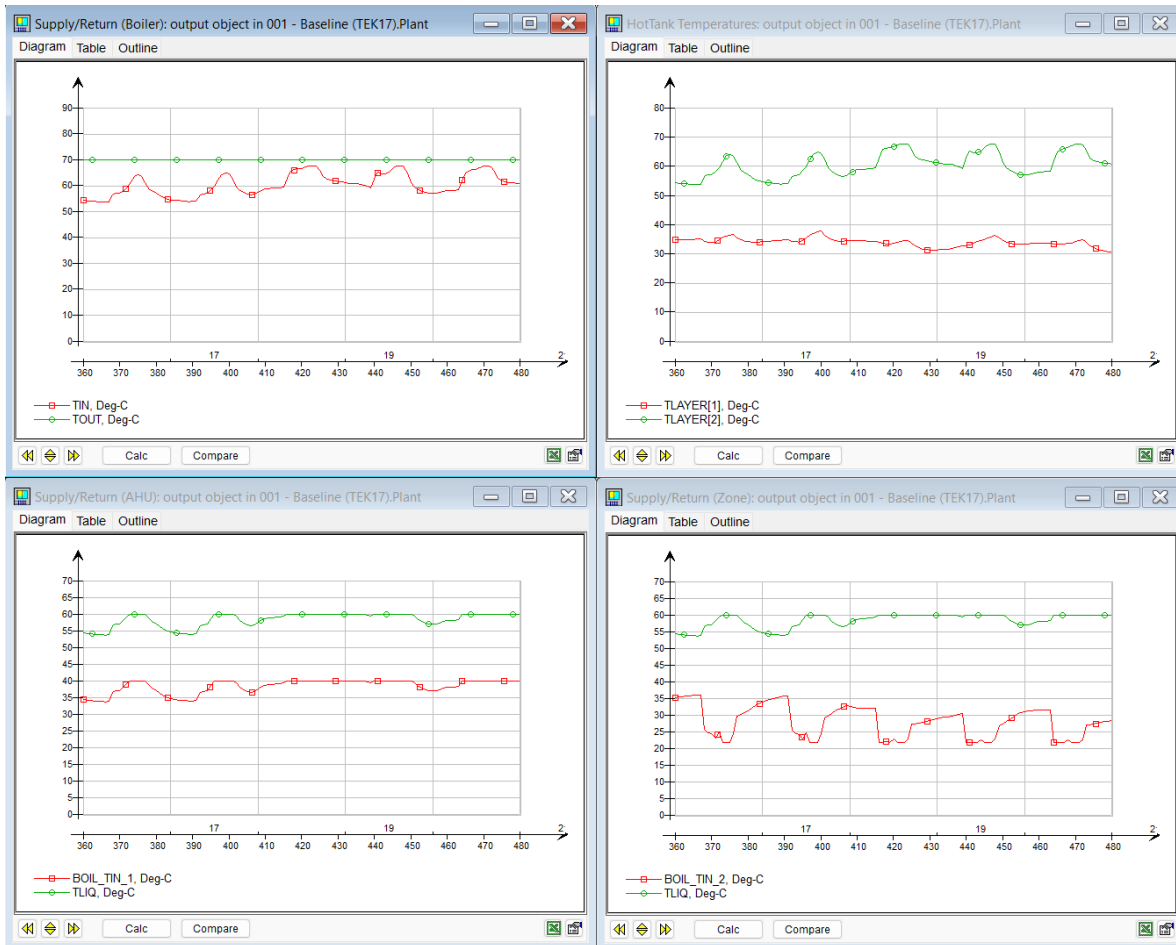


Figure 33: TEK17 case - Simulation 1. From left to right, top to bottom: Supply/Return temperatures for boiler circuit, Temperature of top and bottom layer of HotTank, Supply/Return temperatures for AHU circuit, Supply/Return temperatures for Zone heating circuit

Figure 34 shows the same data as the previous figure, but for PH-S1. The main difference between the two cases is that PH-S1 has less fluctuating temperatures for the bottom HotTank layer (top right graph) and the zone return (bottom right graph). The AHU temperatures remain unchanged, as expected, considering that they are not affected by the building envelope, but rather related to the outdoor air temperature and supply air setpoint temperature, which are being handled by the same AHU as in TEK17-S1, and where the latter is controlled using the same setpoint as TEK17-S1.

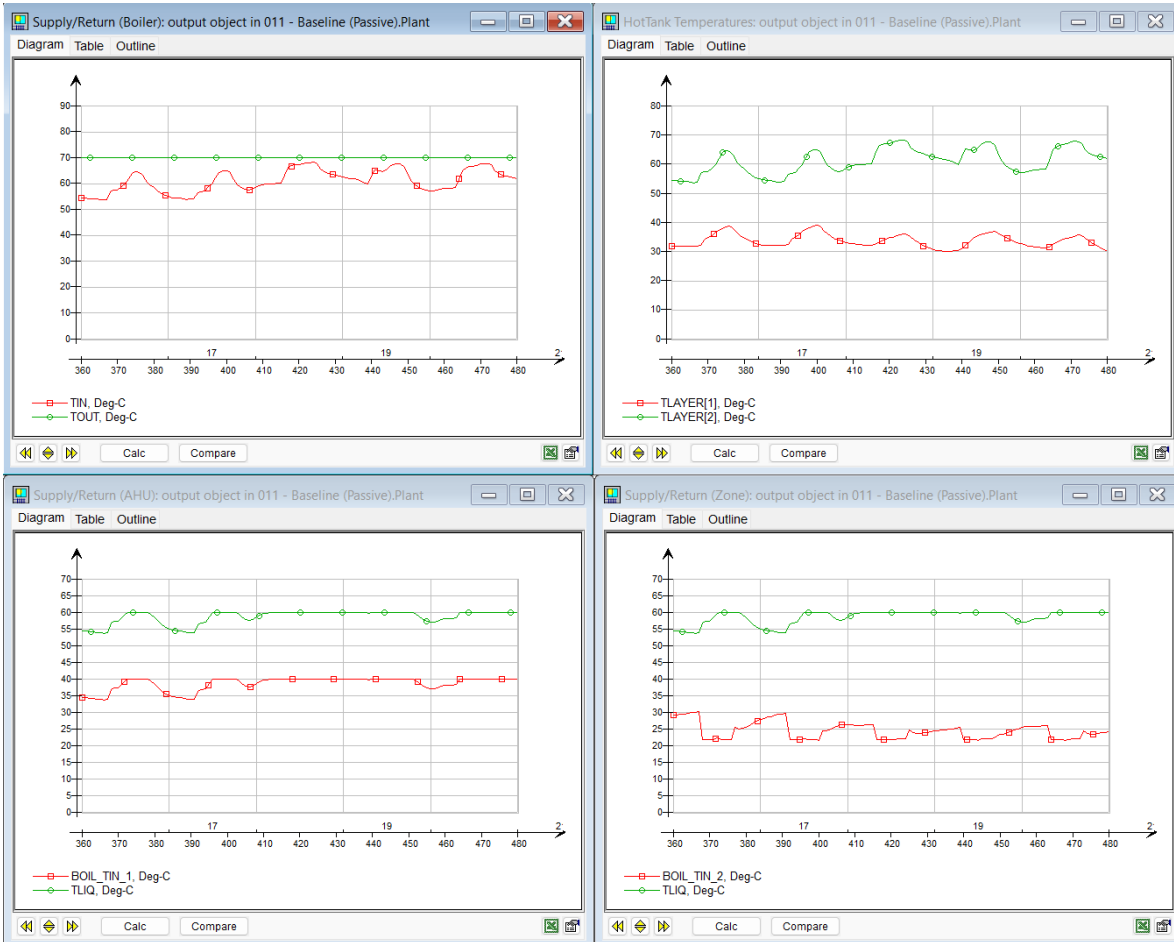


Figure 34: PH case - Simulation 1. From left to right, top to bottom: Supply/Return temperatures for boiler circuit, Temperature of top and bottom layer of HotTank, Supply/Return temperatures for AHU circuit, Supply/Return temperatures for Zone heating circuit

Figure 35 shows the mass flow rates for the boiler circuit (top), AHU circuit (bottom left), and zone circuit (bottom right) for TEK17-S1. The main pump appears to maintain a somewhat stable output throughout the week, with a slight increase during the working days, which could be correlated to both the colder outdoor temperature increasing the heating demand, as well as the presence of occupants increasing the air volume that needs to be heated in the AHU. The AHU graph further strengthens these claims, as there is a clear increase in flow rate in the morning of the first two, colder days. As for the mass flow rate of the zone heating, there is a clear increase early in the morning, especially for the two colder days, with a significant decrease once occupants are present in the zone. The decrease in flow rate correlates to the increased difference between supply and return temperatures that was reported for the corresponding set of supply/return temperature graphs for this circuit. This response follows Equation 2 below, which highlights how a reduction in heat demand, symbolized by rate of heat transferred to the room (\dot{Q} [W]), entails a reduction in mass flow rate (\dot{m} [kg/s]) when the (c_p [J/(kg*°C)]) and the temperature difference (ΔT [°C]) between supply and return temperatures are constant.

$$\dot{Q} = \dot{m} * c_p * \Delta T \quad (2)$$

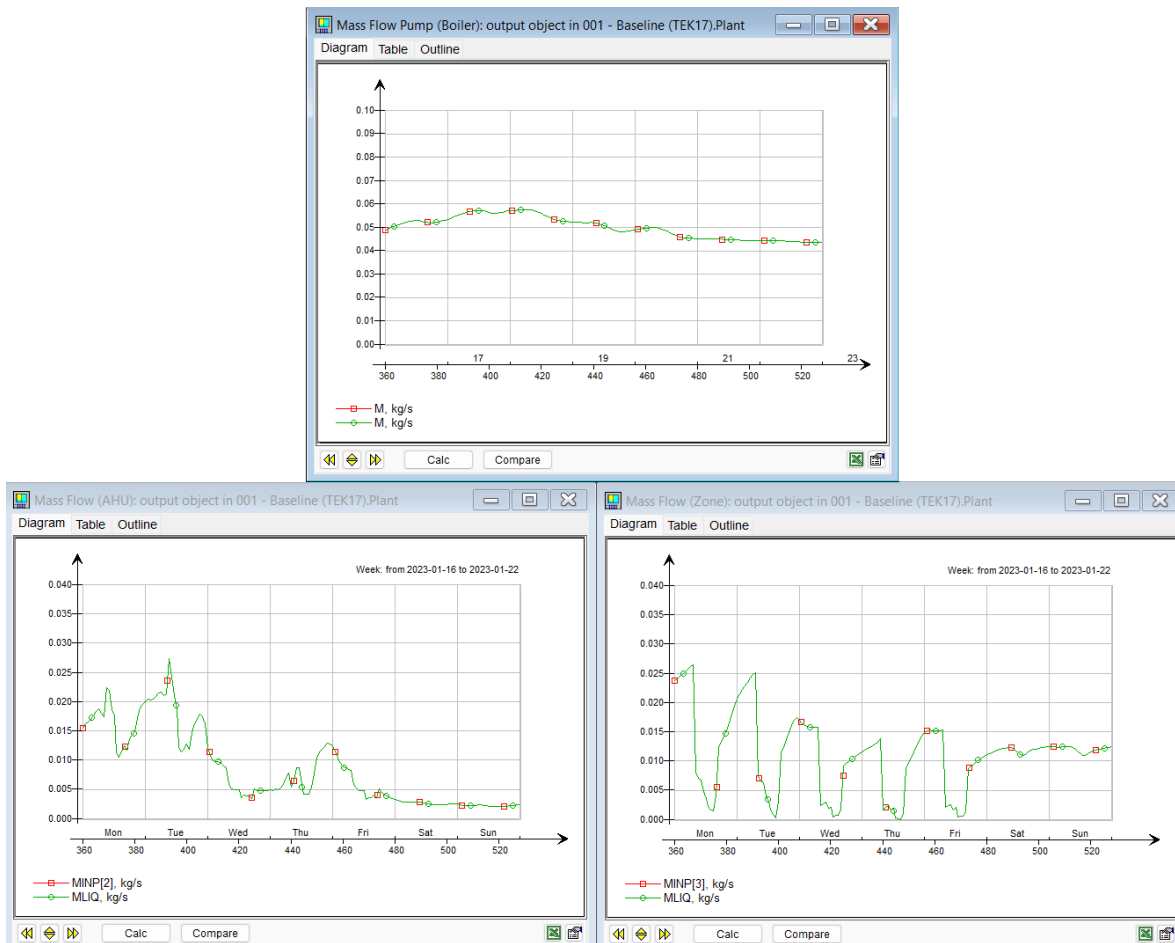


Figure 35: Mass flow rates for TEK17 case - Simulation 1. From top to bottom, left to right: Mass flow of main pump, mass flow of AHU pump, mass flow of zone pump

Figure 36 contains the mass flow rates for the boiler circuit (top), AHU circuit (bottom left), and zone circuit (bottom right) for PH-S1. The main pump follows the same pattern as TEK17-S1, albeit with lower flow rates overall. As with the supply and return temperatures, the mass flow rate for the AHU remains unchanged from TEK17-S1, as it is not affected by the improvement in building envelope properties. The zone heating flow rate, however, is nearly cut in half compared to TEK17-S1. The peak on January 17th, marked as "Tue" for Tuesday above the x axis of the graph, is reduced from 0.025 to around 0.013 kg/s. Furthermore, the minimal flow rate for the zone heating reaches zero for varying durations on all working days, even on the coldest days. This reduction can be directly correlated to the reduced heating demand both outside of and during working hours, which itself is the result of the improved characteristics of a PH compared to more common TEK17 constructions. With no mass flow through the zone circuit for a considerable duration, the internal loads cover the vast majority of the heating demand for the given period.

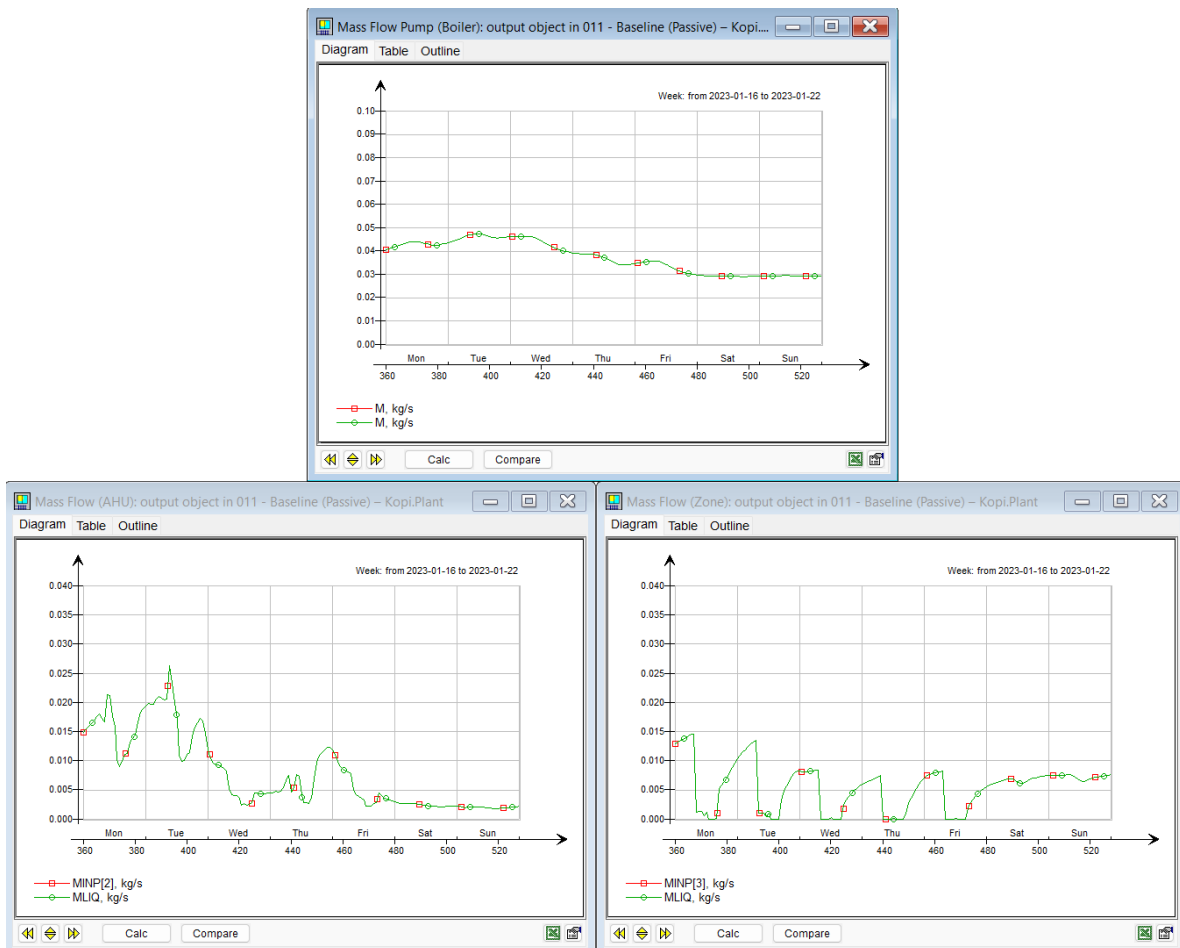


Figure 36: Mass flow rates for PH case - Simulation 1. From top to bottom, left to right: Mass flow of main pump, mass flow of AHU pump, mass flow of zone pump

5.2 Simulation 2

Figure 37 shows the main temperatures (left) and PPD (right) for TEK17-S2, while Figure 38 shows the same data for PH-S2. In both cases, the temperature falls after the boiler is shut off. TEK17-S2, however, shows a significantly steeper drop than PH-S2. While TEK17-S2 drops by 0.5 °C down to 20 °C on January 17th, PH-S2 only drops by 0.2 °C down to 20.8 °C. The temperature drops on the three following days are even less pronounced for PH-S2, staying above 21 °C for all three days. TEK17-S2 also sees similar relative improvement for the three last days, but dips below 21 °C nonetheless. These results can be compared to the results achieved in an experiment by Arteconi et al. [84], who also found that such a shutdown of three hours could maintain temperatures above 20 °C most of the time. The similarities are, in part, due to both their experiment and this simulation utilizing a form of TES, even though it is supposed to symbolize the piping network in the simulations of this thesis.

Although both TEK17-S2 and PH-S2 stay above the lower operative temperature limit of 20 °C, the PPD graphs show a noticeable difference between the two cases. The PPD values show a much clearer increase for the first three days in TEK17-S2, reaching higher than 9 % on January 17th, while for PH-S2 they remain between 7-8 % for the first two days, and even below 7 % starting from the third day. At the same time, the PPD does not reach the limit of 10 % in either case, indicating that the thermal comfort is maintained - at the very least on paper.

On the flip side, it could also be argued that TEK17-S2 already is in a precarious state during the first two days, even without the boiler being shut off. While the reduction in temperature down to 20 °C only appears as a point in the graph, the one hour time steps used for the IDA ICE simulations indicate that this temperature is maintained for around an hour. Given the many components and circuits that are affected by the changes made in Simulation 2, as well as the difference in perceived thermal comfort between men and women, which was pointed out in Section 2.1, one could most certainly expect some complaints regarding thermal discomfort from occupants - particularly the female ones. This negative effect could be further amplified by possible problems in an actual experiment that are not accounted for in this simulation.

With all these aspects in mind, for a duration of three hours, these results appear rather promising, particularly for PH-S2.

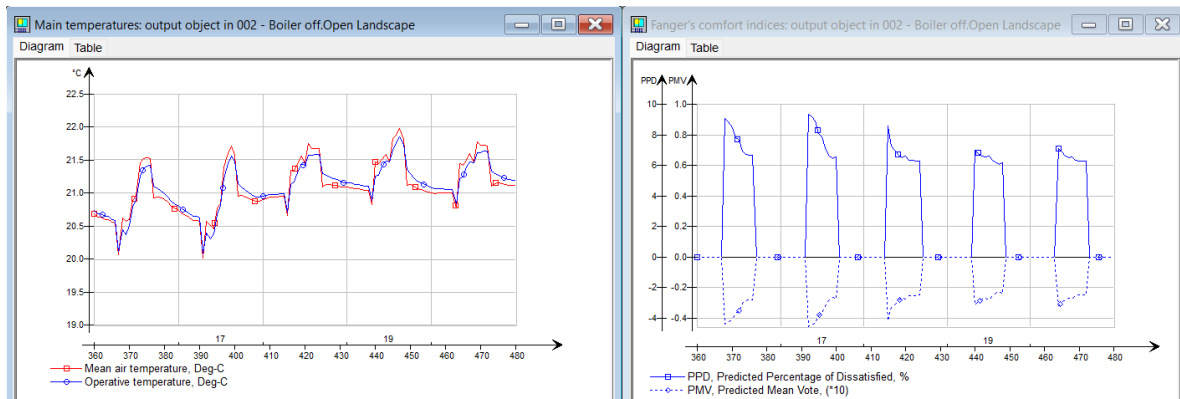


Figure 37: Main temperatures (left) and PPD (right) from Simulation 2 for TEK17 case

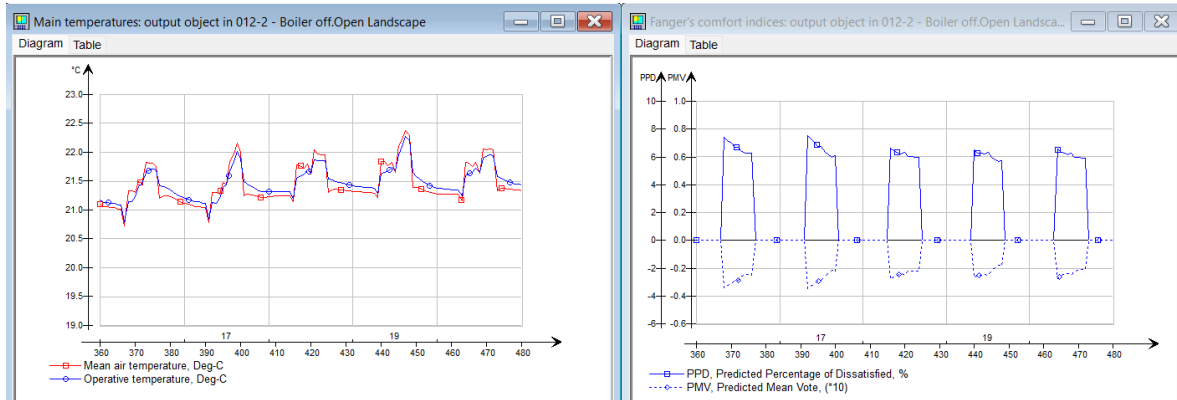
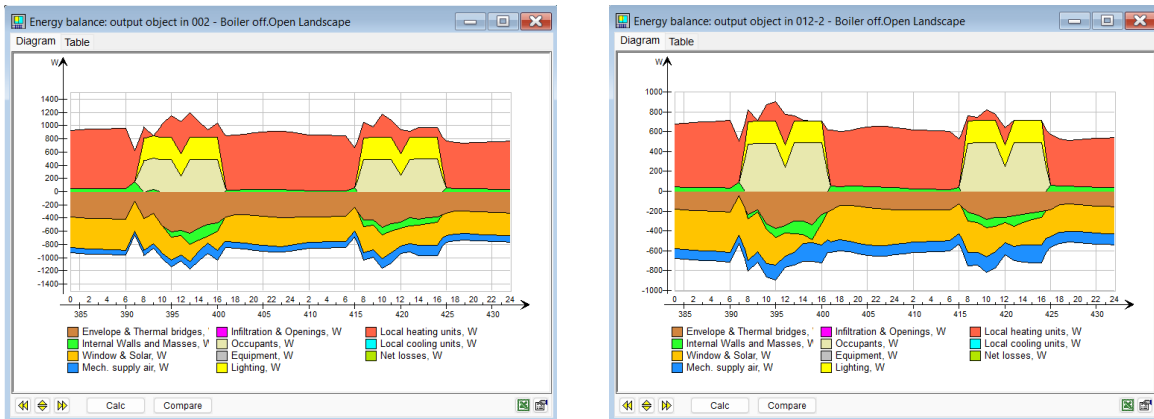


Figure 38: Main temperatures (left) and PPD (right) from Simulation 2 for PH case

Figure 39 shows the energy balances for TEK17-S2 (a) and PH-S2 (b) for January 17th and 18th. The reduction in supplied heat from the radiators can be seen in both cases for both days, and is, for January 17th, around 300 W for TEK17-S2, and 200 W for PH-S2. The reduction only makes up around a third of the emitted power prior to the shutdown period, indicating that there is still energy available for heating in the water volume. The internal walls and masses also provide more heat during the shutdown period than they did in the reference simulation. It appears that for both cases, the supplied heat from the radiators after the boiler is turned on again increases somewhat, followed by a quick drop, before it picks pack up again. While the initial increase can be explained by the radiators receiving more heat to reinstate the temperature setpoint, it is unclear why the output appears to oscillate in the following hours. One explanation could be the impact of the occupants' presence schedule. For January 18th, there is minimal change in the pattern when compared to Simulation 1, apart from the obvious reduction in delivered power from the radiators and the slight increase in heat from the internal walls and masses. The reduction is, naturally, less pronounced than on January 17th.



(a) TEK17 case

(b) PH case

Figure 39: Energy balance from Simulation 2 for TEK17 case (a) and PH case (b)

Figure 40 shows the boiler outputs for TEK17-S2 (a) and PH-S2 (b). While similar in pattern, there are two main differences between the two cases. First of all, for January 17th, TEK17-S2 requires the boiler to operate on maximum available boiler power of 3,836 kW to maintain thermal comfort, while PH-S2 utilizes less than 3,2 kW. Secondly, while both cases utilize the full capacity of the boiler after the shutdown period is over, on January 17th, PH-S2 maintains this for three hours compared to four hours for TEK17-S2. This one our difference also applies to January 18th. It is possible that if the boiler of the PH construction were also designed using its own heating load simulation, it would require a longer duration at maximum power to reach the setpoint temperatures in the system after a shutdown period.

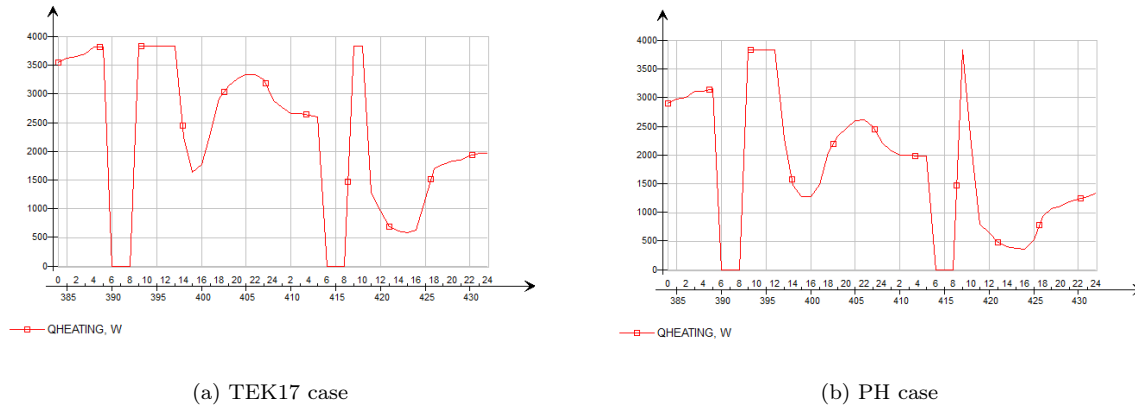


Figure 40: Boiler output for TEK17 case (a) and PH case (b) from Simulation 2

Figure 41 shows how the reduction in boiler power results in reduced temperature for all the water circuits. Since the main pump is still running when the boiler is off, and both the supply and return connections from the boiler to the HotTank are connected roughly at the same height, the supply and return temperatures for the boiler circuit (top left graph) essentially show how the HotTank temperature changes in the upper layer during the shutdown stage. It is clear that once the boiler is shut off, the supply and return temperatures become identical, as the water is simply being pumped in the circuit without any heat exchange taking place. Once the boiler is turned back on, both the supply and return temperatures increase closer to their previous states.

A similar response can be observed in the HotTank layer temperatures (top right graph) as well, with both temperatures decreasing during shutdown, and the top layer even surpassing the setpoint of 60 °C after the boiler is turned back on. Unlike the boiler circuit, however, there is a difference in the HotTank layer temperatures throughout the entire shutdown period, which is caused by the two layers being connected to either supply or return pipes for the AHU and zone circuits. It is also clear that the supply and return graphs decrease significantly more for both layers during the coldest two first days, reaching as low as 20 and 10 °C, respectively. For the last three days, the supply and return temperatures only sink to around 37 and 27 °C, respectively.

Between the AHU (bottom left) and zone heating (bottom right) circuits, the main difference is in the return temperatures. While the AHU still maintains the same 20 °C difference between supply and return, the zone heating circuit remains virtually unchanged from the reference simulation.

There are no major differences between PH-S2 and TEK17-S2, apart from the temperatures falling slightly less in general for PH-S2, and the return temperature for the zone circuit fluctuating less. Hence, the graphs for this case are designated to the appendix list under Appendix Q.

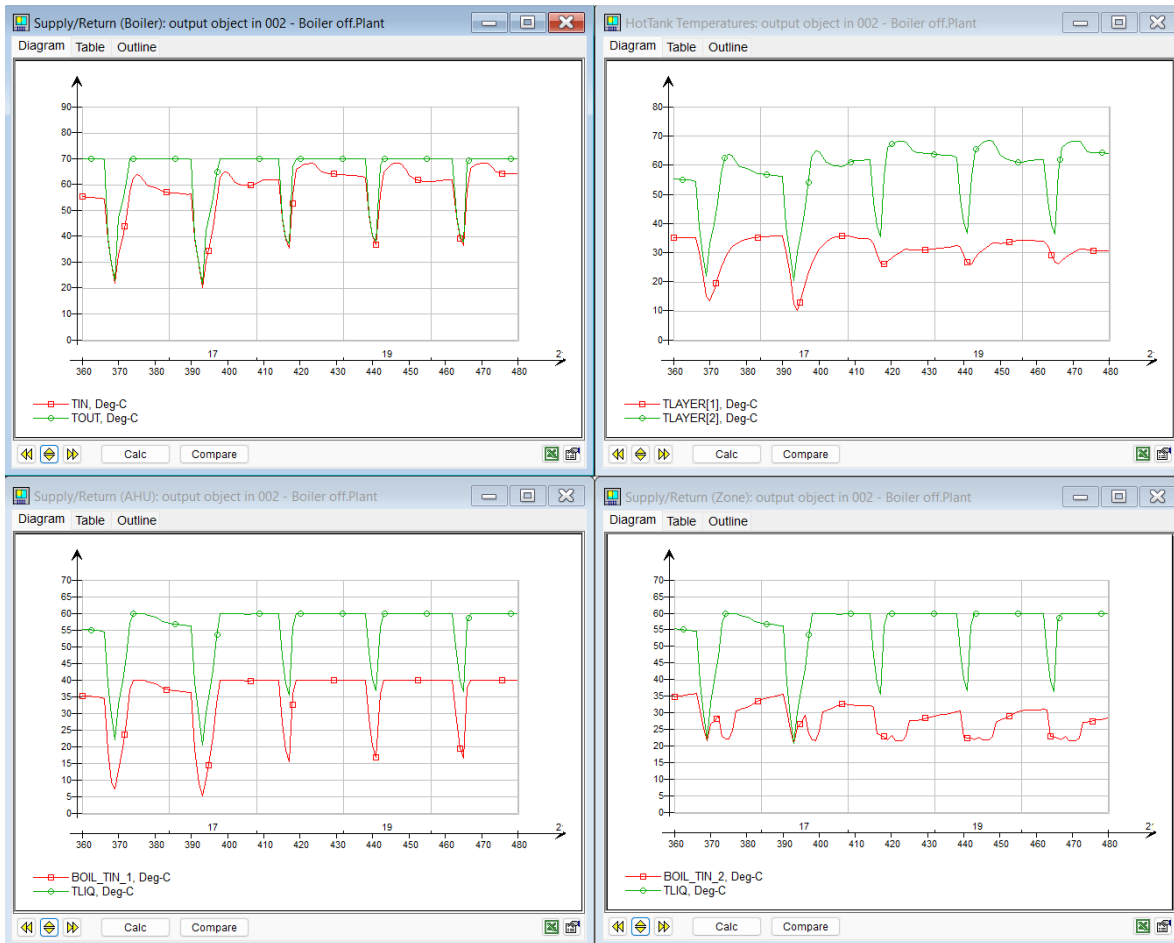


Figure 41: TEK17 case - Simulation 2. From left to right, top to bottom: Supply/Return temperatures for boiler circuit, Temperature of top and bottom layer of HotTank, Supply/Return temperatures for AHU circuit, Supply/Return temperatures for Zone heating circuit

Figure 42 shows the mass flow rates from TEK17-S2 for the boiler circuit (top), AHU circuit (bottom left), and the zone heating circuit (bottom right). The mass flow of the boiler circuit has increased from under 0.060 kg/s in TEK17-S1 to just above 0.080 kg/s in TEK17-S2. Additionally, the AHU mass flow peaks during the coldest first two days have increased noticeably, with the highest peak on January 17th going from 0.027 to 0.037 kg/s between TEK17-S1 and TEK17-S2. It is assumed that, with the supply temperature falling, as shown in Figure 41, the AHU must increase the flow rate to be able to heat up the below $-17\text{ }^{\circ}\text{C}$ outdoor air up to the setpoint of $19\text{ }^{\circ}\text{C}$. The same response of increasing the mass flow to supply enough heat can be seen for the zone heating circuit as well.

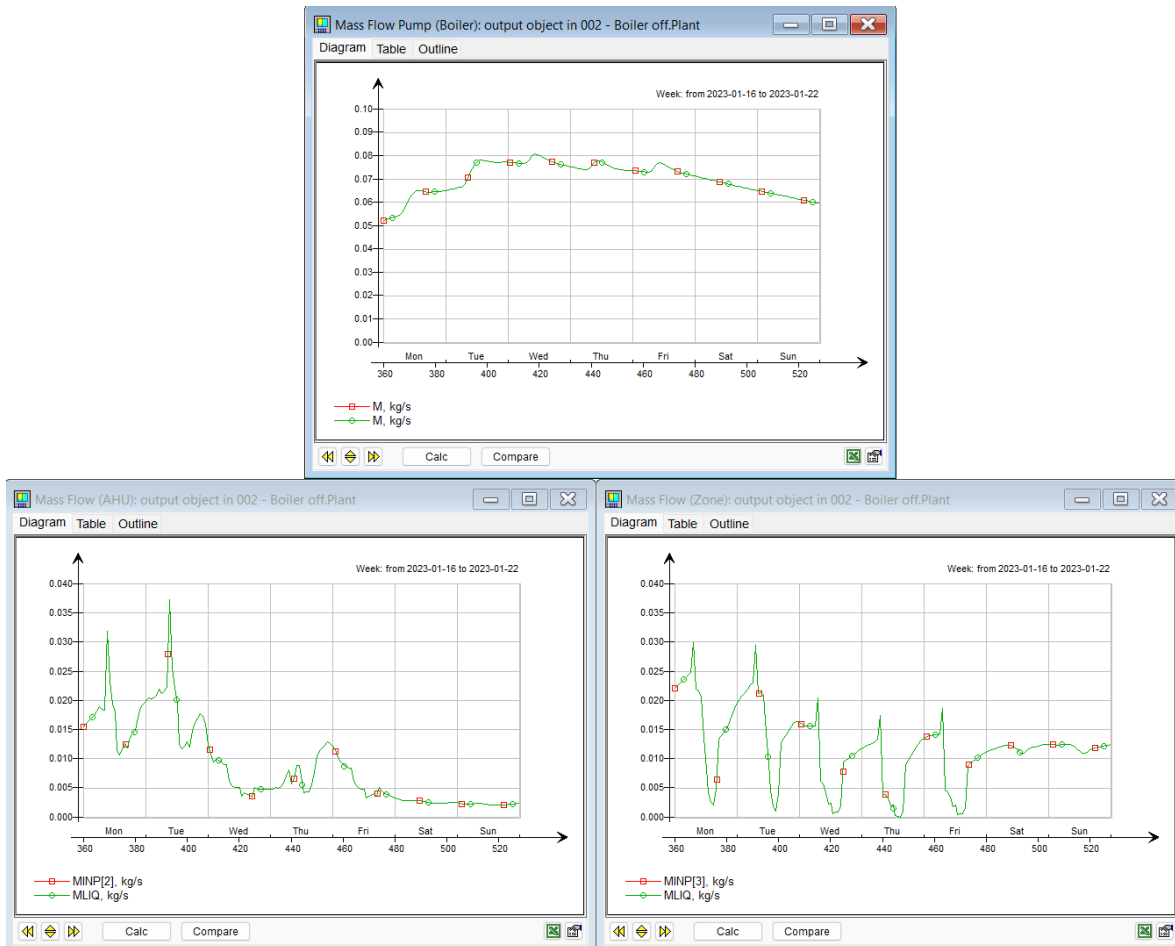


Figure 42: Mass flow rates for TEK17 case - Simulation 2. From top to bottom, left to right: Mass flow of main pump, mass flow of AHU pump, mass flow of zone pump

Figure 43 shows the same data as Figure 42, but for PH-S2. Compared to TEK17-S2, the mass flow rate of the boiler circuit for PH-S2 is lower, as was the case with the comparison between TEK17-S1 and PH-S1. Nonetheless, it increases somewhat, from a peak of 0.050 kg/s for PH-S1 to 0.065 kg/s for PH-S2. The AHU circuit peaks also increase somewhat, similarly as TEK17-S2, while the zone heating mass flow also develops new spikes in peaks in the shutdown period. Compared to PH-S1, in this simulation, the highest AHU circuit goes from 0.025 to 0.032 kg/s, while the zone circuit peak goes from 0.015 to 0.020 kg/s.

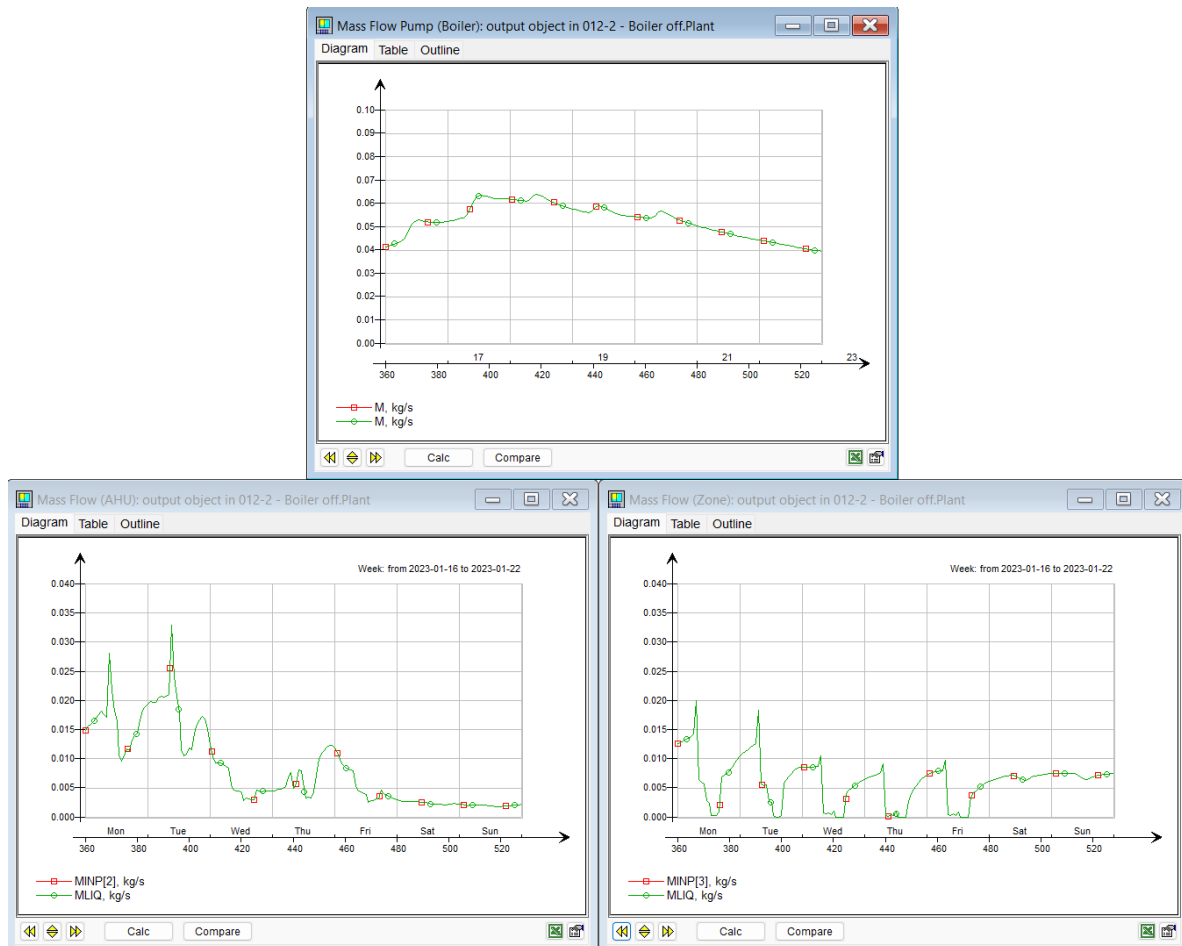


Figure 43: Mass flow rates for PH case - Simulation 2. From top to bottom, left to right: Mass flow of main pump, mass flow of AHU pump, mass flow of zone pump

5.3 Simulation 3

Figure 44 shows the main temperatures (left) and PPD (right) from TEK17-S3. Compared to TEK17-S2, the drop in both mean air temperature and operative temperature is slightly smaller, with the operative temperature minimum on January 17th going from reaching 20 °C to just above the temperature. For the last three days, the minima are all closer to the setpoint of 21 °C, indicating that this strategy is more suitable for days with less extreme negative temperatures. Practically speaking, however, all these changes are insignificant, as the PPD graph indicates. The only notable change is the reduction in the unexpected PPD peak that occurred in TEK17-S2 for January 18th, with the other four days remaining unchanged with regard to PPD.

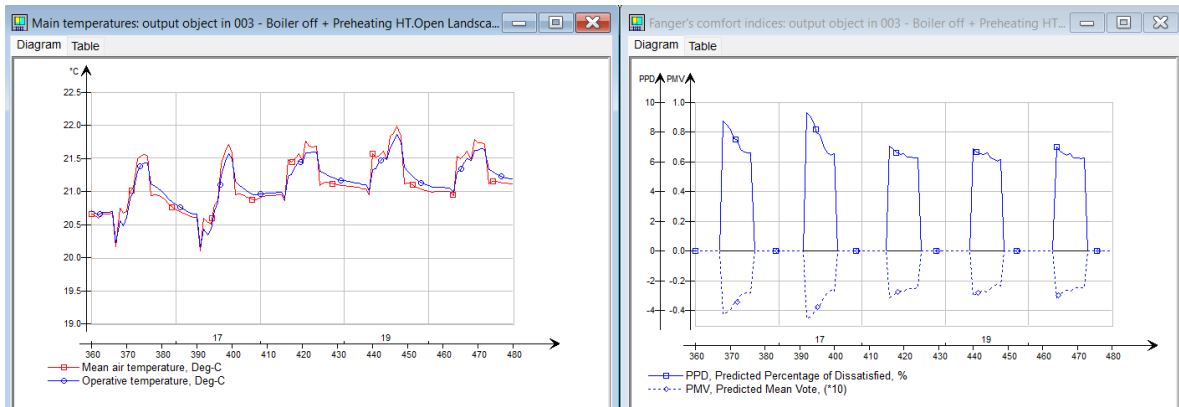


Figure 44: Main temperatures (left) and PPD (right) from Simulation 3 for TEK17 case

In Figure 45, the same data as Figure 44 is presented for PH-S3. Similarly to TEK17-S3, the only improvement compared to PH-S2 is the fact that the operative temperature minima for the two first days are raised back up to the setpoint of 21 °C.

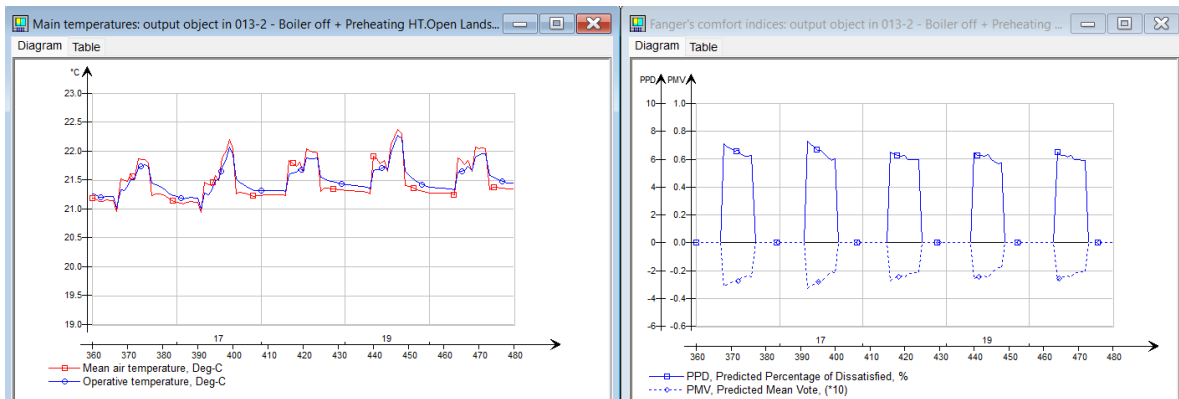


Figure 45: Main temperatures (left) and PPD (right) from Simulation 3 for PH case

It is important to point out that the amount of heat available during shutdown is not only dependent on the increased setpoint, but also the ability of the boiler to supply the temperature. Seeing how the boiler was designed to maintain thermal comfort with a specific maximum power and HotTank temperature setpoint, increasing the temperature setpoint without changing the available power is most likely the cause for the minimal improvement from TEK17-S2 to TEK17-S3. Nonetheless, for an electric boiler, there will be a maximum power available, and if it can not facilitate the current temperature increase of $10\text{ }^{\circ}\text{C}$, this is simply an unfit strategy for such a heating system. Ideally, the preheating strategy should be tested for a building connected to a DHN, where a higher power is available in the pre-preak hours in the morning.

In Figure 46, the energy balances for TEK17-S3 (a) and PH-S3 (b) can be seen. As with the main temperatures, there are minimal changes in this aspect for Simulation 3 compared to Simulation 2. For January 18th, the dip in power delivered by the radiators is mostly filled in for both cases, but January 17th shows no change.

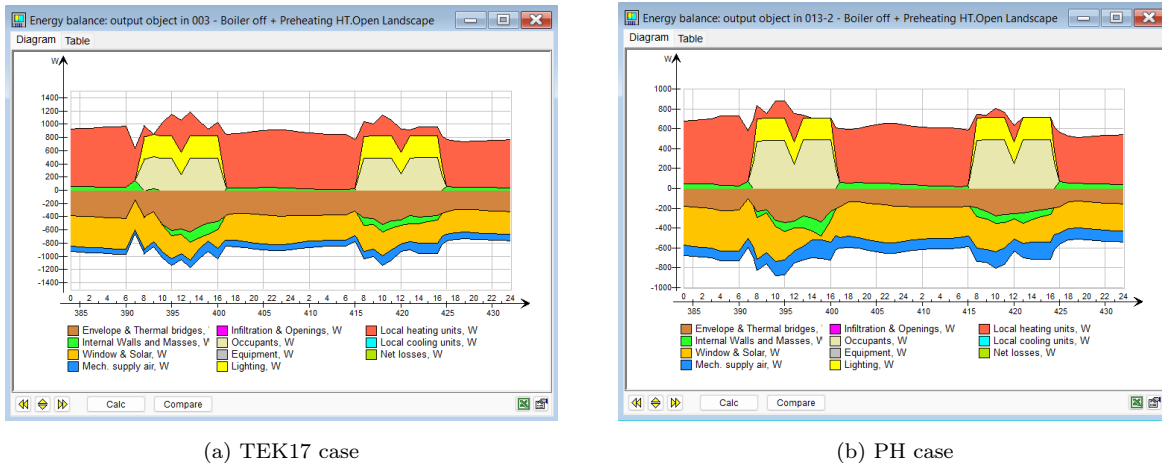


Figure 46: Energy balance from Simulation 3 for TEK17 case (a) and PH case (b)

Power output of the boiler for both TEK17-S3 (a) and PH-S3 (b) is presented in Figure 47. As expected, the power output is running on maximum both during the preheating stages, as well as in the reheating stage after shutdown, for both cases. January 17th yet again requires a longer duration to reach the setpoint temperatures in the HotTank after the shutdown period, compared to January 18th. For PH-S3, the boiler does not run at full power for the entire preheating stage, while TEK17-S3 does.

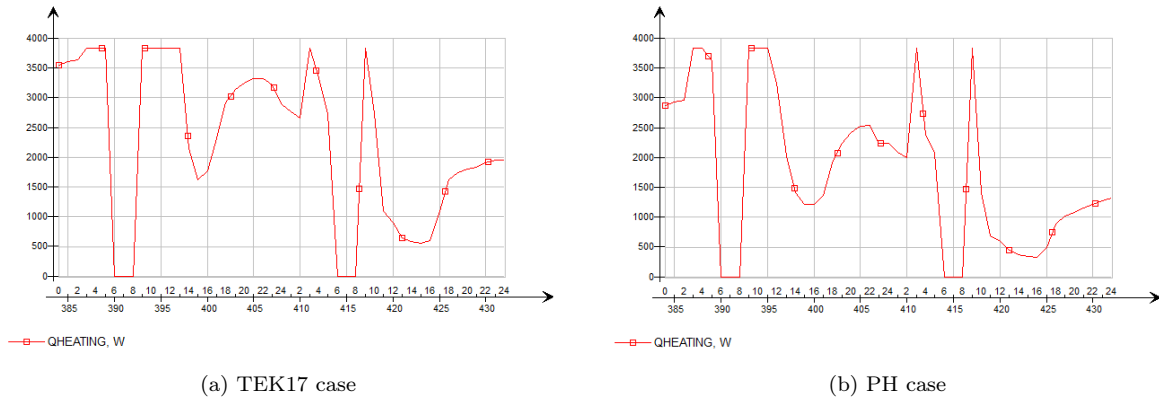


Figure 47: Boiler output for TEK17 case (a) and PH case (b) from Simulation 3

From Figure 48, one can see the degree to which the preheating effects all the circuits and the HotTank. The boiler circuit (top left graphs) shows an increase in both supply and return water temperatures, although only the last three days actually reach the new setpoint of $(70 + 10) \text{ }^\circ\text{C} = 80 \text{ }^\circ\text{C}$. For January 16th, the supply temperature increases from a stable $70 \text{ }^\circ\text{C}$ for TEK17-S2 to a peak of around $75 \text{ }^\circ\text{C}$ for TEK17-S3, while the increase on January 17th is negligible. Both days fail to reach the new setpoint, presumably due to both the insufficient boiler capacity, as well as the increased heat demand on these colder days, further highlighting the cascade effect that occurs between the outdoors and the boiler through the entire heating system. The HotTank temperatures (top right graphs) for these two days both increase more in the reheating stage, which in all likelihood as a consequence of the occupant presence and lighting supplying heat to the zone, leaving less to be covered by the heating system. The temperature minima on the last three days also increase noticeably in all graphs, apart from the bottom HotTank layer and zone heating return, where the increase is slightly lower. The increase in HotTank return temperature being less pronounced is the result of the HotTank containing the sum of water in both the AHU and Zone circuits.

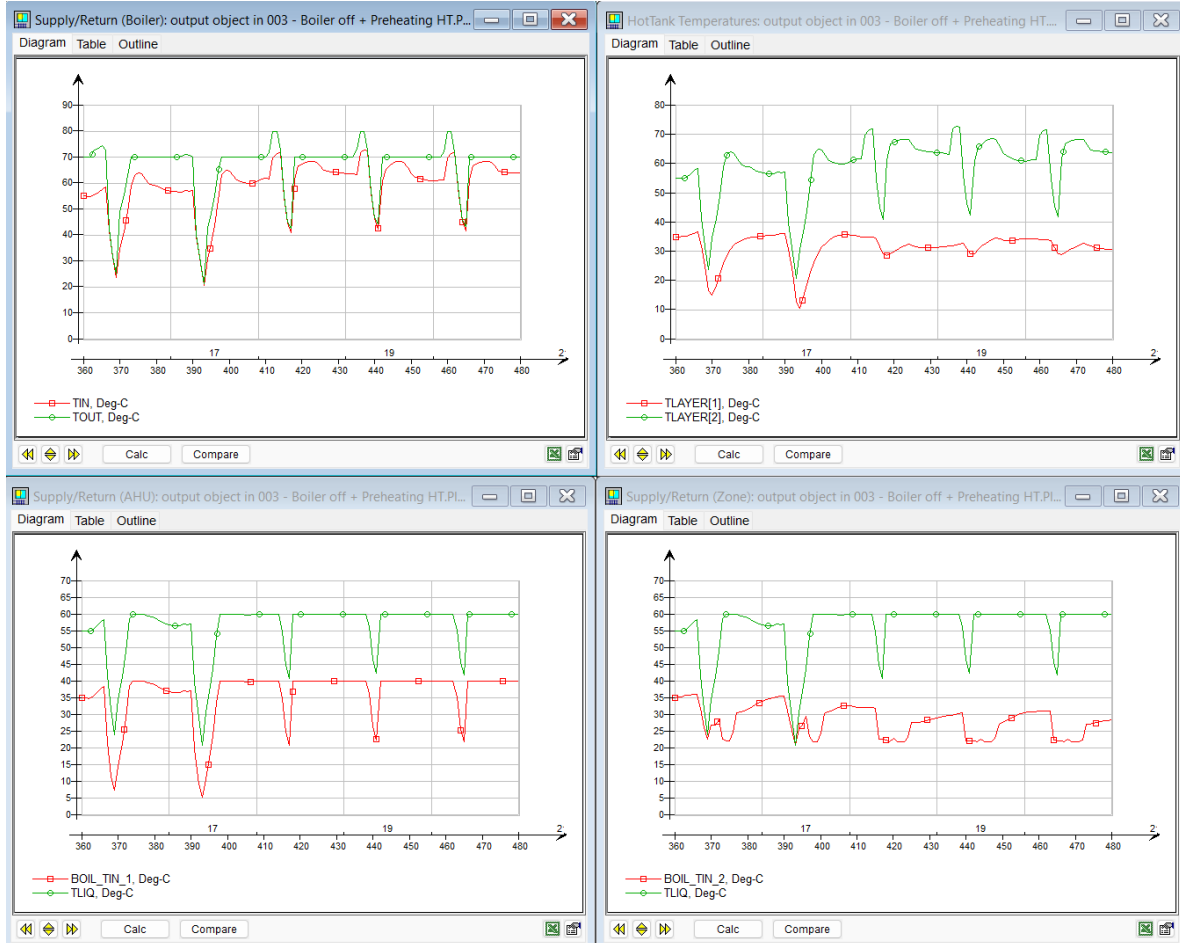


Figure 48: TEK17 case - Simulation 3. From left to right, top to bottom: Supply/Return temperatures for boiler circuit, Temperature of top and bottom layer of HotTank, Supply/Return temperatures for AHU circuit, Supply/Return temperatures for Zone heating circuit

Figure 49 shows more promising results for PH-S3, as was expected, given that the system is technically designed with a larger capacity than a baseline heating load simulation in IDA ICE would require for a PH. The supply temperature of $70 + 10$ °C from the boiler is achieved for all five days (see top left graph), while the top layer setpoint of 70 °C only reaches or surpasses the setpoint for the last three days. Nonetheless, the first two days do reach a HotTank top layer temperature above 60 °C, which was not the case for TEK17-S3.

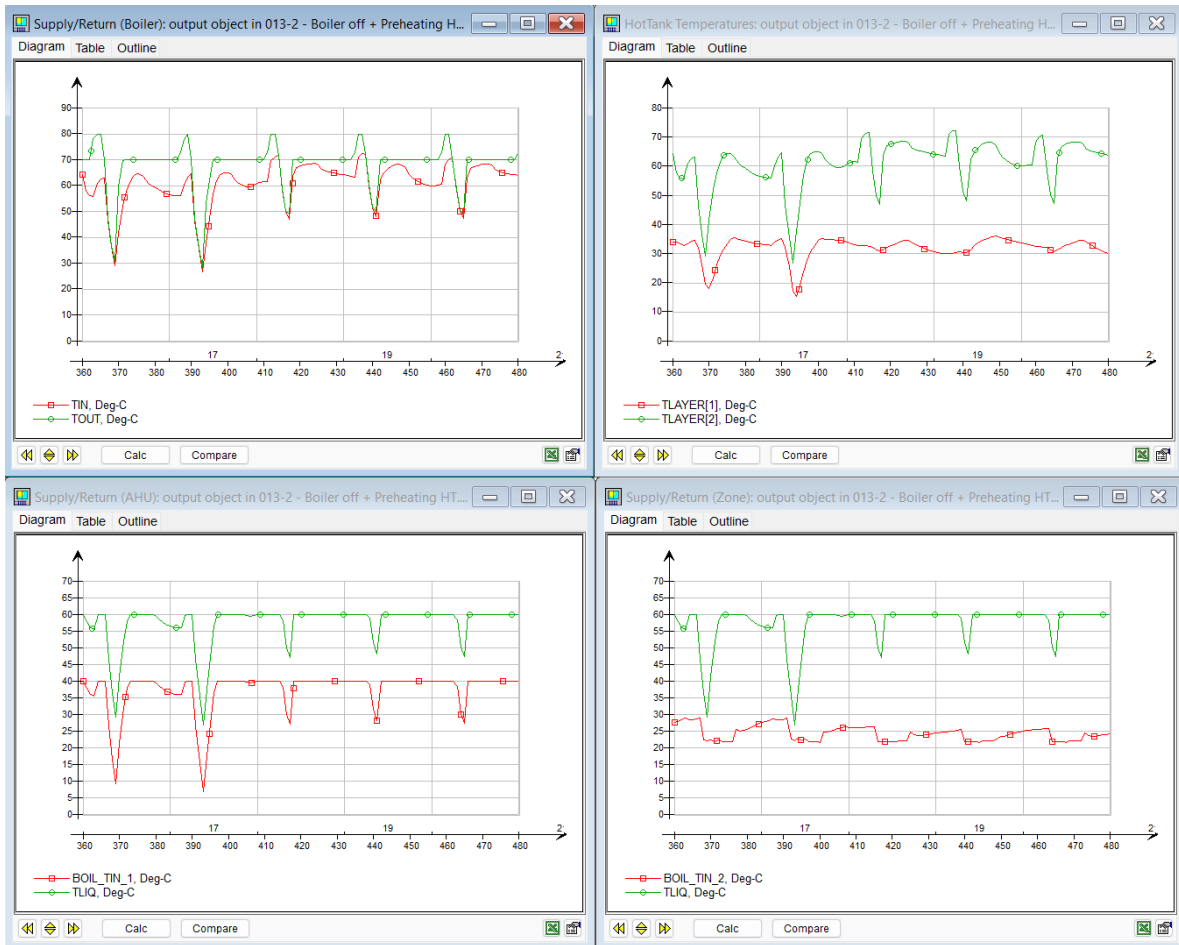


Figure 49: PH case - Simulation 3. From left to right, top to bottom: Supply/Return temperatures for boiler circuit, Temperature of top and bottom layer of HotTank, Supply/Return temperatures for AHU circuit, Supply/Return temperatures for Zone heating circuit

The mass flow rates from TEK17-S3 showed only minimal reductions from TEK17-S2, and are therefore available in Appendix R. The most noticeable change was the reduction of the three spikes in mass flow for January 18th through 20th. The reason no change was observed for the first two days could be the limited capacity of the boiler, which, although it manages to improve the performance of the system on the warmer days compared to TEK17-S2, still remains insufficient for the coldest days.

The mass flow rates from PH-S3, shown in Figure 50 below, exhibit more noticeable changes than the previous TEK17 comparison for the same simulations. These changes are related to the first two days, where the spikes in mass flow rate for the AHU and the zone heating are reduced. This can be attributed to the temperatures being increased more in this case compared to the TEK17 case, as previously described in connection with the supply and return temperatures in Figure 48 and Figure 49.

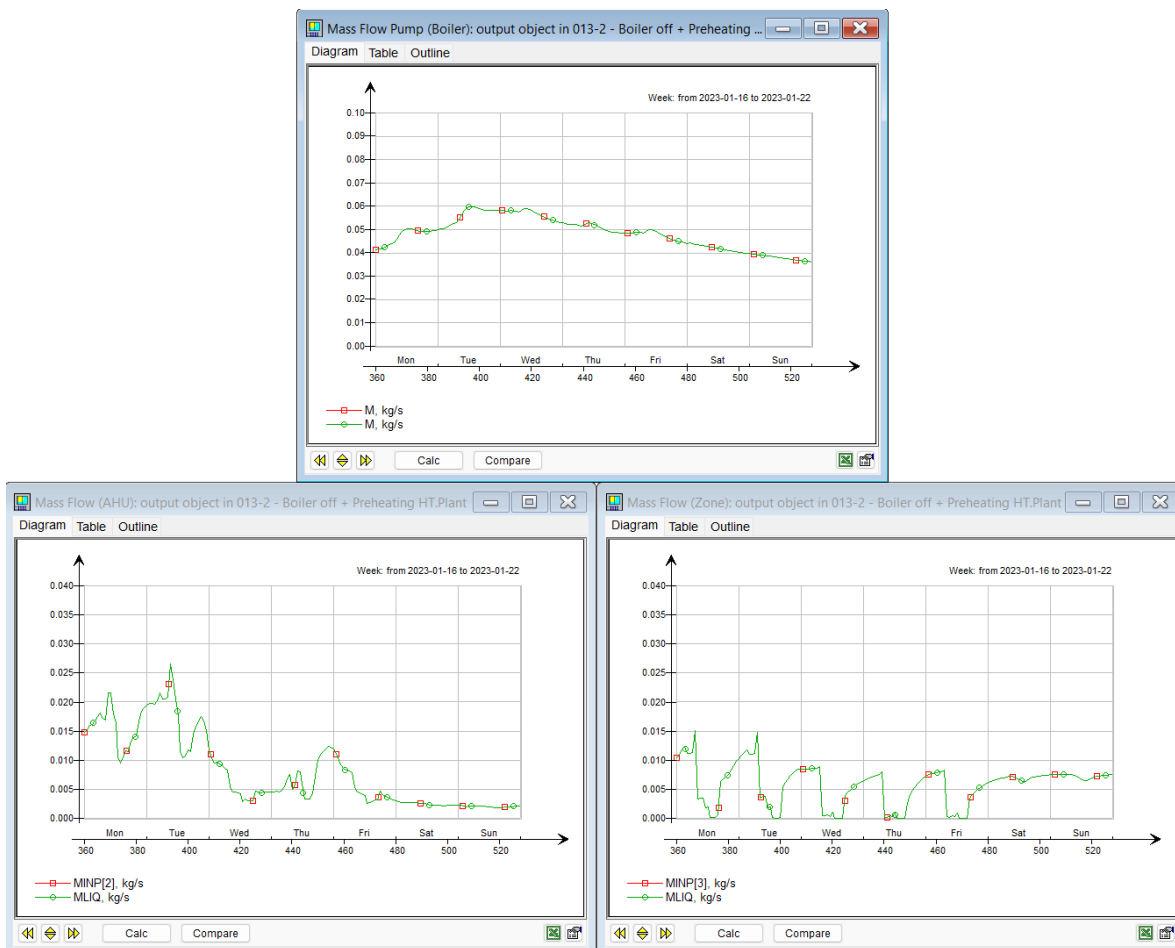


Figure 50: Mass flow rates for PH case - Simulation 3. From top to bottom, left to right: Mass flow of main pump, mass flow of AHU pump, mass flow of zone pump

5.4 Simulation 4

From Figure 51 it is clear that Simulation 4 does not yield the intended results for the TEK17 case. The main temperatures (left) show a decrease to nearly 19 °C on January 17th, while PPD (right) reaches above 14 % for the same day. Both of these are the lowest recorded values in their respective categories so far, which suggests that the strategy tested in Simulation 4 is inadequate with regard to maintaining a comfortable indoor environment, at least given the current setup.

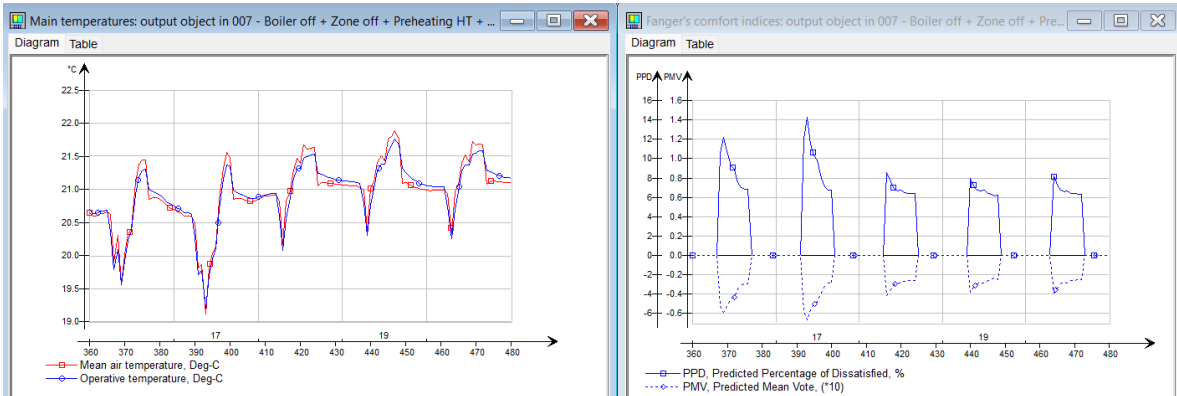


Figure 51: Main temperatures (left) and PPD (right) from Simulation 4 for TEK17 case

For the PH case, the results are similar, as can be seen in Figure 52. The main temperatures both reach as low as 20.5 °C on January 17th, with PPD reaching 8 % at the same point of the day. Despite performing better than TEK17-S4, PH-S4 nonetheless results in lower main temperatures and higher PPD than both PH-S3 and PH-S2.

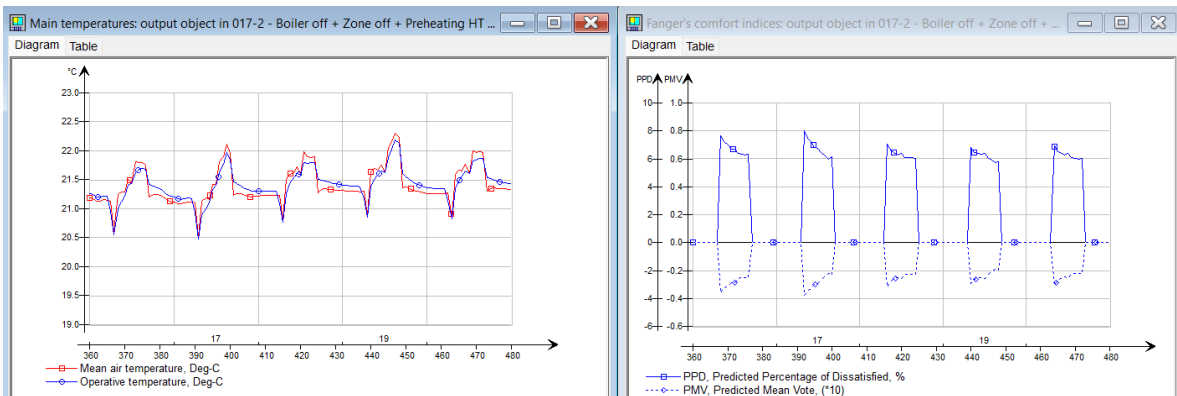


Figure 52: Main temperatures (left) and PPD (right) from Simulation 4 for PH case

Figure 53, showing the supply and return air temperatures (left) and mechanical inflow (right) for TEK17-S4, gives an indication as to why the main temperatures develop as they do throughout the five-day period. The supply temperature (green graph) shows that the increase in temperature setpoint for the supply air is initially successful. However, after about an hour on both January 16th and 17th, the temperature begins to fall drastically, reaching a minimum of about 9.5 °C on January 17th. The mechanical inflow (red graph) increases to the maximum possible value of 112 L/s on both these dates, and reaches over four times the maximum over the past three simulations on all three last days as well.

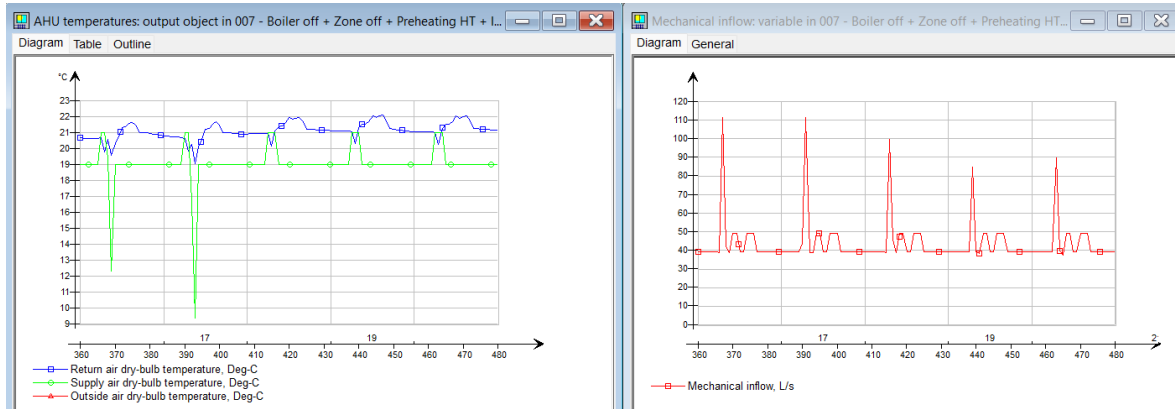


Figure 53: Supply & return air temperatures (left) and mechanical ventilation inflow (right) from Simulation 4 for TEK17 case

Figure 54 shows similar changes as in TEK17-S3 for PH-S4 with regard to the mechanical inflow, albeit with lower peaks that never exceeded 65 L/s. Additionally, such peaks only occur on January 16th and 17th, while the rest of the week remains unchanged from PH-S3.

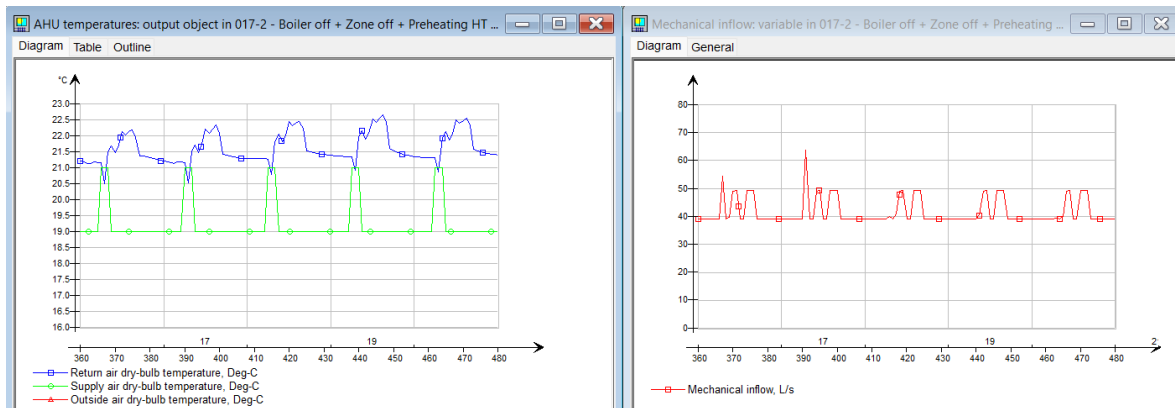
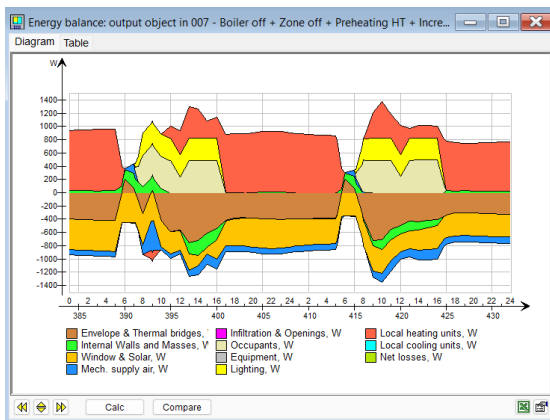


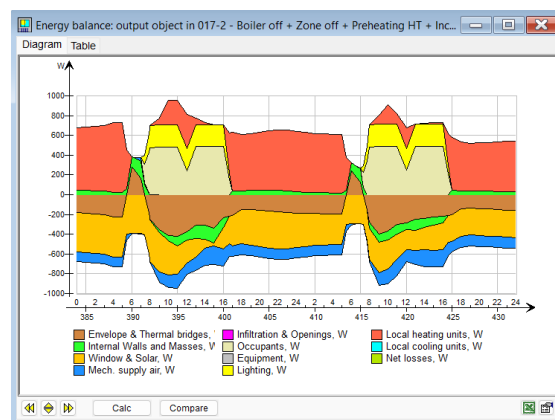
Figure 54: Supply & return air temperatures (left) and mechanical ventilation inflow (right) from Simulation 4 for PH case

Figure 55 shows the energy balances for TEK17-S4 (a) and PH-S4 (b). Clearly, turning off the zone heating circuit during the shutdown phase results in a cut in power emitted from the radiators in both cases. During the shutdown, there is some heat contribution from the supplied air in TEK17-S4. For PH-S4, there is only a negligible contribution from the supplied air on January 17th, but nothing on January 18th. The difference between TEK17-S4 and PH-S4 is most likely related to the building envelopes and larger than baseline capacity for the PH case. For TEK17-S4, the supply air functions as a source of heating considering the low main temperatures in the zone and higher losses than PH-S4, while for PH-S4 the main temperatures remain closer to setpoint. Hence, the supply air in PH-S4, maintaining the same setpoint of 21 °C, does not have any major effect on the heat balance. In addition, there is an increased supply of heat from internal walls and masses during the shutdown for all cases and dates, and even some immediately after the shutdown on January 17th for TEK17-S4. This is related to the operation of the radiators, as described below.

Once the boiler and zone pump are turned back on the energy balances continue to differ between the different cases and dates. While the radiators begin emitting heat nearly immediately after the shutdown is over for both days of PH-S4 and the second day of TEK17-S4, on January 17th TEK17-S4 they yield the exact opposite result. For the latter case, the radiators appear to be a source of heat *loss*, as for the period around 9:00, the red field of the local heating in Figure 55 is in the negative side of the x-axis. Furthermore, the lower limit for operative temperature of 20 °C is not reached until around 12:00 for TEK17-S4 on January 17th, which is a whole three hours after the boiler and radiators are turned back on. This is particularly concerning, considering that the internal loads are the only source of heat in this period, and, as stated earlier, that when the occupants give off heat, they are themselves being cooled down.



(a) TEK17 case



(b) PH case

Figure 55: Energy balance from Simulation 4 for TEK17 case (a) and PH case (b)

Figure 56 shows the boiler outputs on January 17th and 18th for TEK17-S4 (a) and PH-S4 (b). The only noticeable change from TEK17-S3 to TEK17-S4 is the fact that the maximum boiler output after the shutdown period is maintained for about an hour longer on both January 17th and 18th. For PH-S4 there is no noticeable difference from PH-S3 for either of the two days.

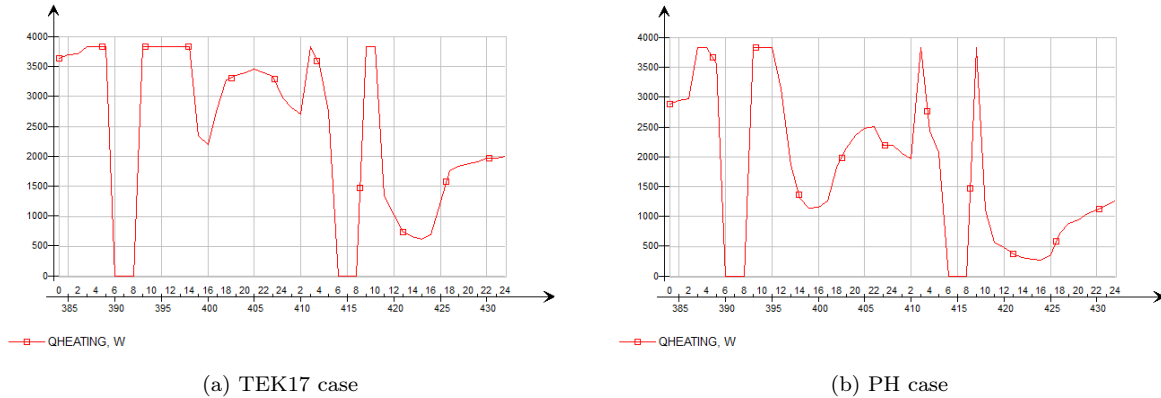


Figure 56: Boiler output [W] for TEK17 case (a) and PH case (b) from Simulation 4

Figure 57 shows that the most noticeable changes in the temperatures in the heating system for TEK17-S4 are the larger temperature declines on January 16th and 17th. The drop for all circuits and layers on these days is between 10 and 15 °C on the supply side. For the boiler circuit (top left) and the HotTank layers, this applies to both supply and return sides. For the AHU circuit (bottom left), the supply side temperature is reduced, while the return temperature remains the same. It is also clear that a positive temperature difference between supply and return on the AHU circuit is maintained, which means the energy in the water is still being used to heat the supply air. For the zone heating circuit (bottom right), however, the case is the opposite, as there is a negative temperature difference between supply and return, which corresponds to the observed post-shutdown cooling effect of the local heating units from Figure 55 (a).

For PH-S4, there was practically no change for the first two days, while for the three last days, supply and return temperatures were marginally higher for the entire set of graphs, apart from the zone heating circuit, where the return temperature remained unchanged. Due to the minimal changes from PH-S3, the graphs are made available in Figure 106 under Appendix Q.

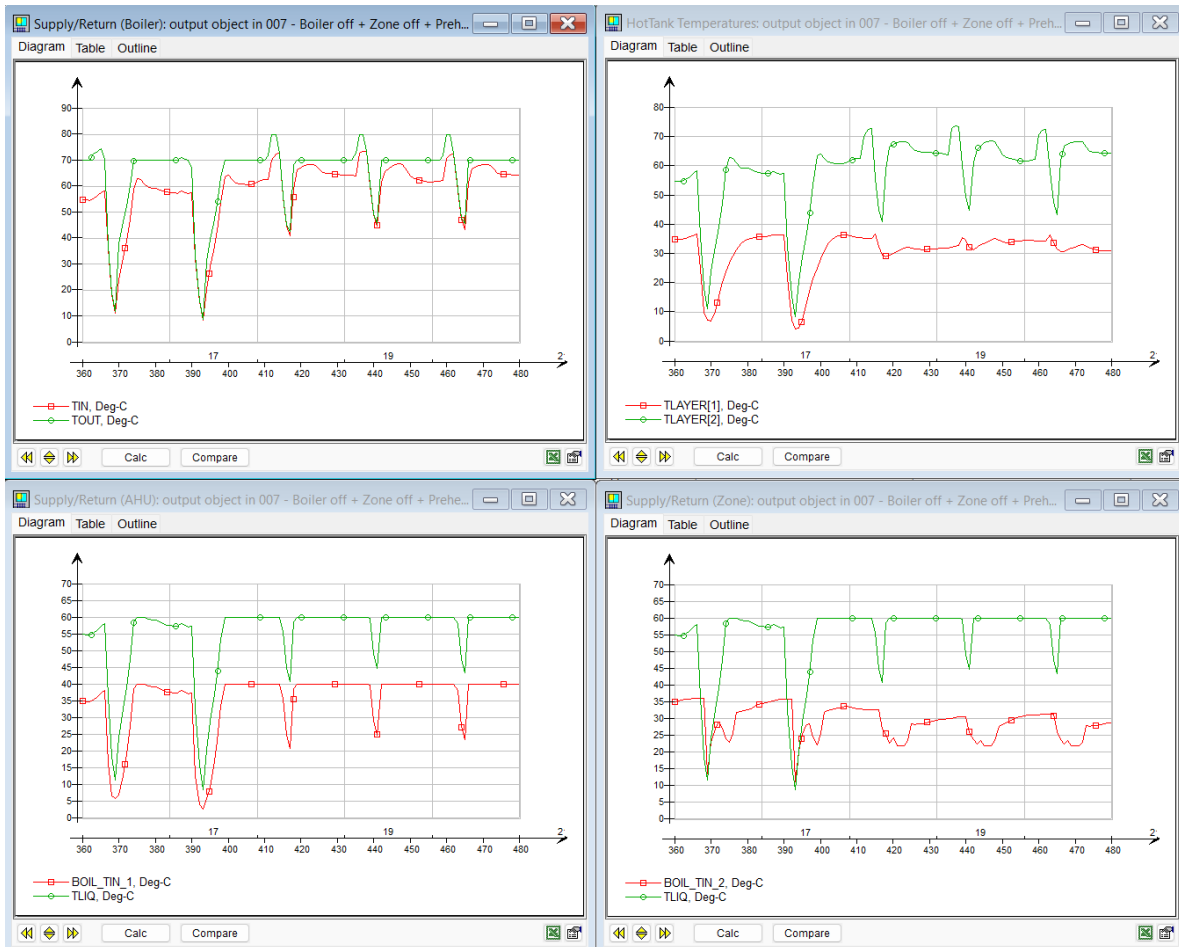


Figure 57: TEK17 case - Simulation 4. From left to right, top to bottom: Supply/Return temperatures for boiler circuit, Temperature of top and bottom layer of HotTank, Supply/Return temperatures for AHU circuit, Supply/Return temperatures for Zone heating circuit

In Figure 58, showing the mass flow rates for TEK17-S4, there are noticeable changes to all three graphs. The mass flow rate peak of the boiler circuit (top graph) reaches 0.09 kg/s, up from 0.08 kg/s for TEK17-S3. For the AHU (bottom left graph), the existing peaks on January 16th and 17th from Simulation 2 and Simulation 3 increase slightly, but the biggest change are the new peaks that occur for the entire workweek during shutdown. For January 17th, the new peak reaches 0.07 kg/s during the shutdown period with increased temperature setpoint for the supply air, while the post-shutdown peaks for the first two days increase by about a third of the values from TEK-S3. For January 18th through 20th, the new AHU peaks occurring during the shutdown period are nearly as high as the post-shutdown peaks were for TEK17-S3, at around 0.03 kg/s. In the graph for the zone heating circuit (bottom right), the height of the peaks stays about the same from TEK17-S3, but they are also shifted to after the shutdown period. This post-shutdown increase is expected, as the system works on getting back to baseline operation. The shutdown period itself can be seen by the mass flow being reduced to zero for three hours on all the workdays.

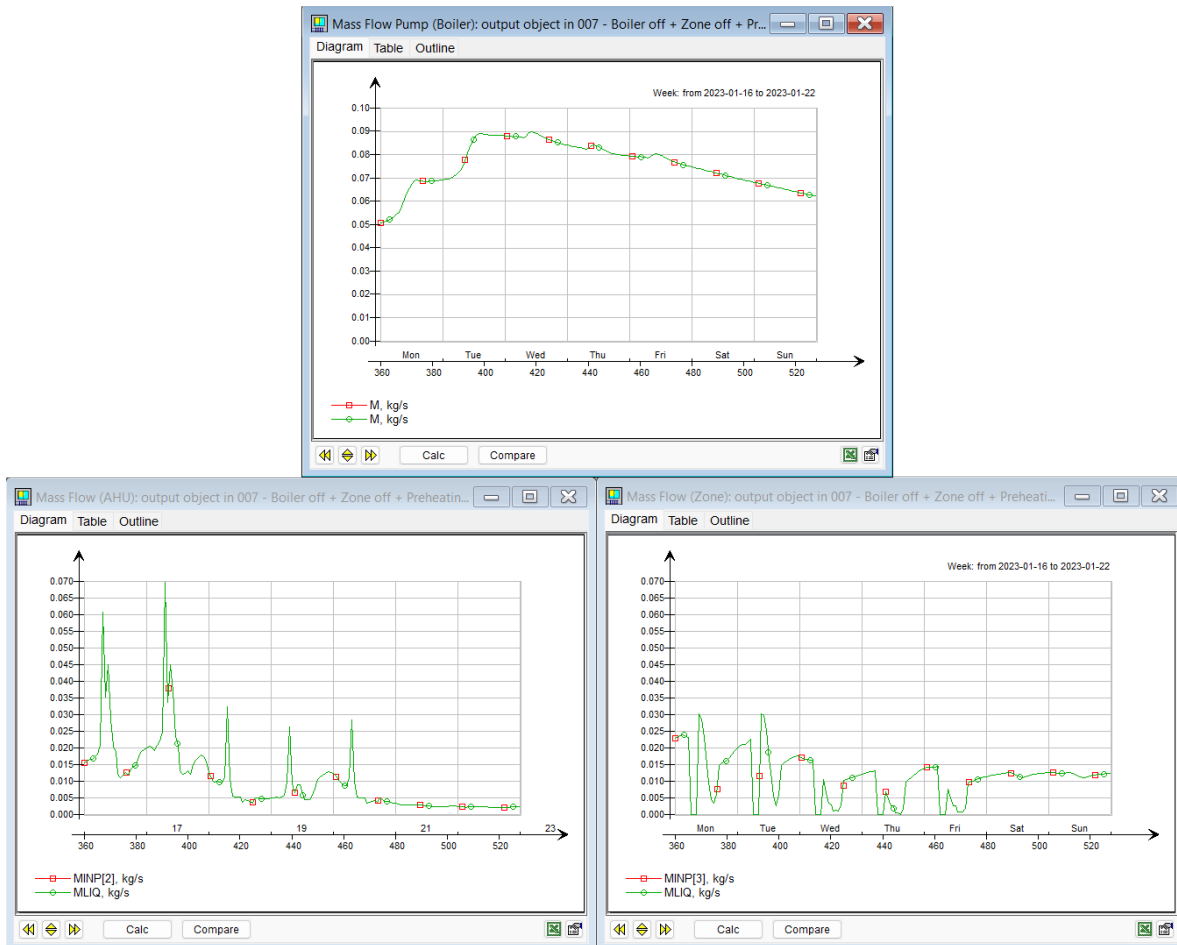


Figure 58: Mass flow rates for TEK17 case - Simulation 4. From top to bottom, left to right: Mass flow of main pump, mass flow of AHU pump, mass flow of zone pump

The mass flow rates for PH-S4, presented in Figure 59, show both similarities and differences compared to PH-S3, depending on which graph that is being evaluated. The mass flow rate of the boiler circuit (top graph) remains virtually unchanged from both PH-S3 and PH-S2. While the post-shutdown peaks for the AHU circuit (bottom left graph) remains unchanged from PH-S3, new peaks occur, with the January 17th peak reaching as high as 0.04 kg/s. The zone heating mass flow rates generally remain unchanged apart from during the shutdown period, when they are zero, and just after for January 16th and 17th, when small peaks occur.



Figure 59: Mass flow rates for PH case - Simulation 4. From top to bottom, left to right: Mass flow of main pump, mass flow of AHU pump, mass flow of zone pump

All these results seem to indicate that there is not enough heat being provided during preheating to enable the intended strategy and achieve the desired outcome for Simulation 4.

5.5 Simulation 5

Figure 60 shows the main temperatures (left) and PPD (right) for TEK17-S5A. The main temperatures on January 17th show a relative improvement compared to TEK17-S4, climbing from 19 to 19.5 °C. The rest of the days remain somewhat consistent. The effect of preheating the ventilation air is barely visible with smaller peaks prior to the shutdown periods, which for the last three days essentially just closes the gap that was present between the mean air and operative temperatures in TEK17-S4. The PPD is also somewhat improved from TEK17-S4, falling from 14 to 13 %. Nonetheless, as previously stated, these are minimal improvements that do not constitute a comfortable indoor climate with regard to thermal conditions. Ideally, a simulation closer resembling the experiment by Foteinaki et al. [79], which was presented in the literature review, should have been tested. While Simulation 5 reduced the load by 100% during shutdown, Foteinaki et al. only reduced the peak load by 87 % through load shifting.

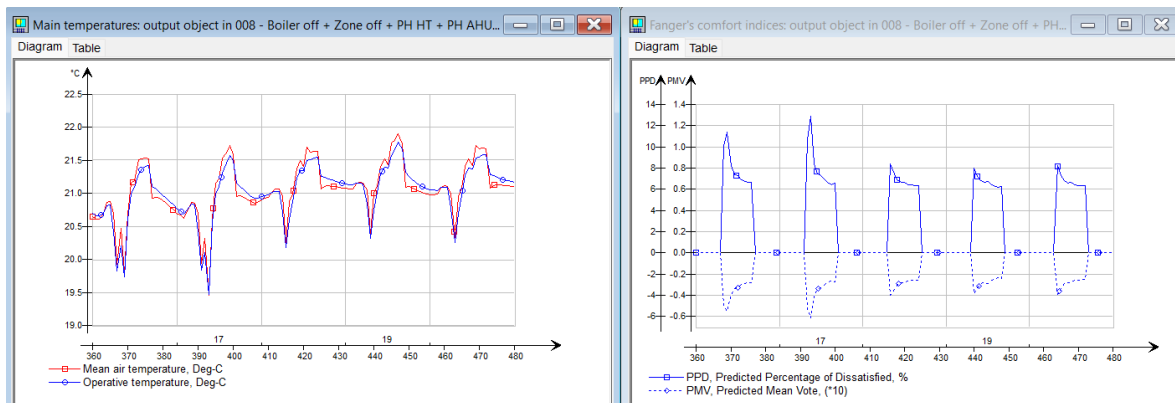


Figure 60: Main temperatures (left) and PPD (right) from Simulation 5A for TEK17 case

Figure 61 shows main temperatures and PPD for TEK17-S5B, which appears to give somewhat better main temperatures and PPD, compared to TEK17-S5A. The lowest operative temperature on January 17th is around 19.7 °C, with the peak PPD for the same day falling below 12 %. These are still not acceptable thermal conditions, but the increased HotTank setpoint appears to have some effect in the correct direction.

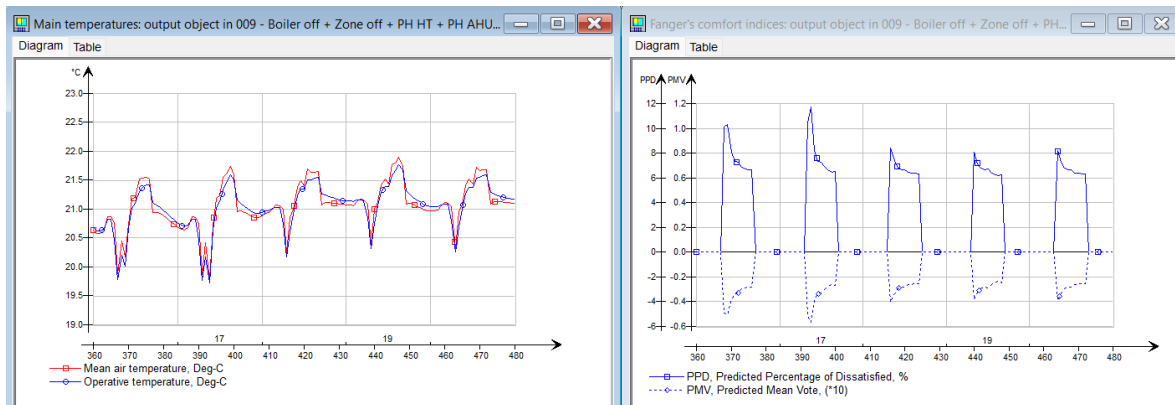


Figure 61: Main temperatures (left) and PPD (right) from Simulation 5B for TEK17 case

The increased HotTank setpoint of 90 °C in TEK17-S5B further improves the thermal conditions, according to Figure 62. The operative temperature (left graph) remains unchanged from TEK17-S5B, but its duration is somewhat reduced, which further improves the PPD to just under 11 % (right graph). Yet again, this is insufficient to ensure thermal acceptable thermal comfort.

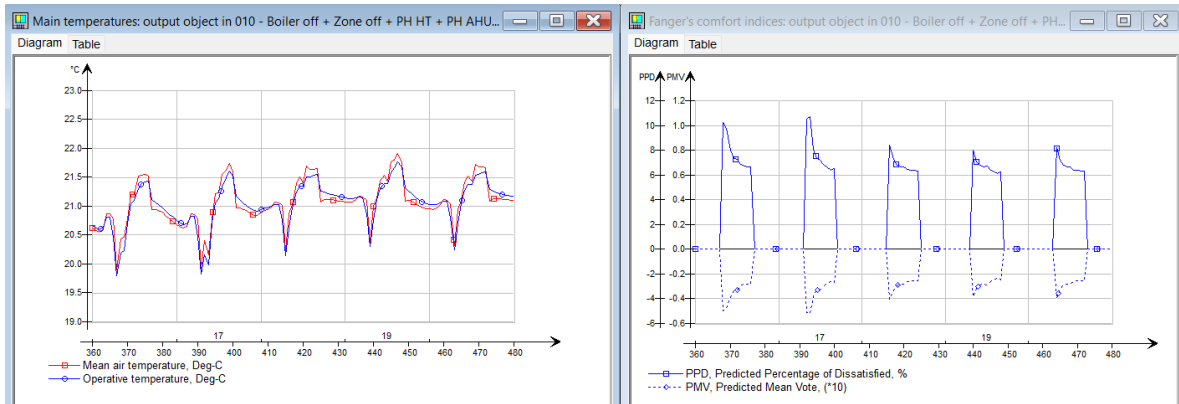


Figure 62: Main temperatures (left) and PPD (right) from Simulation 5C for TEK17 case

Figure 63 shows the AHU supply and return temperatures (left), as well as mechanical ventilation inflow (right) for TEK17-S5A. The increase in supply temperature setpoint clearly begins earlier than in TEK17-S4. However, this does not prevent the drop in supply temperature after the shutdown period begins, as a drop to nearly 11 °C is observed. This is a slight improvement from the 9 °C drop in TEK17-S4, but remains too low to ensure thermal comfort nonetheless. In the preheating stage of the first two days, there are two new increases in the mechanical inflow.

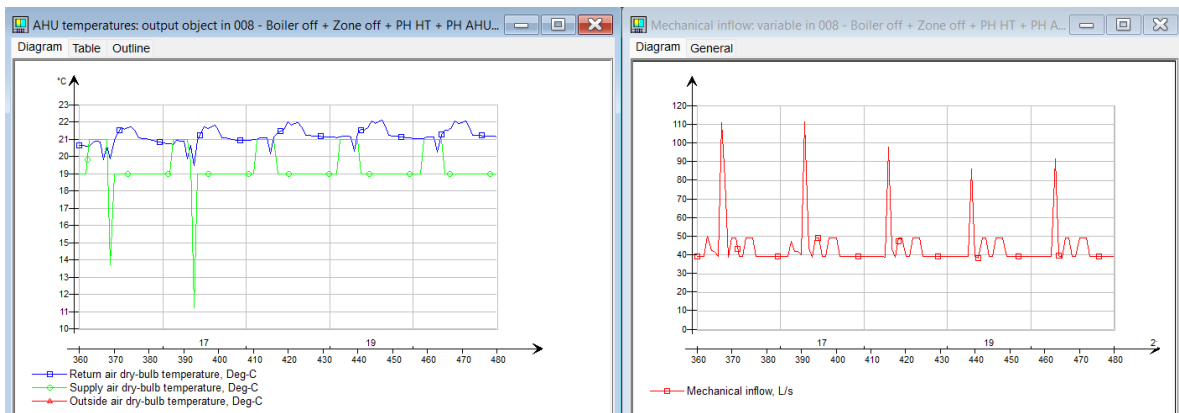


Figure 63: Supply & return air temperatures (left) and mechanical ventilation inflow (right) from Simulation 5A for TEK17 case

The AHU supply and return temperatures, and mechanical inflow, for TEK17-S5B are available in Figure 64. The supply temperature (green graph, left) is somewhat higher than in TEK17-S5B on January 17th, at 14 °C, indicating that the increased preheating temperature for the HotTank has an effect on the available heat for the AHU. The mechanical inflow (right graph) remains unchanged from TEK17-S5A.

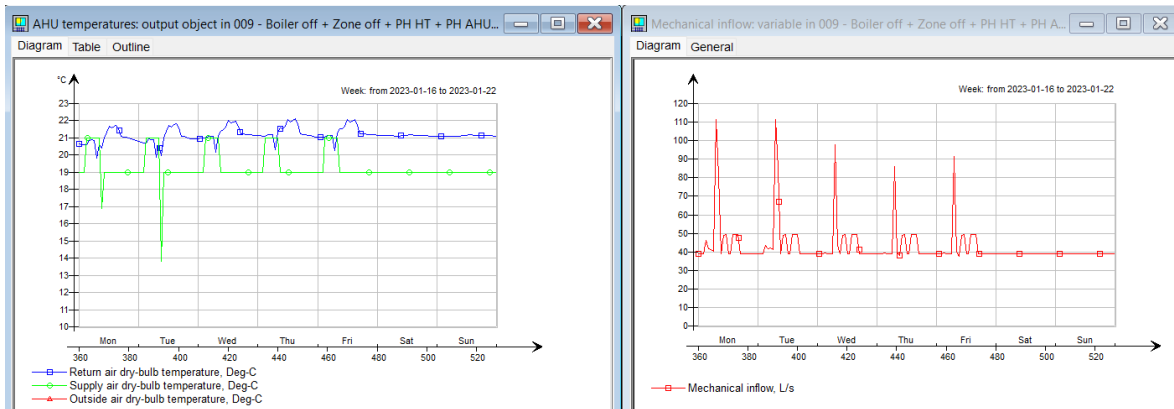


Figure 64: Supply & return air temperatures (left) and mechanical ventilation inflow (right) from Simulation 5B for TEK17 case

TEK17-S5C, presented with supply and return air temperatures and mechanical inflow in Figure 65, shows an even higher supply temperature compared to TEK17-S5B, at 17 °C. This further highlights that the negative effect of shutting off the zone heating is reduced by increasing the preheating temperature. As with the previous two runs, TEK17-S5C shows the same pattern for the mechanical inflow.

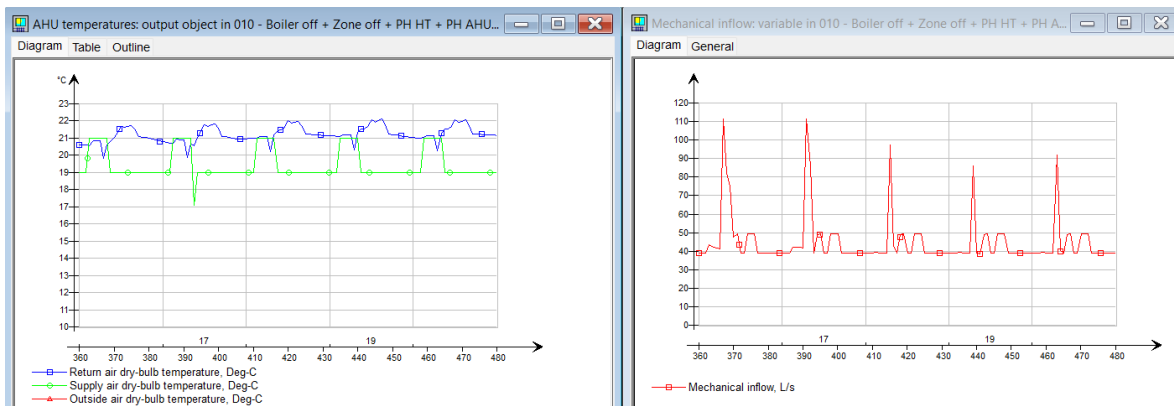
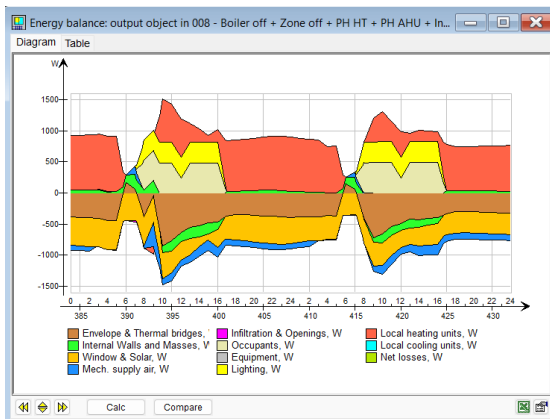


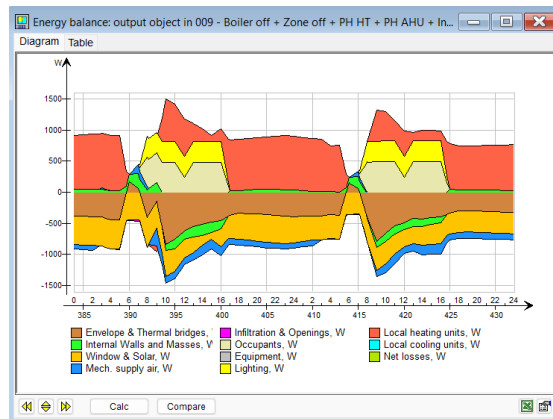
Figure 65: Supply & return air temperatures (left) and mechanical ventilation inflow (right) from Simulation 5C for TEK17 case

Figure 66 shows the energy balances for TEK17-S5A (a), TEK17-S5B (b) & TEK17-S5C (c). It is clear for TEK17-S5A (a) that the increase in supply air temperature results in decreased heat losses, both those caused by the previously sub-room temperature setpoint for the supply air, as well as the cooling effect from the radiators. The post-shutdown increase in power supply from radiators begins faster for all three setpoints in TEK17-S5 than TEK17-S4, even though there is still a short period after restarting the zone pumps where the radiators are the cause of some heat loss.

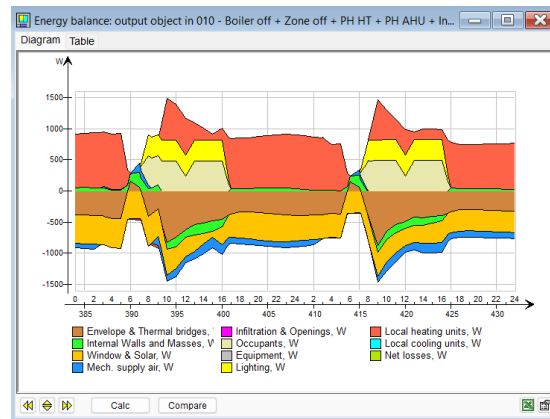
Generally, the main difference between the three runs of TEK17-S5 as the HotTank setpoint increases is more power available for the reheating via radiators post-shutdown period for January 18th, while the cooling effect of the AHU in the same period become less pronounced. Ideally, a shorter shutdown period should have been tested for Simulation 5, either on its own or with a further increase in HotTank setpoint during the preheating. At the same time, higher temperatures would not only cause more rapid deterioration of the water pipes in the distribution system, but would also be significantly higher than what the regulations in TEK17 allow with regard to low temperature heating systems.



(a) TEK17-S5A



(b) TEK17-S5B



(c) TEK17-S5C

Figure 66: Energy balances from Simulation 5A (a), 5B (b), & 5C (c) for TEK17 case

Figure 67 shows the boiler outputs over January 17th and 18th for TEK17-S5A (a), TEK17-S5B (b) & TEK17-S5C (c), as well as the additional simulation run (d) with a HotTank setpoint increase up to 100 °C during the preheating period. The first three runs show that while the preheating peaks kept increasing as the HotTank setpoint increased, the post-shutdown peaks were being reduced. The value of these four simulation runs lays in the leveling of power peaks over the two-day period that was achieved in run (d). As can be seen in Figure 67 (d), the preheating peaks for both days, as well as the post-shutdown peak for January 17th, are all the same height, at 13 kW. While this value is over three times the original value for the electric boiler (3.836 kW), the matching of the power peaks makes the strategy of Simulation 5 seem more promising. Furthermore, one of the reasons these peaks occur, is because the increased power enables quicker preheating before and reheating after the shutdown period, which is evident in that neither of these peaks last as long as the corresponding peaks for the previous simulations, including the reference simulation.

One possible change that could make this case more relevant to Norwegian designs of such systems, would be to incorporate a low-temperature heating system by designing a lower initial HotTank setpoint, resembling a real low temperature water distribution system. That way, the temperature could be increased from its initial value up to 60 °C, which TEK17 has decided is the maximum temperature that what can be considered "low temperature heating". Nonetheless, the runs in Simulation 5 show how important it is to optimize the setpoint temperature to achieve even power distribution when attempting to reduce and/or shift power peaks.

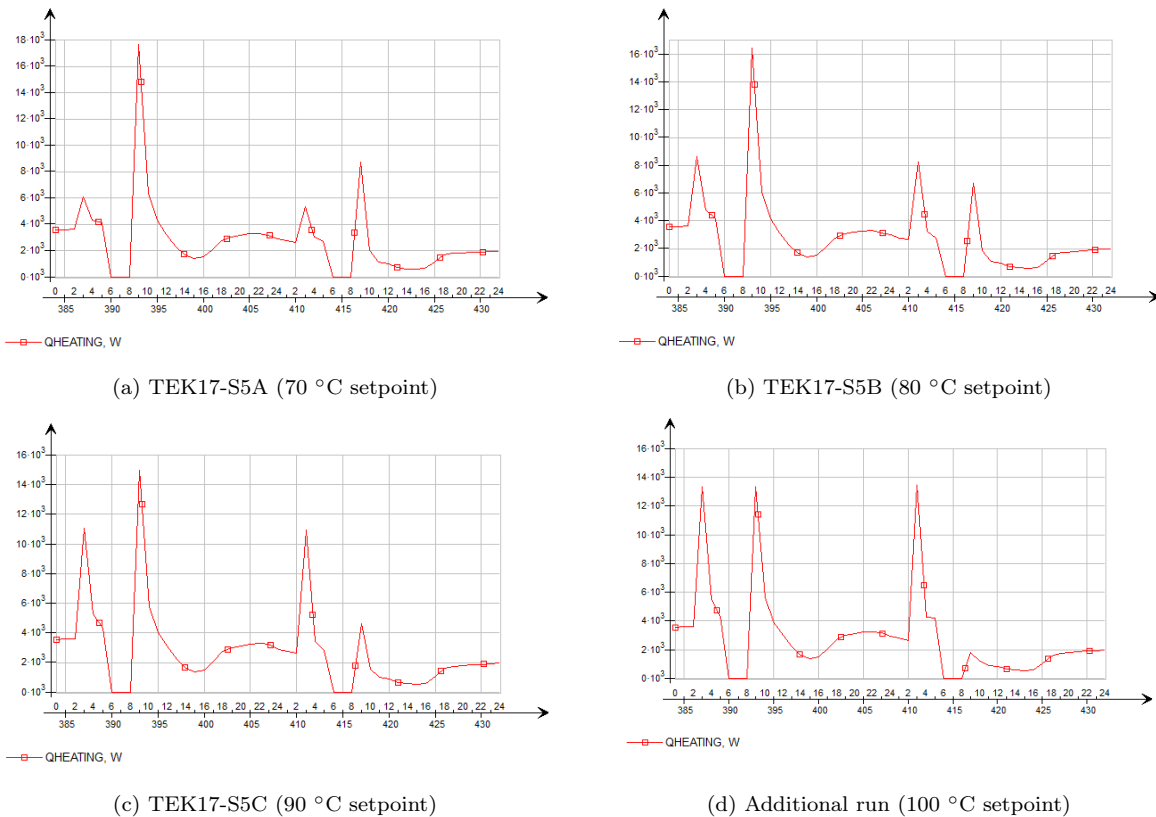


Figure 67: Boiler outputs from Simulation 5A (a), 5B (b), 5C (c), & additional run (d) for TEK17 case

Figure 68 shows the supply and return temperatures for the boiler circuit (top left), AHU circuit (bottom left), zone heating circuit (bottom right), as well as HotTank layer temperatures (top right) for TEK17-S5A. The main difference from TEK17-S4 are the increased supply and top layer temperatures during the preheating stage, made possible by the increased available power after the switch to a DHS. Naturally, increased available power also reduces the reheating duration post-shutdown. The later runs of Simulation 5, TEK17-S5B and TEK17-S5C, reflect the further increase in preheating temperature setpoint, as well as less pronounced temperature decline in supply and return temperatures on the last three days. These graphs are available in Appendix Q, as they do not differ much from TEK17-S5A in any aspects besides the ones mentioned in this paragraph.



Figure 68: TEK17 case - Simulation 5A. From left to right, top to bottom: Supply/Return temperatures for boiler circuit, Temperature of top and bottom layer of HotTank, Supply/Return temperatures for AHU circuit, Supply/Return temperatures for Zone heating circuit

Figure 69 contains the mass flow rates for the boiler circuit (top), AHU circuit (bottom left), and zone heating circuit (bottom right) for TEK-S5A. The flow rate of the boiler circuit is reduced from just under 0.09 kg/s to just above 0.07 kg/s compared to TEK17-S4. In the AHU graph, there is a small increase in flow rate during the preheating stage, while the zone heating circuit sees a slight reduction in duration of the maximum flow rate from TEK17-S4, which can be attributed to the higher power available in the boiler, which means that restoring the design temperatures for the radiators is achieved quicker.

For TEK17-S5B and TEK17-S5C, the graphs with mass flow rates can be seen under Appendix R in Figure 108 and Figure 109, respectively. The graphs are placed in the appendix section, as the only differences between them and TEK17-S5A are the barely distinguishable decreases in mass flow rate for the boiler circuit in general, the preheating phase for the AHU, and the post-shutdown peaks for the zone heating circuit, which was addressed in the previous paragraph.

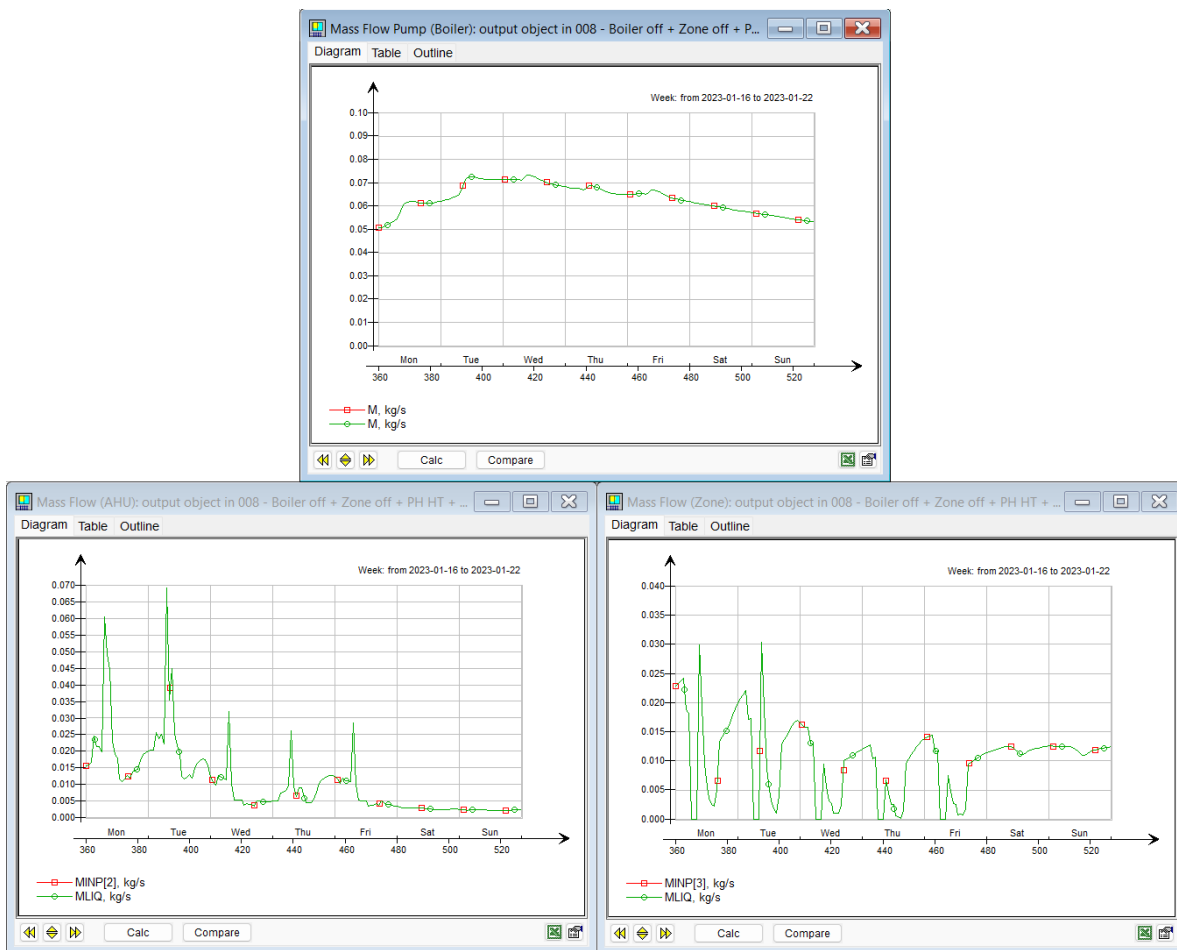


Figure 69: Mass flow rates for TEK17 case - Simulation 5A. From top to bottom, left to right: Mass flow of main pump, mass flow of AHU pump, mass flow of zone pump

6 Conclusion

The main goal of this thesis was to analyze the potential of using temporary power shutdowns in the CHS to achieve power peak reduction in water-borne heating systems while maintaining thermal comfort. The literature review that was conducted indicated that both the building envelope and different operational strategies could be utilized to reduce and/or shift power peaks related to space heating, often without compromising thermal comfort. As expected, constructions following more recent building regulations with better insulation performed better with regard to thermal decay. With regard to operational strategies, the use of DR and MPCs were among the most common solutions.

In addition to the literature review, a series of simulations were performed to analyze the possibility of maintaining thermal comfort during a temporary shutdown of the available power in the CHS of an office building. The potential of exploiting the thermal capacity of the water in the piping network of the building was investigated by employing a two-layered stratified tank was resembling the supply and return sides of the water distribution network, with a volume equal to that of the piping system. The custom controls that were developed to manipulate setpoints and operation schedules of different components in the CHS and AHU performed as expected, as was proven by their logged signals. The simulations were executed in IDA ICE 4.8, for both a TEK17- and a PH-worthy building envelope. Simulation 1 served as a baseline run with no user-defined changes in the operation of the CHS. Simulation 2, which consisted of a temporary shutdown of the electric boiler power in the CHS, established that power could be disconnected completely in the peak hours between 06:00 and 09:00 in the morning without compromising the thermal comfort. Simulation 3 proved first of all that sufficient power in the CHS must be guaranteed in order to facilitate preheating of the water volume to the desired temperature pre-shutdown. By prioritizing heating through the AHU over radiators during the shutdown period, Simulation 4 further highlighted the need for sufficient power to ensure the success of such a strategy. Simulation 5 showed that it is important to optimize preheating temperature setpoints to balance power peaks before and after shutdown when connected to a DHN.

Generally, there appear to be considerable benefits to utilizing the thermal storage capacity of the water volume in the piping system, both for TEK17 and PH-worthy building envelopes, using either electric heating or DH as a heat source. The exploitation of the thermal inertia of both the building envelope and hot water exhibits promising results, which reflect the findings presented in the literature review. While the optimal control strategy varies depending on the case being studied, there is a significant potential for power peak shifting from the temporary shutdown of available power in the CHS.

6.1 Suggestions for Further Research

While interesting results were achieved in the work that was conducted for this thesis, there is always room for improvement in future research. Some of these suggestions are listed below.

- Validate the simulation results to experimental data
- Examine the same strategies for both morning and afternoon power peaks during the same day
- Try only partly reducing boiler capacity to reduce power peaks
- Conduct similar tests for lower-temperature heating systems (e.g. TABS)
- Implement PCMs in the model to further exploit the building mass
- Investigate the potential of power peak reduction and/or shifting in cooling systems as well

References

- [1] United Nations Framework Convention on Climate Change, “The paris agreement. what is the paris agreement?” [Accessed 21-Jan-2023]. [Online]. Available: <https://unfccc.int/process-and-meetings/the-paris-agreement/the-paris-agreement>
- [2] Council of European Union, “Regulation (EU) 2021/1119 (‘European Climate Law’),” Jun 2021, [Accessed 21-Jan-2023]. [Online]. Available: <https://eur-lex.europa.eu/eli/reg/2021/1119>
- [3] Klima- og miljødepartementet, “Nytt norsk klimamål på minst 55 prosent,” *Regjeringen.no*, Nov 2022. [Online]. Available: <https://www.regjeringen.no/no/aktuelt/nytt-norsk-klimamal-pa-minst-55-prosent/id2944876/>
- [4] Klima- og miljødepartementet , “Det grønne skiftet,” Dec 2021. [Online]. Available: <https://www.regjeringen.no/no/tema/klima-og-miljo/innsiktsartikler-klima-miljo/det-gronne-skiftet/id2879075/>
- [5] “Forskrift om forbud mot bruk av mineralolje til oppvarming av bygninger,” Jun 2018. [Online]. Available: <https://lovdata.no/dokument/SF/forskrift/2018-06-28-1060>
- [6] THEMA & Multiconsult, “Har vi fleksibilitet nok til å balansere kraftsystemet fram mot 2050?,” Sep 2022, ISBN: 978-82-8368-118-5. [Online]. Available: <https://www.regjeringen.no/contentassets/5f15fccc3143d1bf9cade7da6afe6e/no/sved/vedlegg4.pdf>
- [7] HM Government, “The Ten Point Plan for a Green Industrial Revolution,” Nov 2020. [Online]. Available: <https://www.gov.uk/government/publications/the-ten-point-plan-for-a-green-industrial-revolution>
- [8] Energikommisjonen, “Mer av alt – raskere,” Feb 2023. [Online]. Available: <https://www.regjeringen.no/no/dokumenter/nou-2023-3/id2961311/?ch=1>
- [9] N. H. Sandberg, S. K. Lien, K. B. Lindberg, and I. Sartori, “Mål om 10 TWh energisparing i bygningsmassen: Hvordan ligger vi an og hva er potensialet?” *Praktisk økonomi & finans*, vol. 38, no. 1, pp. 4–22, 2022. [Online]. Available: <https://doi.org/10.18261/pof.38.1.2>
- [10] Direktoratet for byggkvalitet (DiBK), “TEK17 - § 14-4. Krav til løsninger for energiforsyning,” Jul 2022. [Online]. Available: <https://dibk.no/regelverk/byggteknisk-forskrift-tek17/14/14-4/>
- [11] SINTEF Byggforsk, “552.109 varmtvannssentraler og varmeanlegg,” 1995. [Online]. Available: https://www.byggforsk.no/dokument/521/varmtvannssentraler_og_varmeanlegg
- [12] Thermal Storage UK, “Flexibility for low carbon electric heating,” Oct 2022. [Online]. Available: https://static1.squarespace.com/static/61af158225618e1511f3323f/t/6348080d3e4c696e22f6b8ca/1665665039164/Benefits+of+heat+flexibility_Thermal+Storage+UK_October+2022.pdf
- [13] SINTEF Byggforsk, “Romoppvarming av boliger. prinsipper og systemer,” Apr 2010. [Online]. Available: https://www.byggforsk.no/dokument/518/romoppvarming_av_boliger_prinsipper_og_systemer
- [14] M. R. Heikal and A. J. Miller, “SPACE HEATING,” Feb 2011, [Accessed 21-Feb-2023]. [Online]. Available: https://dx.doi.org/10.1615/AtoZ.s.space_heating

- [15] Norsk Standard, “Ergonomics of the thermal environment - Analytical determination and interpretation of thermal comfort using calculation of the PMV and PPD indices and local thermal comfort criteria (ISO 7730:2005),” Mar 2006. [Online]. Available: <https://www.standard.no/no/nettbutikk/produktkatalogen/produktpresentasjon/?ProductID=158329>
- [16] S. Guenther, “What is pmv? what is ppd? the basics of thermal comfort,” Oct 2022. [Online]. Available: <https://www.simscale.com/blog/what-is-pmv-ppd/>
- [17] S. Byggforsk, “Termisk inneklima. betingelser, tilrettelegging og målinger,” Oct 2017. [Online]. Available: https://www.byggforsk.no/dokument/193/termisk_inneklima_betingelser_tilrettelegging_og_maalinger
- [18] Standard Norge, “NS-EN 16798-1:2019 - Bygningers energiytelse - Ventilasjon i bygninger - Del 1: Inneklimaparametere for dimensjonering og vurdering av bygningers energiytelse inkludert inneluftkvalitet, termisk miljø, belysning og akustikk (Modul M1-6),” Aug 2019. [Online]. Available: <https://www.standard.no/no/Nettbutikk/produktkatalogen/Produktpresentasjon/?ProductID=1055687>
- [19] E. Haselsteine, “Gender Matters! Thermal Comfort and Individual Perception of Indoor Environmental Quality: A Literature Review,” in *Rethinking Sustainability Towards a Regenerative Economy*, M. Andreucci, M. Baltov, A. Marvuglia, and P. Hansen, Eds. Cham, Switzerland: Springer Nature, 2021, ch. 9, pp. 169–200, ISBN: 978-3-030-71819-0.
- [20] H. Gadd and S. Werner, “Daily heat load variations in swedish district heating systems,” *Applied Energy*, vol. 106, pp. 47–55, 2013. [Online]. Available: <https://doi.org/10.1016/j.apenergy.2013.01.030>
- [21] The Norwegian Water Resources and Energy Directorate (NVE), “Energy and effect,” Oct 2018. [Online]. Available: <https://www.nve.no/energy-consumption-and-efficiency/energy-consumption-in-norway/energy-and-effect/>
- [22] P. E. Dodds, I. Staffell, A. D. Hawkes, F. Li, P. Grünewald, W. McDowall, and P. Ekins, “Hydrogen and fuel cell technologies for heating: A review,” *International Journal of Hydrogen Energy*, vol. 40, no. 5, pp. 2065–2083, 2015. [Online]. Available: <https://doi.org/10.1016/j.ijhydene.2014.11.059>
- [23] J. Stene and V. Havellen, “Varmepumper til oppvarming og kjøling i bygninger,” 2016. [Online]. Available: https://byggalliansen.no/wp-content/uploads/2018/11/Varmepumper_Byggalliansen-Tipshefte-7.pdf
- [24] K. Treiakova and K. Ekker, “Energiutredning – alternativer til energiforsyning,” Sep 2013. [Online]. Available: <https://www.merzell.com/lv-lv/m/file/GetFile.ashx?id=44696552&version=1>
- [25] Eurostat, “Shedding light on energy in the EU: What kind of energy do we consume in the EU?” [Accessed 21-Feb-2023]. [Online]. Available: <https://ec.europa.eu/eurostat/cache/infographs/energy/bloc-3a.html>
- [26] I. Bryn, A. Petersen, and S. Gedsø, “Varmeløsninger og deres dekningsgrader,” Jan 2011. [Online]. Available: <https://www.doi.org/10.13140/RG.2.2.14012.56962>
- [27] J. Stene and O. Smedegård, “Hensiktsmessige varme- og kjøleløsninger i bygninger,” Mar 2013. [Online]. Available: https://www.enova.no/upload_images/380D698AC6CC4A0D98695AC29342ECDC.pdf

- [28] ENOVA SF, “Beregning av oppvarmingskarakteren,” Des 2021. [Online]. Available: <https://www.energimerking.no/no/energimerking-bygg/om-energimerkesystemet-og-regelverket/beregning-av-oppvarmingskarakteren/>
- [29] Viessmann, “How does an oil fired boiler work?” Mar 2022. [Online]. Available: <https://www.viessmann.co.uk/en/heating-advice/boilers/how-does-an-oil-fired-boiler-work.html>
- [30] ENOVA SF, “Kjøpsveileder utfasing av oljekjel,” [Accessed 02-Feb-2023]. [Online]. Available: https://www.enova.no/download?objectPath=upload_images/1AE561A7D99143A9982DFFD480422BA8.pdf
- [31] ENOVA SF, “Kjøpsveileder - utfasing av oljefyr/oljekamin,” [Accessed 02-Feb-2023]. [Online]. Available: https://www.enova.no/download?objectPath=/upload_images/EAE34D494E8849F690C6EEC26F6A2A99.pdf
- [32] ENOVA SF, “Biokjel,” [Accessed 02-Mar-2023]. [Online]. Available: <https://www.enova.no/privat/alle-energitiltak/biovarme/biokjel/>
- [33] W. H. O. Institution, “Solar Radiation,” [Accessed 22-Jan-2023]. [Online]. Available: <https://www.who.edu/science/AOPE/mvco/description/SolRad.html>
- [34] D. Rutz, C. Doczekal, R. Zweiler, M. Hofmeister, and L. L. Jensen, “Small Modular Renewable Heating and Cooling Grids - A Handbook,” 2017, ISBN: 978-3-936338-40-9. [Online]. Available: https://www.wip-munich.de/biolyfe-handbook/1_1_D4_1-Handbook-EN.pdf
- [35] N. Connor, “What is Coefficient of Performance – COP – Heat Pump – Definition,” May 2019. [Online]. Available: <https://www.thermal-engineering.org/what-is-coefficient-of-performance-cop-heat-pump-definition/>
- [36] Norsk Varmepumpeforening, “Hva er nordisk modell av varmepumper?” Feb 2023. [Online]. Available: <https://www.varmepumpeinfo.no/sporsmal-og-svar-om-varmepumper/hva-er-nordisk-modell>
- [37] SINTEF Byggforsk, “552.403 varmepumper i bygninger. funksjonsbeskrivelse,” Nov 2009. [Online]. Available: https://www.byggforsk.no/dokument/541/varmepumper_i_bygninger_funksjonsbeskrivelse
- [38] Norges Geologiske Undersøkelse (NGU), “GRUNNVARME,” Nov 2020. [Online]. Available: <https://www.ngu.no/emne/grunnvarme>
- [39] SINTEF Byggforsk, “451.021 klimadata for termisk dimensjonering og frostsikring,” Nov 2018. [Online]. Available: https://www.byggforsk.no/dokument/204/klimadata_for_termisk_dimensjonering_og_frostsikring
- [40] United States Department of Energy, “Geothermal heat pumps,” 2022. [Online]. Available: <https://www.energy.gov/energysaver/geothermal-heat-pumps>
- [41] United States Environmental Protection Agency (EPA), “Geothermal heating and cooling technologies,” Sep 2022. [Online]. Available: <https://www.epa.gov/rhc/geothermal-heating-and-cooling-technologies>
- [42] Office of Energy Efficiency and Renewable Energy (EERE), “Ground-source heat pumps,” Jan 2015. [Online]. Available: <https://basel.pnnl.gov/resource-guides/ground-source-heat-pumps>

- [43] Statkraft, "District heating," [Accessed 23-Feb-2023]. [Online]. Available: <https://www.statkraft.com/what-we-do/district-heating/>
- [44] S. O. Slinde, "Mythbusting: "Burning waste to produce district heating is not climate-friendly",," 2019. [Online]. Available: <https://www.statkraftvarme.no/en/kunnskapssenter/nyheter/2019/mythbusting-burning-waste-to-produce-district-heating-is-not-climate-friendly22/>
- [45] S. Werner, "District heating and cooling," in *Reference Module in Earth Systems and Environmental Sciences*. Elsevier, 2013, ISBN: 978-0-12-409548-9. [Online]. Available: <https://doi.org/10.1016/B978-0-12-409548-9.01094-0>
- [46] ENOVA, "Fjernvarme," 2022. [Online]. Available: <https://www.enova.no/bedrift/energisystem/fjernvarme/>
- [47] D. Basciotti, F. Judex, O. Pol, and R.-R. Schmidt, "Sensible heat storage in district heating networks: a novel control strategy using the network as storage," in *Conference proceedings of the 6th international renewable energy storage conference IRES*, 2011. [Online]. Available: https://www.iea-shc.org/data/sites/1/publications/Task42-Sensible_Heat_Storage_in_District_Heating_Networks.pdf
- [48] M. Koschenz and B. Lehmann, *Thermoaktive Bauteilsysteme tabs*. Springer, 2000, ISBN: 9783905594195. [Online]. Available: <https://doi.org/10.1007/978-3-658-31163-6>
- [49] Uponor, "Thermally activated building systems," [Accessed 25-Jan-2023]. [Online]. Available: <https://www.uponor.com/en-en/products/ceiling-heating-and-cooling/tabs>
- [50] "Analysis of control strategies for thermally activated building systems under demand side management mechanisms," *Energy and Buildings*, vol. 80, pp. 384–393, 2014. [Online]. Available: <https://doi.org/10.1016/j.enbuild.2014.05.053>
- [51] Grant UK, "Maximising the benefits of combined heating technologies," Jun 2020. [Online]. Available: <https://www.grantuk.com/knowledge-hub/tips-advice/maximising-the-benefits-of-combined-heating-technologies/>
- [52] J.-C. Hadorn, *Solar and Heat Pump Systems for Residential Buildings*. Ernst & Sohn, Sep 2015, ISBN: 978-3-433-60484-7.
- [53] A. Lisauskas, "Solar Calculations for the Raseiniai District Heating Plant," Oct 2014. [Online]. Available: https://www.solarthermalworld.org/sites/default/files/news/file/2017-08-03/sdh_calculations_for_raseiniai_planenergi_october2014.pdf
- [54] N. Kraftwerke, "What does peak shaving mean?" [Accessed 2-Feb-2023]. [Online]. Available: <https://www.next-kraftwerke.com/knowledge/what-is-peak-shaving>
- [55] U.S. Energy Information Administration (EIA), "Electric utility demand side management," 2000. [Online]. Available: <https://www.eia.gov/electricity/data/eia861/dsm/>
- [56] Government of Western Australia - Office of Energy, "Demand management," Sep 2010. [Online]. Available: https://web.archive.org/web/20100928011636/http://www.energy.wa.gov.au/2/3203/64/demand_management.pm

- [57] E. Guelpa and V. Verda, "Demand response and other demand side management techniques for district heating: A review," *Energy*, vol. 219, p. 119440, 2021. [Online]. Available: <https://doi.org/10.1016/j.energy.2020.119440>
- [58] U.S. Energy Department - Office of Electricity, "Demand response," [Accessed 12-Apr-2023]. [Online]. Available: <https://www.energy.gov/oe/demand-response>
- [59] H. Gadd and S. Werner, *Thermal energy storage systems for district heating and cooling*, 1st ed. Woodhead Publishing, 2015, p. 467–478, ISBN: 978-1-78242-088-0. [Online]. Available: <http://urn.kb.se/resolve?urn=urn:nbn:se:hh:diva-27091>
- [60] L. Olsson Ingvarson and S. Werner, "Building mass used as short term heat storage," 2008. [Online]. Available: <http://urn.kb.se/resolve?urn=urn:nbn:se:hh:diva-6035>
- [61] J. A. Noël, S. Kahwaji, L. Desgrosseilliers, D. Groulx, and M. A. White, "Chapter 13 - phase change materials," in *Storing Energy*, T. M. Letcher, Ed. Oxford: Elsevier, 2016, pp. 249–272, ISBN: 978-0-12-803440-8. [Online]. Available: <https://doi.org/10.1016/B978-0-12-803440-8.00013-0>
- [62] C. A. Cruickshank and C. Baldwin, "19 - sensible thermal energy storage: diurnal and seasonal," in *Storing Energy (Second Edition)*, second edition ed., T. M. Letcher, Ed. Elsevier, 2022, pp. 419–441, ISBN: 978-0-12-824510-1. [Online]. Available: <https://doi.org/10.1016/B978-0-12-824510-1.00018-0>
- [63] B. Baeten, F. Rogiers, and L. Helsen, "Reduction of heat pump induced peak electricity use and required generation capacity through thermal energy storage and demand response," *Applied Energy*, vol. 195, pp. 184–195, 2017. [Online]. Available: <https://doi.org/10.1016/j.apenergy.2017.03.055>
- [64] Simenergi, "Simien - om oss," [Accessed 07-Apr-2023]. [Online]. Available: <https://simien.no/om-oss/>
- [65] Simenergi, "Simien PRO," [Accessed 07-Apr-2023]. [Online]. Available: <https://simien.no/simien-pro/>
- [66] TRNSYS, "TRNSYS: Transient System Simulation Tool," [Accessed 07-Apr-2023]. [Online]. Available: <https://www.trnsys.com/#1>
- [67] EnergyPlus, "EnergyPlus," [Accessed 07-Apr-2023]. [Online]. Available: <https://energyplus.net/>
- [68] EQUA Simulation AB, "IDA Indoor Climate and Energy," [Accessed 07-Apr-2023]. [Online]. Available: <https://www.equa.se/en/ida-ice>
- [69] EQUA Simulation AB, "Validations certifications," [Accessed 07-Apr-2023]. [Online]. Available: <https://www.equa.se/en/ida-ice/validation-certifications>
- [70] G. Salvalai, "Implementation and validation of simplified heat pump model in IDA-ICE energy simulation environment," *Energy and Buildings*, vol. 49, pp. 132–141, 2012. [Online]. Available: <https://doi.org/10.1016/j.enbuild.2012.01.038>
- [71] EQUA Simulation AB, "Exhaust air heat pump for residential," [Accessed 07-Apr-2023]. [Online]. Available: <https://www.equa.se/en/ida-ice/case-studies/exhaust-air>
- [72] M. Airaksinen and M. Vuolle, "Heating energy and peak-power demand in a standard and low energy building," *Energies*, vol. 6, no. 1, p. 235–250, Jan 2013. [Online]. Available: <http://dx.doi.org/10.3390/en6010235>

- [73] A. Hayati, J. Akander, and M. Eriksson, "A case study of mapping the heating storage capacity in a multifamily building within a district heating network in mid-sweden," *Buildings*, vol. 12, no. 7, p. 1007, Jul 2022. [Online]. Available: <http://dx.doi.org/10.3390/buildings12071007>
- [74] J. Heier, C. Bales, and V. Martin, "Thermal energy storage in swedish single family houses: a case study," in *InnoStock The 12th International Conference on Energy Storage: Book of Abstract*, 2012, ISBN: 978-84-938793-4-1. [Online]. Available: <http://urn.kb.se/resolve?urn=urn:nbn:se:kth:diva-118729>
- [75] V. Fransson, H. Bagge, and D. Johansson, "Investigating parameters affecting the indoor temperature drop after a power cut - in-situ measurements and simulations," *Building and Environment*, vol. 125, pp. 401–413, 2017. [Online]. Available: <https://doi.org/10.1016/j.buildenv.2017.07.028>
- [76] E. Guelpa, "Impact of thermal masses on the peak load in district heating systems," *Energy*, vol. 214, p. 118849, 2021. [Online]. Available: <https://doi.org/10.1016/j.energy.2020.118849>
- [77] J. Hirsche, Z. Li, K. R. Gluesenkamp, T. J. LaClair, and S. Graham, "Demand reduction and energy saving potential of thermal energy storage integrated heat pumps," *International Journal of Refrigeration*, vol. 148, pp. 179–192, 2023. [Online]. Available: <https://doi.org/10.1016/j.ijrefrig.2023.01.026>
- [78] T. Benakopoulos, W. Vergo, M. Tunzi, R. Salenbien, J. Kolarik, and S. Svendsen, "Energy and cost savings with continuous low temperature heating versus intermittent heating of an office building with district heating," *Energy*, vol. 252, p. 124071, 2022. [Online]. Available: <https://doi.org/10.1016/j.energy.2022.124071>
- [79] K. Foteinaki, R. Li, T. Péan, C. Rode, and J. Salom, "Evaluation of energy flexibility of low-energy residential buildings connected to district heating," *Energy and Buildings*, vol. 213, p. 109804, 2020. [Online]. Available: <https://doi.org/10.1016/j.enbuild.2020.109804>
- [80] D. Basciotti and R.-R. Schmidt, "Demand side management in district heating networks: Simulation case study on load shifting," *Euroheat and Power (English Edition)*, vol. 10, pp. 43–46, 01 2013. [Online]. Available: https://www.researchgate.net/publication/288189851_Demand_side_management_in_district_heating_networks_Simulation_case_study_on_load_shifting
- [81] H. Hajian, K. Ahmed, and J. Kurnitski, "Dynamic heating control measured and simulated effects on power reduction, energy and indoor air temperature in an old apartment building with district heating," *Energy and Buildings*, vol. 268, p. 112174, 2022. [Online]. Available: <https://doi.org/10.1016/j.enbuild.2022.112174>
- [82] P. Ala-Kotila, T. Vainio, and J. Heinonen, "Demand response in district heating market—results of the field tests in student apartment buildings," *Smart Cities*, vol. 3, no. 2, p. 157–171, Mar 2020. [Online]. Available: <http://dx.doi.org/10.3390/smartcities3020009>
- [83] A. Arteconi, D. Costola, P. Hoes, and J. Hensen, "Analysis of control strategies for thermally activated building systems under demand side management mechanisms," *Energy and Buildings*, vol. 80, pp. 384–393, 2014. [Online]. Available: <https://doi.org/10.1016/j.enbuild.2014.05.053>
- [84] A. Arteconi, N. Hewitt, and F. Polonara, "Domestic demand-side management (dsm): Role of heat pumps and thermal energy storage (tes) systems," *Applied Thermal Engineering*, vol. 51, no. 1, pp. 155–165, 2013. [Online]. Available: <https://doi.org/10.1016/j.applthermaleng.2012.09.023>

- [85] J. Tarragona, C. Fernández, L. F. Cabeza, and A. de Gracia, “Economic evaluation of a hybrid heating system in different climate zones based on model predictive control,” *Energy Conversion and Management*, vol. 221, p. 113205, 2020. [Online]. Available: <https://doi.org/10.1016/j.enconman.2020.113205>
- [86] B. Alimohammadisagvand, S. Alam, M. Ali, M. Degefa, J. Jokisalo, and K. Sirén, “Influence of energy demand response actions on thermal comfort and energy cost in electrically heated residential houses,” *Indoor and Built Environment*, vol. 26, no. 3, pp. 298–316, 2017. [Online]. Available: <https://doi.org/10.1177/1420326X15608514>
- [87] B. Baeten, F. Rogiers, and L. Helsen, “Reduction of heat pump induced peak electricity use and required generation capacity through thermal energy storage and demand response,” *Applied Energy*, vol. 195, pp. 184–195, 2017. [Online]. Available: <https://doi.org/10.1016/j.apenergy.2017.03.055>
- [88] M. D. Knudsen, L. Georges, K. S. Skeie, and S. Petersen, “Experimental test of a black-box economic model predictive control for residential space heating,” *Applied Energy*, vol. 298, p. 117227, 2021. [Online]. Available: <https://doi.org/10.1016/j.apenergy.2021.117227>
- [89] V. Amato, R. Hedegaard, M. Knudsen, and S. Petersen, “Room-level load shifting of space heating in a single-family house – a field experiment,” *Energy and Buildings*, vol. 281, p. 112750, 2023. [Online]. Available: <https://doi.org/10.1016/j.enbuild.2022.112750>
- [90] F. Li, G. Zheng, and Z. Tian, “Optimal operation strategy of the hybrid heating system composed of centrifugal heat pumps and gas boilers,” *Energy and Buildings*, vol. 58, pp. 27–36, 2013. [Online]. Available: <https://doi.org/10.1016/j.enbuild.2012.09.044>
- [91] Standard Norge, “NS 3701:2012 - Criteria for passive houses and low energy buildings - Non-residential buildings,” September 2012. [Online]. Available: <https://www.standard.no/no/Nettbutikk/produktkatalogen/Produktpresentasjon/?ProductID=587802>
- [92] P. Schild, “EPW Climate Files.” SINTEF Building Research Design Guides, 2014.
- [93] Direktoratet for byggkvalitet (DiBK), “TEK17 - § 13-3. Ventilasjon i byggverk for publikum og arbeidsbygning,” [Accessed 2-Mar-2023]. [Online]. Available: <https://dibk.no/regelverk/byggteknisk-forskrift-tek17/13/i/13-3>
- [94] Arbeidstilsynet, “Ventilasjon på arbeidsplassen,” [Accessed 2-Mar-2023]. [Online]. Available: <https://www.arbeidstilsynet.no/tema/inneklima/ventilasjon/>
- [95] Forbrukerrådet, “Spotpriser,” [Accessed 1-Apr-2023]. [Online]. Available: <https://www.strompris.no/spotpriser>

Appendix

A IDA ICE Climate for Blindern

The screenshot shows the 'Location' dialog box in IDA ICE. The 'Location' dropdown is set to 'Oslo - Blindern (Location)'. The 'Position' section contains the following data:

Country	Norway		
City	Oslo - Blindern		
Latitude	59.66047 N °	Elevation	94 m
Longitude	10.78199 E °	Time zone	1 E h

The 'Climate description' dropdown is also set to 'Oslo - Blindern'. The 'Design day data' section is divided into 'Winter' and 'Summer' columns:

	Winter	Summer	
Dry-bulb min	-22.5	16.3	°C
Dry-bulb max	-17.5	26.7	°C
Wet-bulb max	-17.712	17.4	°C
Wind direction	360	180	°
Wind speed	0.7	1	m/s
Clearness number	0	1	0-1

The 'Object' section shows the 'Name' as 'Oslo - Blindern (Location)' and an empty 'Description' field. At the bottom, there are buttons for 'OK', 'Cancel', 'Save as...', and 'Help'.

Figure 70: Location data for IDA ICE model

B Thermal Bridge inputs

Thermal bridges: object in 001 - Baseline (TEK17)

Envelope area definition

Internal
 Overall internal
 External
 External incl. floor slab
 Preserve wall volume

Thermal bridges

Category	Quality	Value	Unit
External wall / internal slab	Good	-0.0686	W/K/(m joint)*
External wall / internal wall	Good	-0.0686	W/K/(m joint)*
External wall / external wall	Typical	0	W/K/(m joint)
External windows perimeter	Typical	0	W/K/(m perim)
External doors perimeter	Typical	0	W/K/(m perim)
Roof / external walls	Typical	0	W/K/(m joint)
External slab / external walls	Typical	0	W/K/(m joint)
Balcony floor / external walls	Typical	0	W/K/(m joint)
External slab / Internal walls	Typical	-0.0686	W/K/(m joint)*
Roof / Internal walls	Typical	-0.073	W/K/(m joint)*
External walls, inner corner	Poor	0	W/K/(m joint)
External slab / external walls, inner corner	Poor	0	W/K/(m joint)
Roof / external walls, inner corner	Poor	0	W/K/(m joint)
Total envelope (incl. roof and ground) <small>(alternatively enter W/K/(m² floor area))</small>		0.029279	W/K/(m² envelope)

NB! When the area definition is changed here, envelope areas and U-values will also change. Make sure to verify, under Loss factor for thermal bridges in the zone form, that the final computation of thermal bridge losses matches your intentions. The reference construction (construction without thermal bridge losses) is visible in the 3D view when Wall thickness has been activated.

* total for both adjacent zones

IDA

Thermal bridge per m2 floor area

0.05

Ok Cancel

Figure 71: Input of thermal bridge value for TEK17 case building. Note that the required value of 0,05 $W/(m^2 \cdot K)$ is given per m^2 of floor area, hence requiring input in the red box.

Thermal bridges: object in 011 - Baseline (Passive)

Envelope area definition

Internal
 Overall internal
 External
 External incl. floor slab
 Preserve wall volume

Thermal bridges

	Good	Typical	Poor	Very poor	Value	Unit
External wall / internal slab					-0.0686	W/K/(m joint)*
External wall / internal wall					-0.0686	W/K/(m joint)*
External wall / external wall					0.0	W/K/(m joint)
External windows perimeter					0	W/K/(m perim)
External doors perimeter					0	W/K/(m perim)
Roof / external walls					0.0	W/K/(m joint)
External slab / external walls					0	W/K/(m joint)
Balcony floor / external walls					0	W/K/(m joint)
External slab / Internal walls					-0.0686	W/K/(m joint)*
Roof / Internal walls					-0.073	W/K/(m joint)*
External walls, inner corner					0.0	W/K/(m joint)
External slab / external walls, inner corner					0.0	W/K/(m joint)
Roof / external walls, inner corner					0.0	W/K/(m joint)
Total envelope (incl. roof and ground)					0.017568	W/K/(m² envelope)

(alternatively enter W/K/(m² floor area))

NB! When the area definition is changed here, envelope areas and U-values will also change. Make sure to verify, under Loss factor for thermal bridges in the zone form, that the final computation of thermal bridge losses matches your intentions. The reference construction (construction without thermal bridge losses) is visible in the 3D view when Wall thickness has been activated.

* total for both adjacent zones

IDA

Thermal bridge per m2 floor area

0.03

Ok Cancel

Figure 72: Input of thermal bridge value for Passive House case building. Note that the required value of 0,03 $W/(m^2 \cdot K)$ is given per m^2 of floor area, hence requiring input in the red box.

C Occupancy Schedules

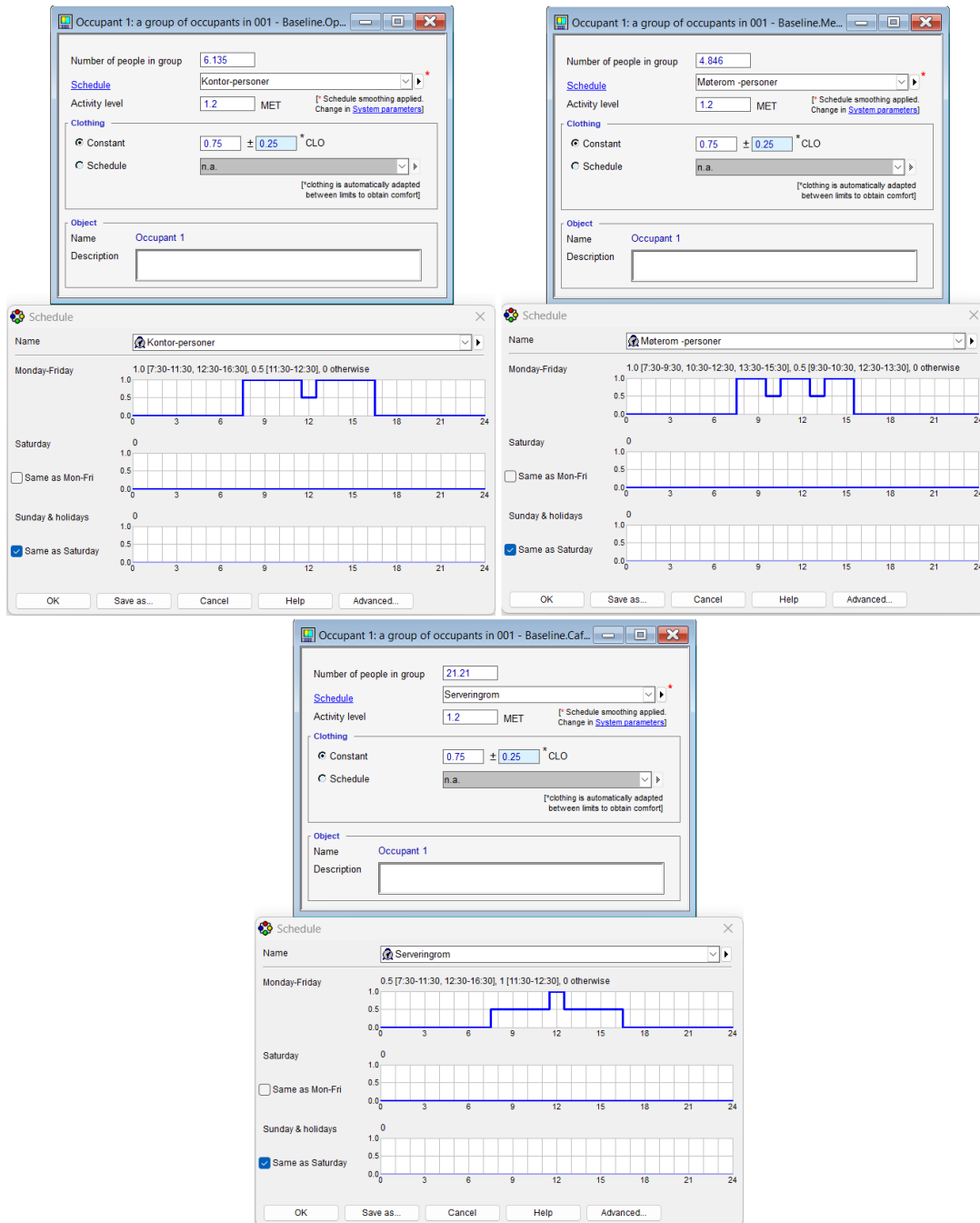


Figure 73: Occupancy schedules used in different zones. From upper left corner moving clockwise: Open Landscape, Meeting Room, Cafeteria

D Lighting Schedules

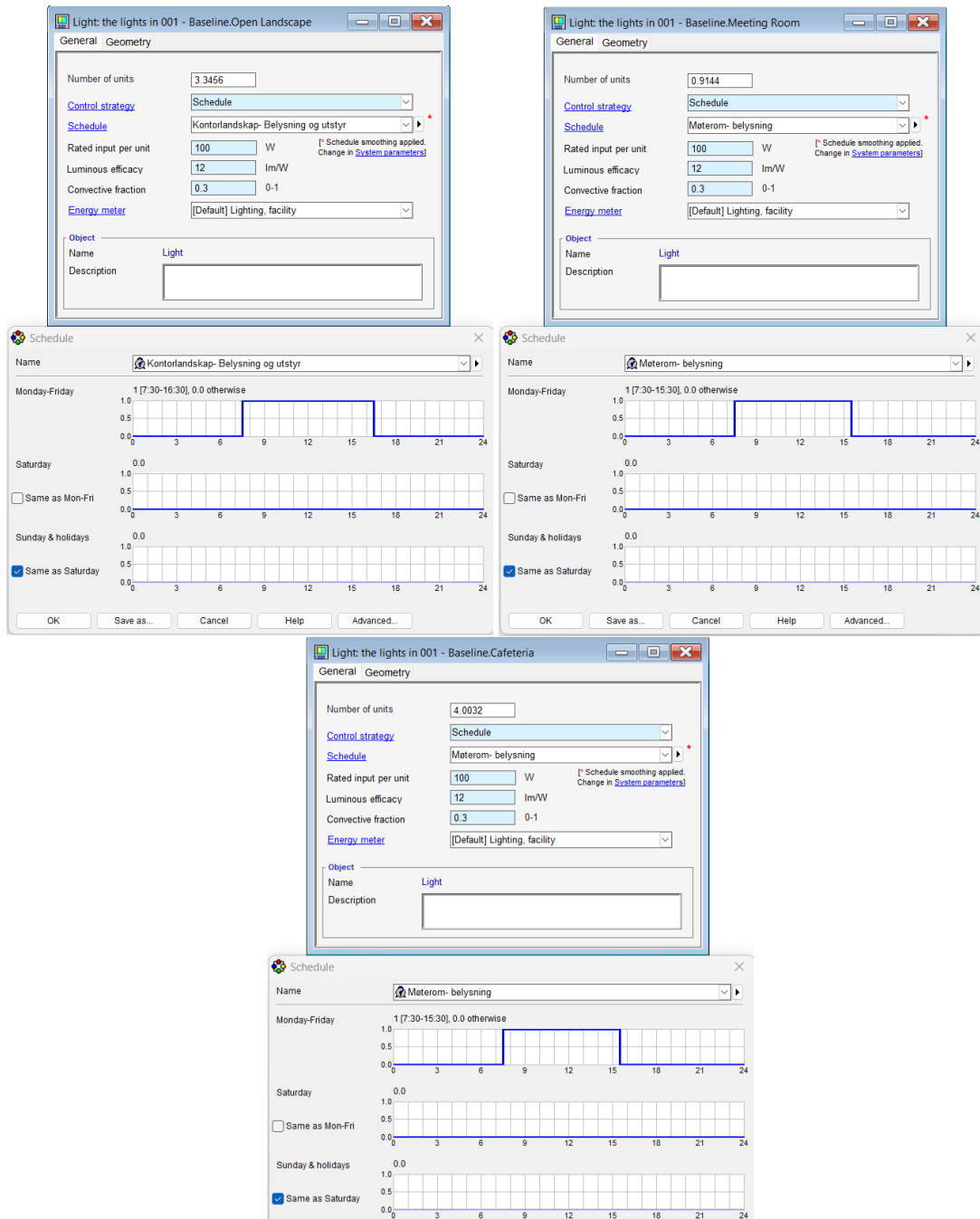


Figure 74: Lighting schedules used in different zones. From upper left corner moving clockwise: Open Landscape, Meeting Room, Cafeteria

E TEK17 & Passive House Window Details

Name	Type	Group	Zone	Face	Sill height from ground, m	Sill height from floor, m	Asmuth, Deg	Slope, Deg	Width, m	Height, m	Area, m ²	Glazing	g (SHGC)	T	Tvs	Glazing U, W/(m ² K)	Frame fract_0,1	Frame U, W/(m ² K)	Win total U, W/(m ² K)	Recess depth, m	Int shading	Control
Cafeteria Wall 3...	Window (detail...)	Cafete...	Buildin...	0.78	0.78	0.0	90.0	1.623	1.71	2.775	0.5	0.34	0.604	0.911	0.13	2.0	1.053	0.0	Generi...	Sun		
Cafeteria Wall 3...	Window (detail...)	Cafete...	Buildin...	0.78	0.78	0.0	90.0	1.623	1.71	2.775	0.5	0.34	0.604	0.911	0.13	2.0	1.053	0.0	Generi...	Sun		
Meeting Room...	Window (detail...)	Meetin...	Buildin...	0.75	0.75	0.0	90.0	1.0	1.9	1.9	0.5	0.34	0.604	0.911	0.14	2.0	1.063	0.0	Generi...	Sun		
Open Landsca...	Window (detail...)	Open...	Buildin...	0.8	0.8	270.0	90.0	1.0	1.8	1.8	0.5	0.34	0.604	0.911	0.13	2.0	1.053	0.0	Generi...	Sun		

Figure 75: Data regarding all the windows in the TEK17 case

Name	Type	Group	Zone	Face	Sill height from ground, m	Sill height from floor, m	Asmuth, Deg	Slope, Deg	Width, m	Height, m	Area, m ²	Glazing	g (SHGC)	T	Tvs	Glazing U, W/(m ² K)	Frame fract_0,1	Frame U, W/(m ² K)	Win total U, W/(m ² K)	Recess depth, m	Int shading	Control
Cafeteria Wall 3...	Window (detail...)	Cafete...	Buildin...	0.78	0.78	0.0	90.0	1.623	1.71	2.775	0.5	0.34	0.604	0.682	0.13	1.5	0.7883	0.0	Generi...	Sun		
Cafeteria Wall 3...	Window (detail...)	Cafete...	Buildin...	0.78	0.78	0.0	90.0	1.623	1.71	2.775	0.5	0.34	0.604	0.682	0.13	1.5	0.7883	0.0	Generi...	Sun		
Meeting Room...	Window (detail...)	Meetin...	Buildin...	0.75	0.75	0.0	90.0	1.0	1.9	1.9	0.5	0.34	0.604	0.682	0.14	1.5	0.7965	0.0	Generi...	Sun		
Open Landsca...	Window (detail...)	Open...	Buildin...	0.8	0.8	270.0	90.0	1.0	1.8	1.8	0.5	0.34	0.604	0.682	0.13	1.5	0.7883	0.0	Generi...	Sun		

Figure 76: Data regarding all the windows in the Passive House case

Detailed window construction

Name: Glass U=0,9

Layers

- Pane: PLANILUX 4mm.SGG (WIN7) (flipped)
- Gap: 10.0 mm Argon - EN673 (WIN7)
- Pane: LOW-E_5_LOF (WIN7)
- Gap: 10.0 mm Argon - EN673 (WIN7)
- Pane: Energy_glass-EN14501

Data for selected layer

Pane: PLANILUX 4mm.SGG (WIN7)

Flipped:

Glazing properties at reference conditions

Solar heat gain coefficient: 0.5

Solar transmittance: 0.34

Visible transmittance: 0.604

Glazing U-value: 0.911 W/(m²K)

Calculate

(a) TEK17 window glazing

Detailed window construction

Name: Glass U=0,682

Layers

- Pane: PLANILUX 4mm.SGG (WIN7) (flipped)
- Gap: 18.0 mm Argon - EN673 (WIN7)
- Pane: LOW-E_5_LOF (WIN7)
- Gap: 18.0 mm Argon - EN673 (WIN7)
- Pane: Energy_glass-EN14501

Data for selected layer

Pane: PLANILUX 4mm.SGG (WIN7)

Flipped:

Glazing properties at reference conditions

Solar heat gain coefficient: 0.5

Solar transmittance: 0.34

Visible transmittance: 0.604

Glazing U-value: 0.682 W/(m²K)

Calculate

(b) Passive House window glazing

Figure 77: Detailed window constructions for TEK17 case (a) and Passive House case (b)

F Materials for TEK17 External Walls

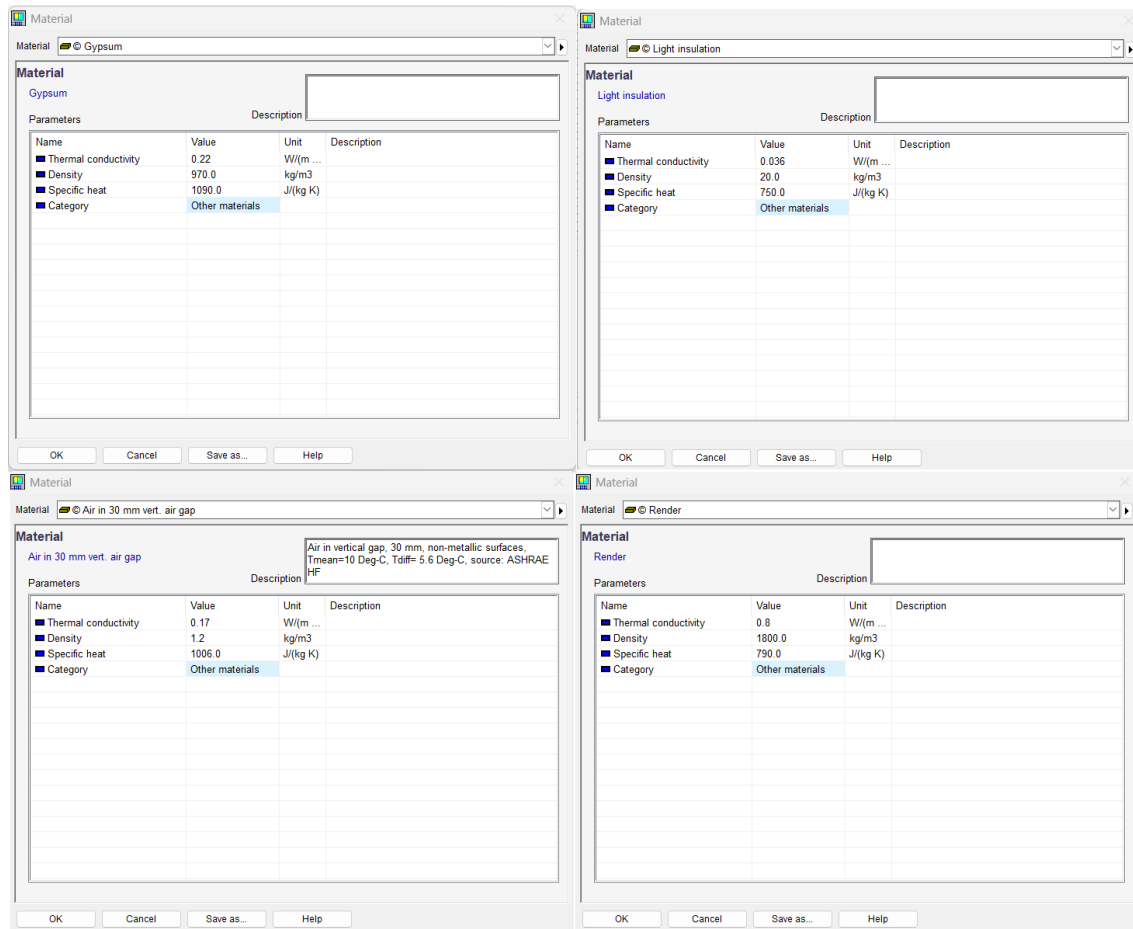


Figure 78: Construction materials for external walls in TEK17 case

G Materials for TEK17 Slab Towards Ground

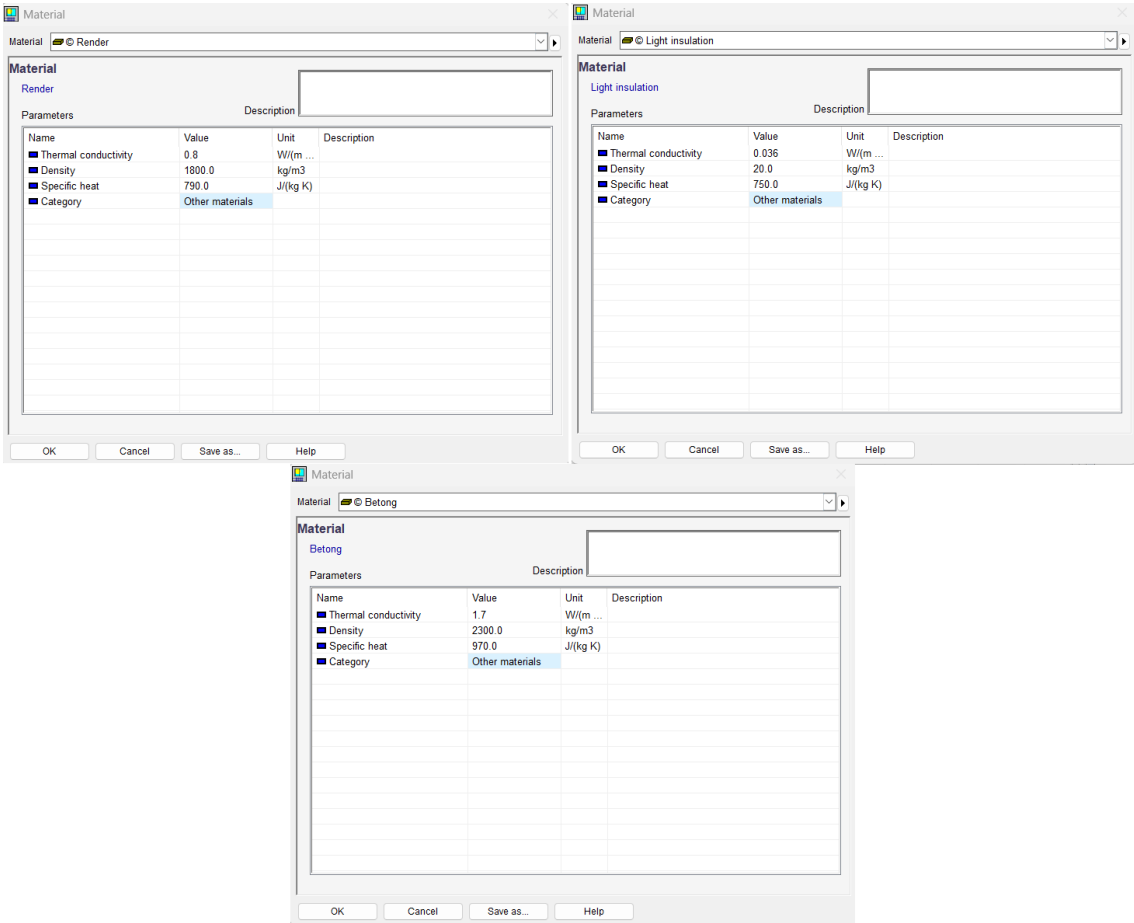


Figure 79: Construction materials for slab towards ground in TEK17 case

H Materials for Passive House External Walls

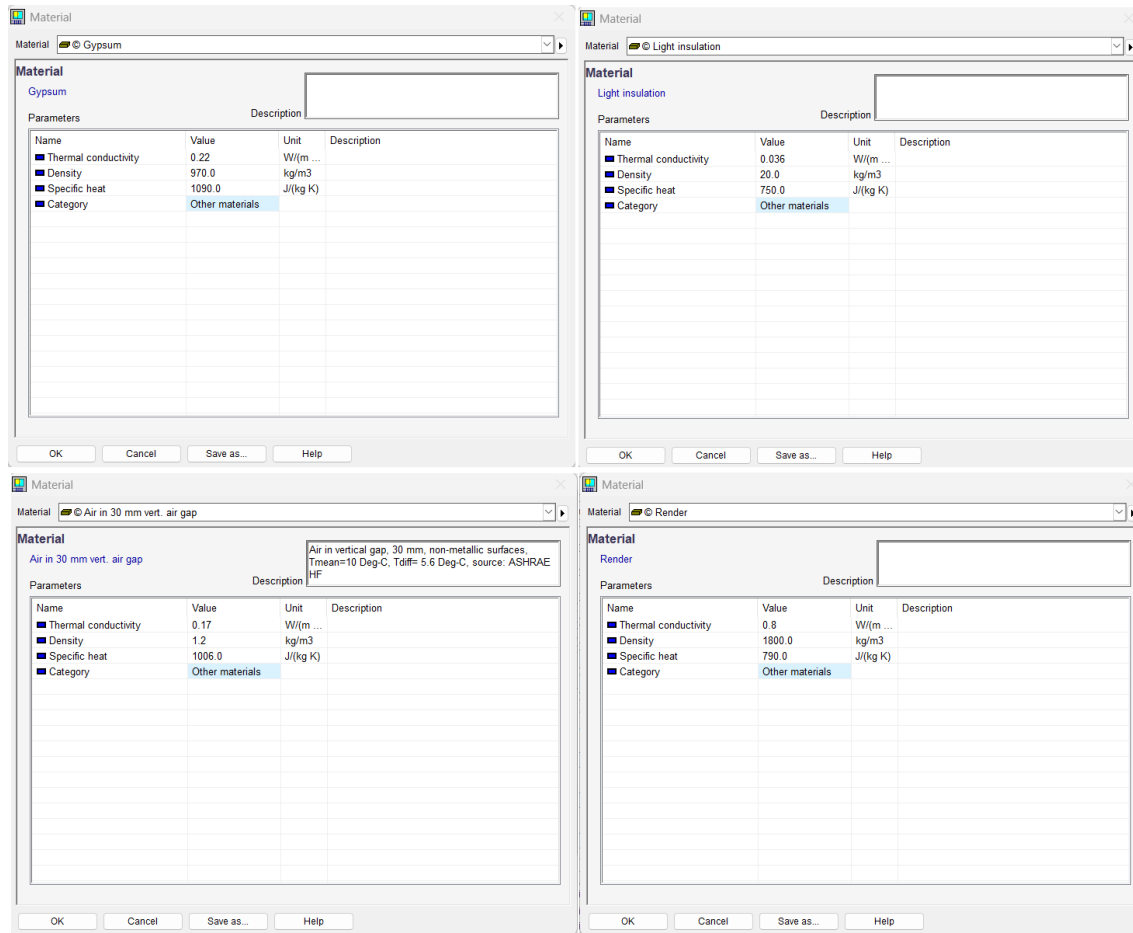


Figure 80: Construction materials for external walls in Passive House case

I Materials for Passive House Slab Towards Ground

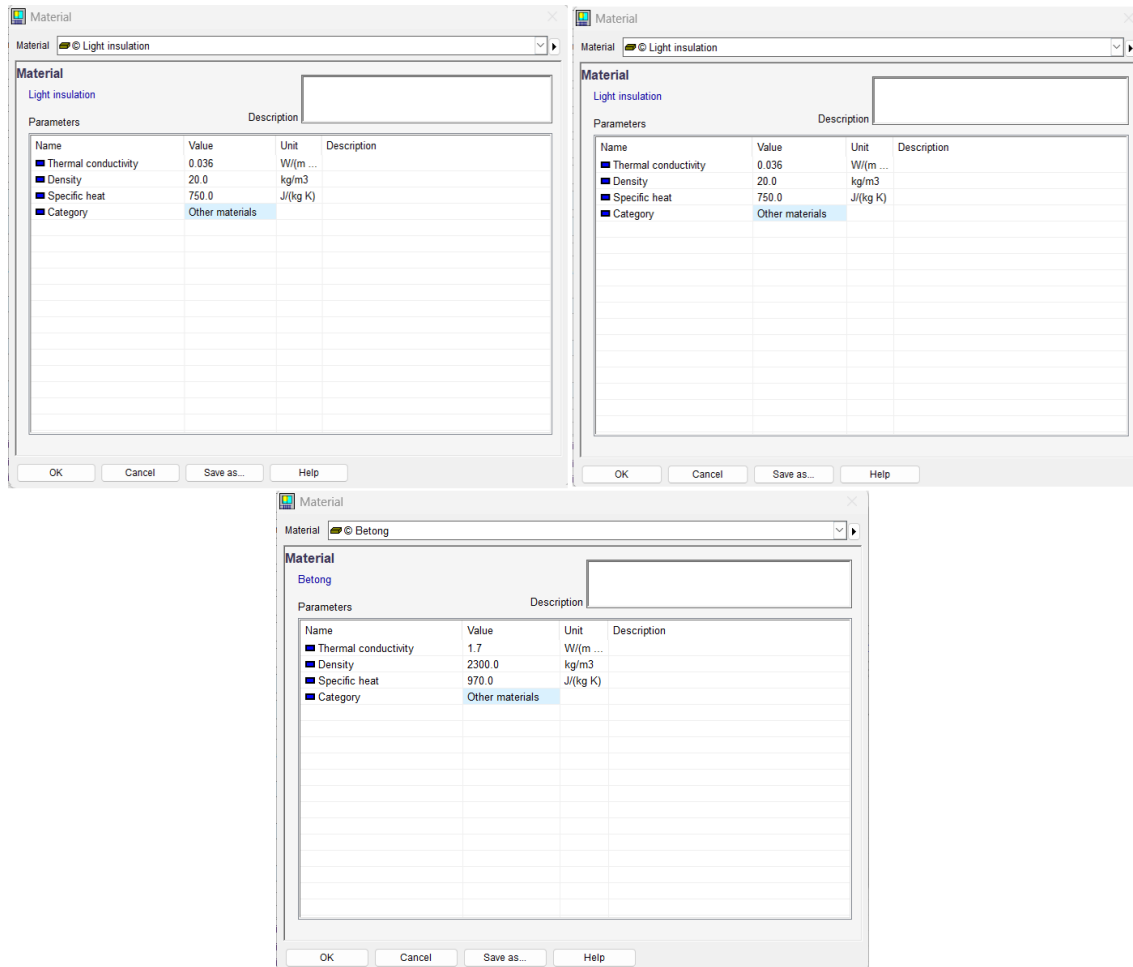



Figure 81: Construction materials for slab towards ground in Passive House case

J Heating Load Simulations

 EQUA SIMULATION TECHNOLOGY GROUP		<h3>Heating Load Report</h3>	
Project		Building	
Customer		Model floor area	137.7 m ²
Created by	Albin Zahiti	Model volume	371.9 m ³
Location	Oslo - Blindern (Location)	Model ground area	142.2 m ²
Climate file	Oslo - Blindern Climate	Model envelope area	254.1 m ²
Case	001 - Baseline (TEK17)	Window/Envelope	9.7 %
Simulated	27.04.2023 10:21:52	Average U-value	0.2506 W/(m ² K)
		Envelope area per Volume	0.6834 m ² /m ³

Zone Heating Loads

Zone	Group	Area, m ²	Heat supplied*, W	Time	Room unit heat, W	Vent. heat loss**, W	Temp., °C	Sup airflow, L/s
Cafeteria		66.7	794.2	16 Jan 07:12	862.5	68.9	20.2	46.9
Meeting Room		15.2	257.1	16 Jan 07:12	273.1	16.1	20.3	10.7
Open Landscape		55.8	866.1	17 Jan 06:59	927.4	61.0	20.2	39.3

* Maximum heat supplied by air and room units

** Heat lost through ventilation and infiltration at time of maximum heat supply

Air Handling Unit Heating Loads


Air Handling Unit	Heating*, W	Time	AHU heat recovery, W
AHU	2367.0	17 Jan 09:19:06	4448.0

* Total (sensible and latent) heat load

Total for Building

	Max., kW	Time
Zone heating	2.0	
AHU heating	1.8	
Total	3.8	17 Jan 06:05

Figure 82: Initial heating load simulation report

 EQUA SIMULATION TECHNOLOGY GROUP		<h2>Heating Load Report</h2>	
Project		Building	
		Model floor area	137.7 m ²
Customer		Model volume	371.9 m ³
Created by	Albin Zahiti	Model ground area	142.2 m ²
Location	Oslo - Blindern (Location)	Model envelope area	254.1 m ²
Climate file	Oslo - Blindern Climate	Window/Envelope	9.7 %
Case	001 - Baseline (TEK17)	Average U-value	0.2506 W/(m ² K)
Simulated	18.05.2023 11:57:39	Envelope area per Volume	0.6834 m ² /m ³

Zone Heating Loads

Zone	Group	Area, m ²	Heat supplied*, W	Time	Room unit heat, W	Vent. heat loss**, W	Temp., °C	Sup airflow, L/s
Cafeteria		66.7	677.2	15 Jan 14:30	747.4	68.8	20.4	46.9
Meeting Room		15.2	234.2	16 Jan 07:10	249.1	14.8	20.2	10.7
Open Landscape		55.8	809.1	17 Jan 07:12	878.0	68.9	20.4	39.3

* Maximum heat supplied by air and room units

** Heat lost through ventilation and infiltration at time of maximum heat supply

Air Handling Unit Heating Loads

Air Handling Unit	Heating*, W	Time	AHU heat recovery, W
AHU	2362.0	17 Jan 09:20:23	4456.0

* Total (sensible and latent) heat load

Total for Building

	Max., kW	Time
Zone heating	1.8	
AHU heating	1.8	
Total	3.6	17 Jan 06:04

Figure 83: Actual heating load simulation report

K Boiler Data

Name	Value	Start	Unit	Connected to	Logged to	Description
TEN	10		items			10
ETAPRIMARY	1.0		dimless			Boiler Overall efficiency
ELGENEFF	0.0		dimless			Electric generation efficiency
QMAX	3.836		kW			Maximum heating capacity
QIDLE	0.0		W			Power consumption when inactive
CPLIQ	4187.0		J/(kg K)			Liquid specific heat
MASS	10.0		kg			Boiler and circuit mass
NOMTERMEFF	0.0					Nominal thermal efficiency (if zero, overall efficiency is used)
TOUTLOW	30.0		°C			Min temperature
TOUTHIGH	85.0		°C			Max temperature
TAU	1.0		dimless			Time constant for TOUT (sec)
BEFF[1:10]	{0.0 0.0 0.0 0.0 0.0 0.0 0.0 0.0 0.0 0.0}					Coefficients in bicubic fcn(PLR,T) for boiling efficiency curve output
TBOIL	70.0	70.0	°C		[off]	Boiler temperature
TOUT	70.0		°C	topPump.TLIQIN	[off]	Temp of leaving liquid
P	0.0		Pa	HotTank.P[1]; to...	[off]	Pressure
M	0.04891		kg/s	HotTank.MOUT[1]; to...	[off]	Mass Flow Pum...
TOUTREQ	70.0		°C	<-- topAdd10...	[off]	Requested leaving temperature
TIN	60.77		°C	HotTank.TOUT[1]	[off]	Supply/Return (...)
BOILON	1.0	1.0	dimless	<-- Start value	[off]	Boil control signal
TOUTAS	70.0	60.0	°C		[off]	Temp of leaving liquid
MODE	1.0	1.0			[off]	Boiler mode 0 = Off 1 = Normal regime 2 = Full capacity
QSUP	1890.0		W		[off]	Supplied meter energy for heating
QREQ	1890.0		W		[off]	Requested heating power
QHEATING	1890.0		W		[off]	Boiler Output [W]
Q	1890.0		W		[off]	Plant details.TO...
PW	0.0		W		[off]	Electric Power generated
TOUTLIM	24.0		°C		[off]	Temp of leaving liquid used in fcn
QAVAIL	4000.0		W		[off]	Available cooling power
PLR	24.0				[off]	Part load ration
BOILEFF	1.0		dimless		[off]	Boiler efficiency
INLET				HotTank.OUT[1]		Entering liquid
OUTLET				topPump.INLET		Leaving liquid
TEMPSETP	70.0		°C	topAdd10.OUTS...	[off]	leaving liquid temperature setpoint
HEATCONTROL	1.0	1.0	dimless		[off]	Boil control signal
Energy meter	[Default] Electric heating					
PROD-ACCO...	[Default] CHP electricity					
Energy carrier	[Default] Electricity					

Figure 84: Input data for boiler in ESBO plant

L HotTank Data

Name	Value	Start	Unit	Connected to	Logged to	Description
IDEAL	1		items			1 for ideal tank
N_LAYER	2		items			number of tank layers
NAUX	0		items			number of auxilliary heaters
NIN	3		items			number of fittings for inlet
NOUT	3		items			number of fittings for outlet
NHX	1		items			number of internal heat exchangers (helix or segment of internal tank)
NREADTEMP	1		items			number of measurement points for tank temperature
NREADTEMPHX	1		items			number of measurement points for heat exchanger temperature
HOTORCOLD	HOT					hot or cold tank
SHUNT	Yes					Shunt used (default)
RTANK	0.1898		m			inner radius of tank
TNKWALTKN	0.002		m			wall Thickness of tank excluding insulation
HBULG	0.0		m			height of bulge at tank top
UCOAT	0.3		W/(m2 ...			General U-value of tank coat
UTOP	0.3		W/(m2 ...			U-value of tank top
UBOTTOM	0.3		W/(m2 ...			U-value of tank bottom
Q_DHW_LOSS	0.0		W			heat from losses in DHW circuit
ZOUT0	1.0		m			height of tank outlet 0
RHOLIQU	1000.0		kg/m3			water density
CPLIQU	4187.0		J/(kg K)			water mass heat capacity
LAMBDAWAT	0.6		W/(m K)			water heat conductivity
TNKWALCOND	50.0		W/(m K)			material heat conductivity of the tank wall
DLMAX	1.0		dimless			Max relative change between layers for in/out flows
DELTA	1.0		°C			minimal tempdiff to lower/upper neighbour for strat. loading
TAU	30.0		dimless			Time constant for TOUT (sec)
TAU	30.0		dimless			Time constant for min/max temp setpoints (sec)
MMIN	1.0E-8		kg/s			Min mass flow
PFACT	1.0		dimless			Factor
QLOSSPRV	500.0		W/K			Factor for Heat loss due to activation of pressure relief valve
TSETPRV	100.0		°C			Boiling temp of the fluid to open Press Relief Valve
FCOND	100000.0		dimless			Conductivity factor for temperature inversion
H_LAYER[1:2]	{0.949 0 ...		m			height of layer node
ZAUX[1:0]	{}		m			height of auxilliary heater
QMAX[1:0]	{}		W			maximal supplied heat to layer by auxiliary heater
ZIN[1:3]	{0.1 0.1 0...}		m			height of tank inlet
UAIN[1:3]	{0.0 0.0 0...}		W/K			UA-Value for heatloss of inlet
ZOUT[1:3]	{1.1 1.1 1...}		m			height of tank outlet
UAOUT[1:3]	{0.0 0.0 0...}		W/K			UA-Value for heatloss of outlet
ZHXIN[1:1]	{0.07923}		m			height of internal heat exchanger inlet
ZHXOUT[1:1]	{0.1585}		m			height of internal heat exchanger outlet
UAHX[1:1]	{400}		W/K			Heat transfer coefficient heatexchanger -> tank
VHX[1:1]	{0.01}		m3			total volume of internal heat exchanger
UAHXIN[1:1]	{0.0}		W/K			UA-Value for heatloss of internal heat exchanger inlet
UAHXOUT[1:1]	{0.0}		W/K			UA-Value for heatloss of internal heat exchanger outlet
LIQTYPE[1:1]	{Ethylene...}					Liquid type
TFREEZE[1:1]	{-25}		°C			Liquid freezing point temperature
ZREADTEMP[1:1]	{100}		m			height of temperatur reader
Energy meter	[Default] ...					

Figure 85: Parameters for HotTank in ESBO plant

M Controller Setpoints for Open Landscape

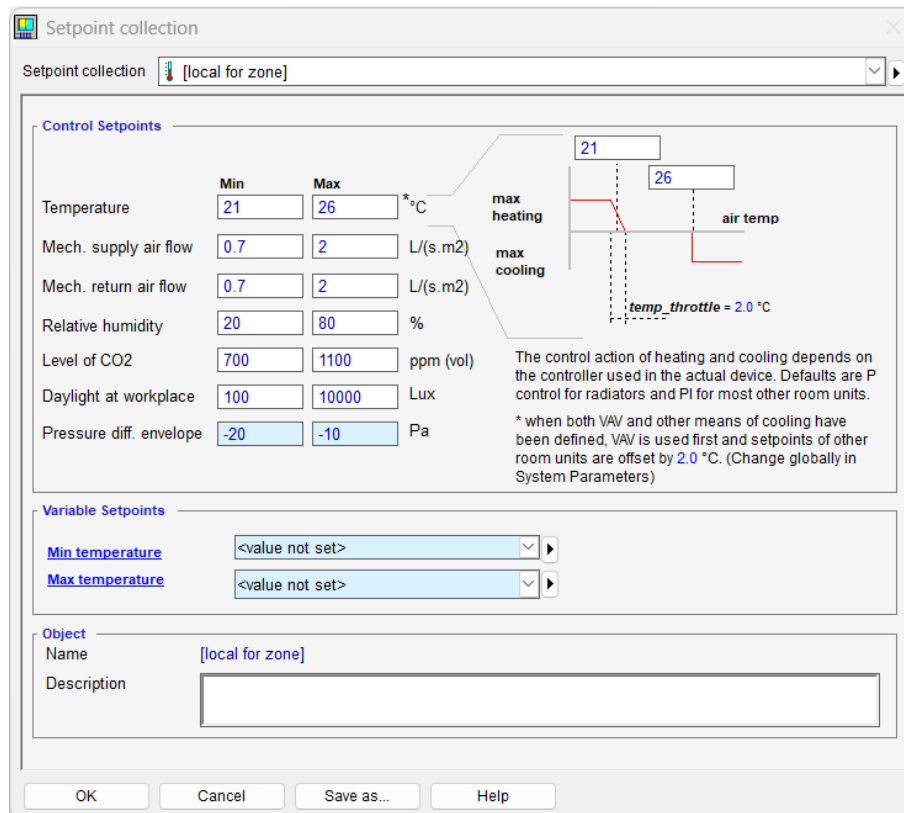


Figure 86: Setpoints for Open Landscape zone

N Main Temperatures & PPD for Open Landscape Zone

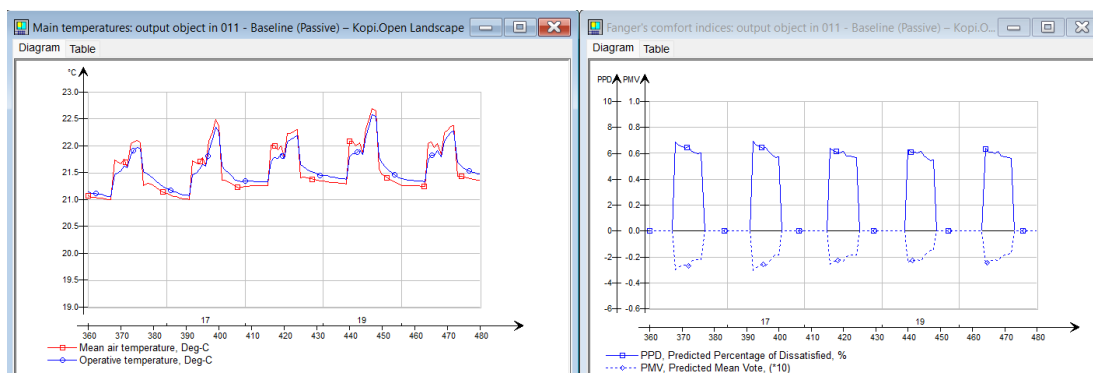


Figure 87: Main temperatures (left) and PPD (right) in Open Landscape zone from Simulation 1 for Passive House case

O AHU Temperatures & Mechanical Inflows for Open Landscape Zone

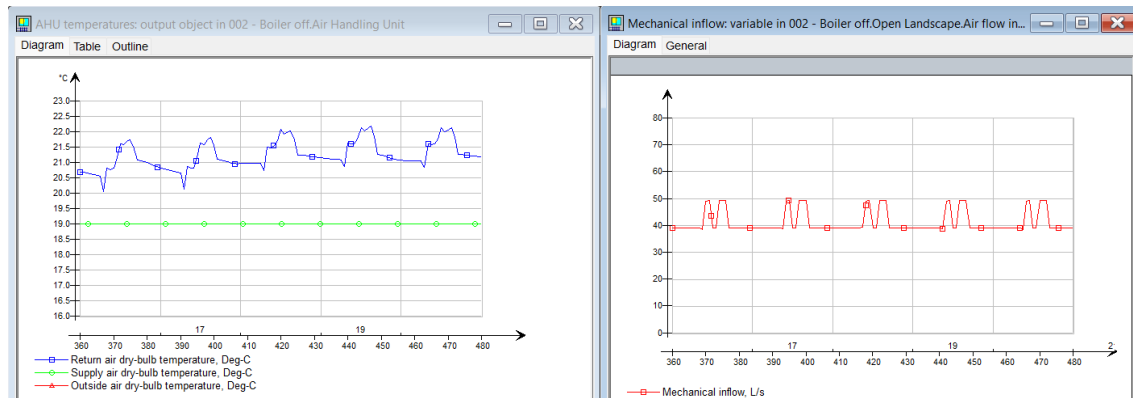


Figure 88: Supply & return air temperatures (left) and mechanical ventilation inflow (right) in Open Landscape zone from Simulation 2 for TEK17 case

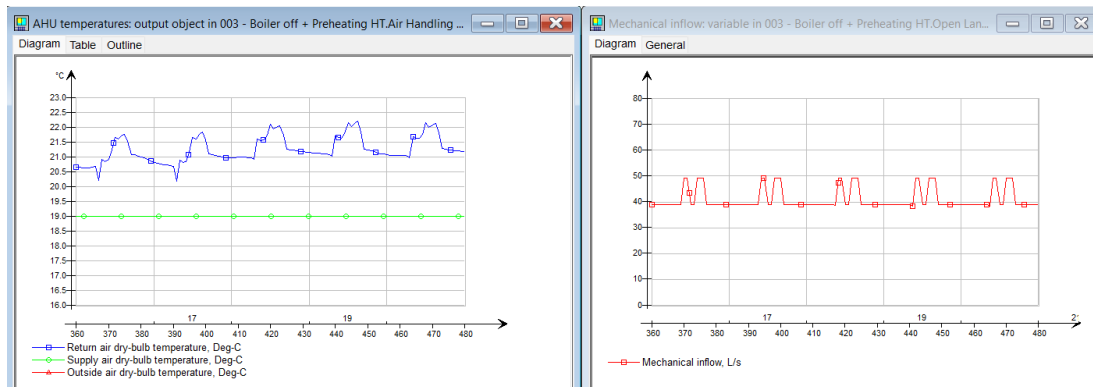


Figure 89: Supply & return air temperatures (left) and mechanical ventilation inflow (right) in Open Landscape zone from Simulation 3 for TEK17 case

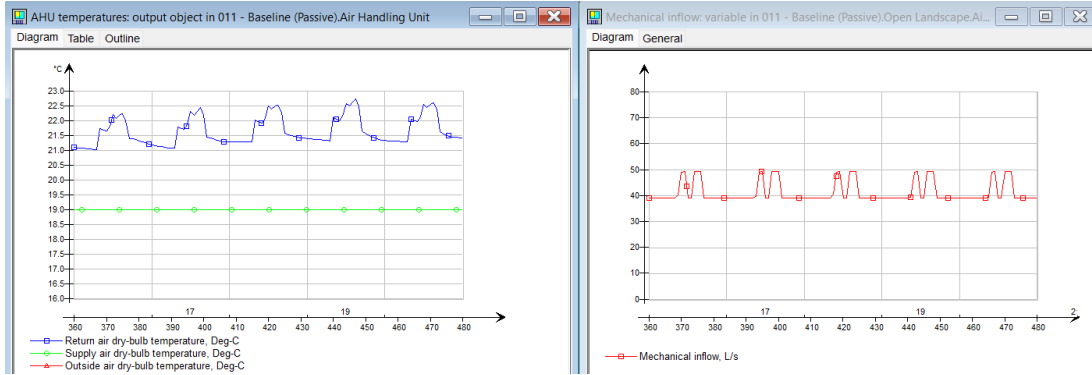


Figure 90: Supply & return air temperatures (left) and mechanical ventilation inflow (right) in Open Landscape zone from Simulation 1 for Passive House case

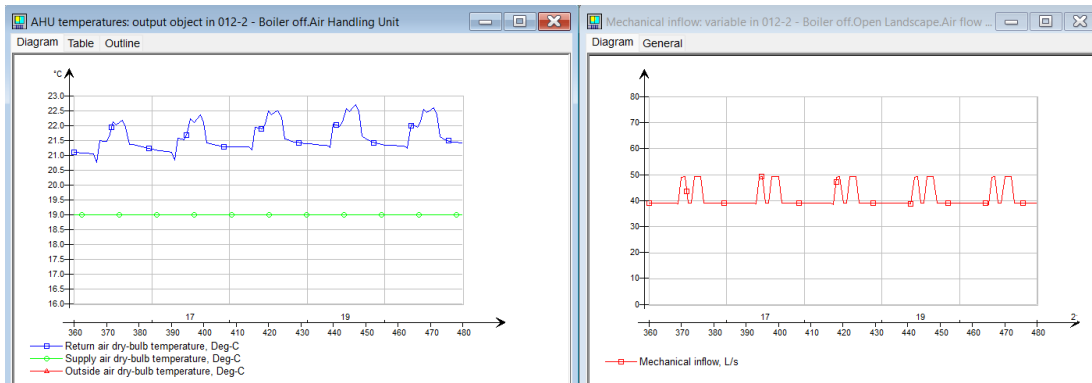


Figure 91: Supply & return air temperatures (left) and mechanical ventilation inflow (right) in Open Landscape zone from Simulation 2 for Passive House case

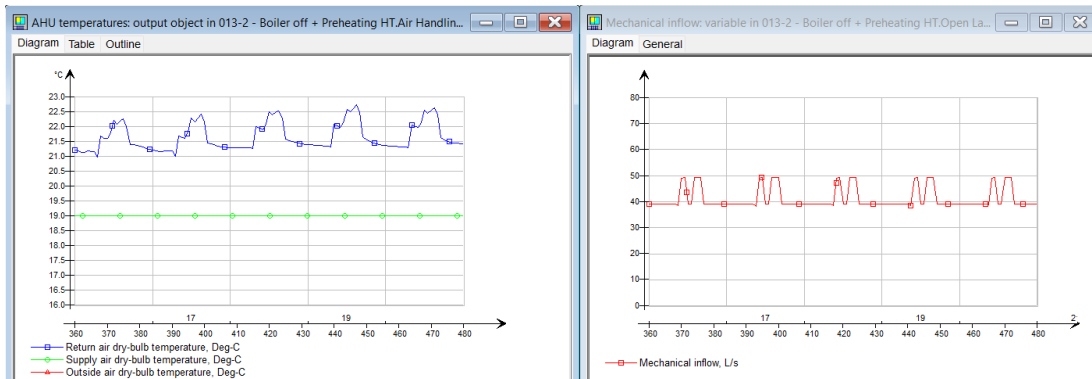


Figure 92: Supply & return air temperatures (left) and mechanical ventilation inflow (right) in Open Landscape zone from Simulation 3 for Passive House case

P Signals & Boiler Output (17.-18. January)

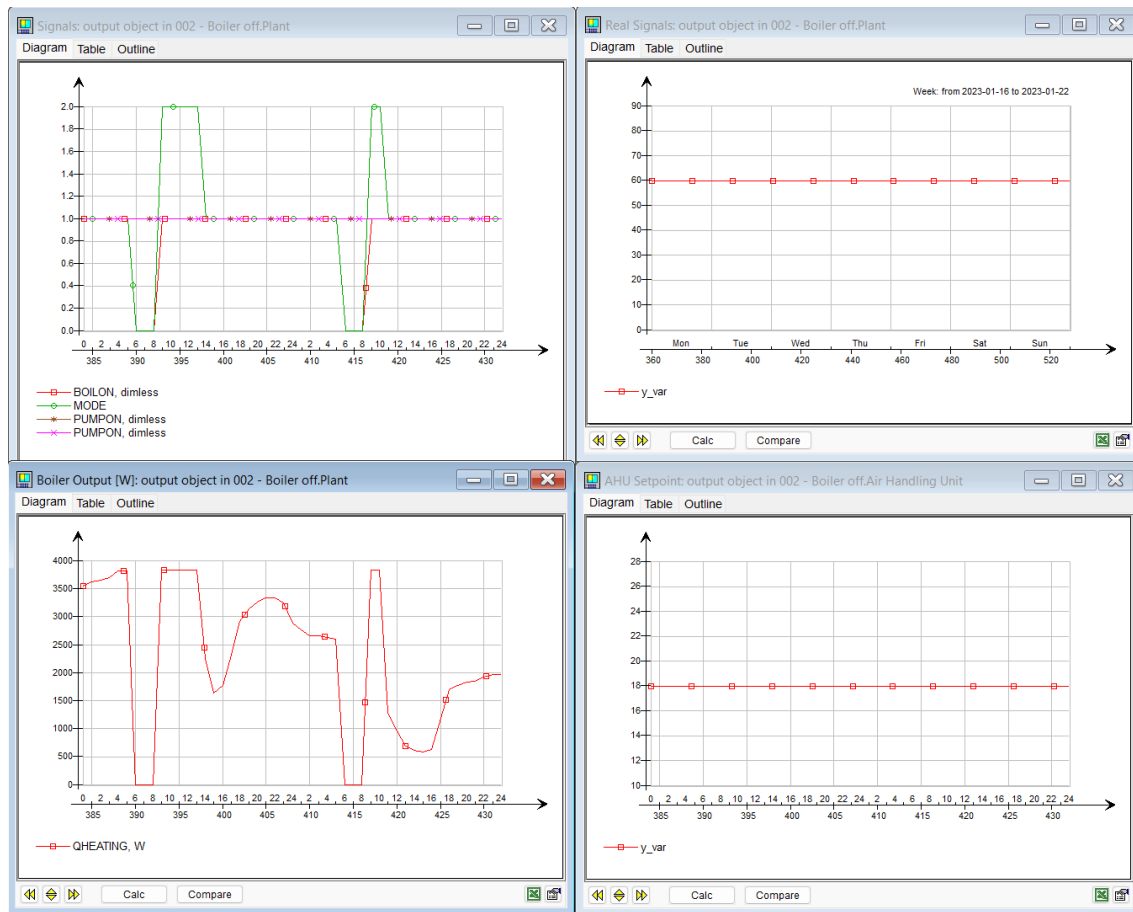


Figure 93: Signals and boiler output from Simulation 2 for TEK17 case. From left to right, top to bottom: Control signals (Boiler + AHU & zone pumps), Setpoint of boiler and PI controller [$^{\circ}\text{C}$], Boiler output [W], AHU controller SP [$^{\circ}\text{C}$] (Note that this is 1°C lower than resulting setpoint due to 1°C increase over supply fan).

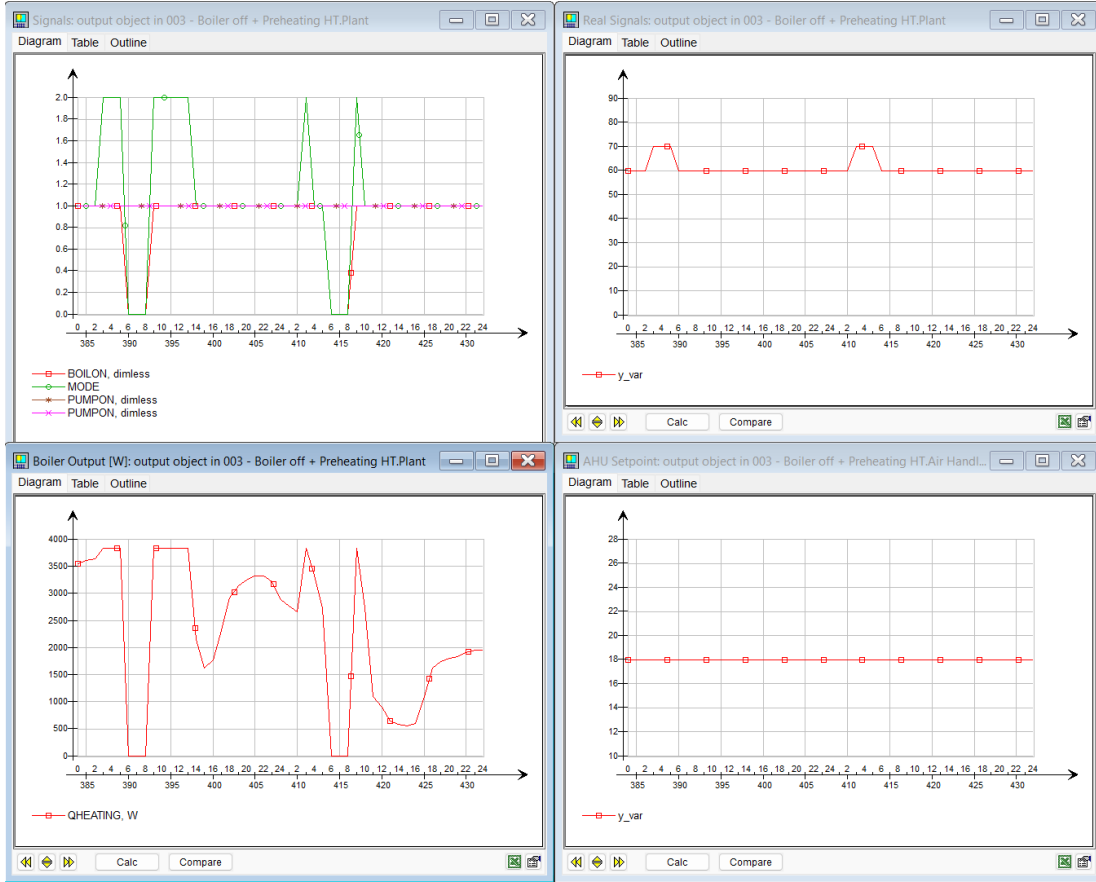


Figure 94: Signals and boiler output from Simulation 3 for TEK17 case. From left to right, top to bottom: Control signals (Boiler + AHU & zone pumps), Setpoint of boiler and PI controller [°C], Boiler output [W], AHU controller SP [°C] (Note that this is 1 °C lower than resulting setpoint due to 1 °C increase over supply fan).

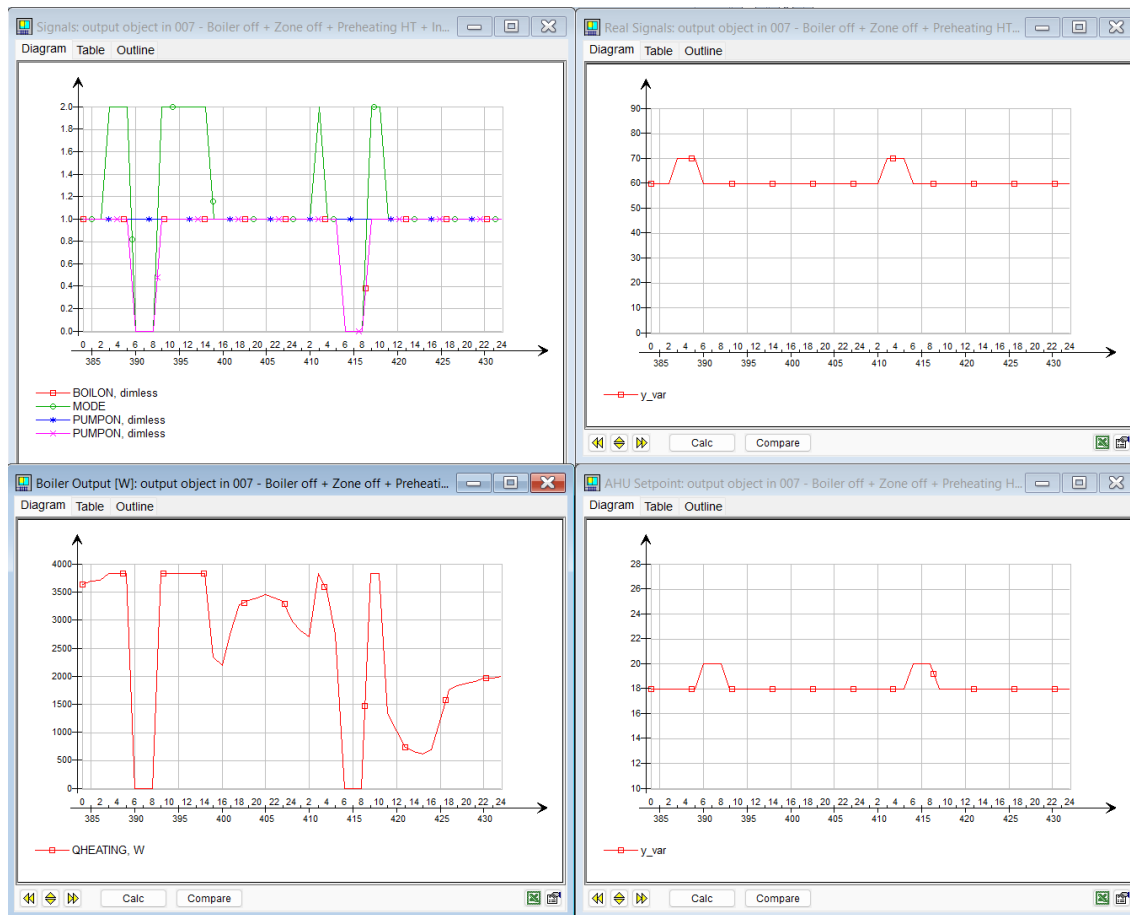


Figure 95: Signals and boiler output from Simulation 4 for TEK17 case. From left to right, top to bottom: Control signals (Boiler + AHU & zone pumps), Setpoint of boiler and PI controller [$^{\circ}\text{C}$], Boiler output [W], AHU controller SP [$^{\circ}\text{C}$] (Note that this is 1°C lower than resulting setpoint due to 1°C increase over supply fan).

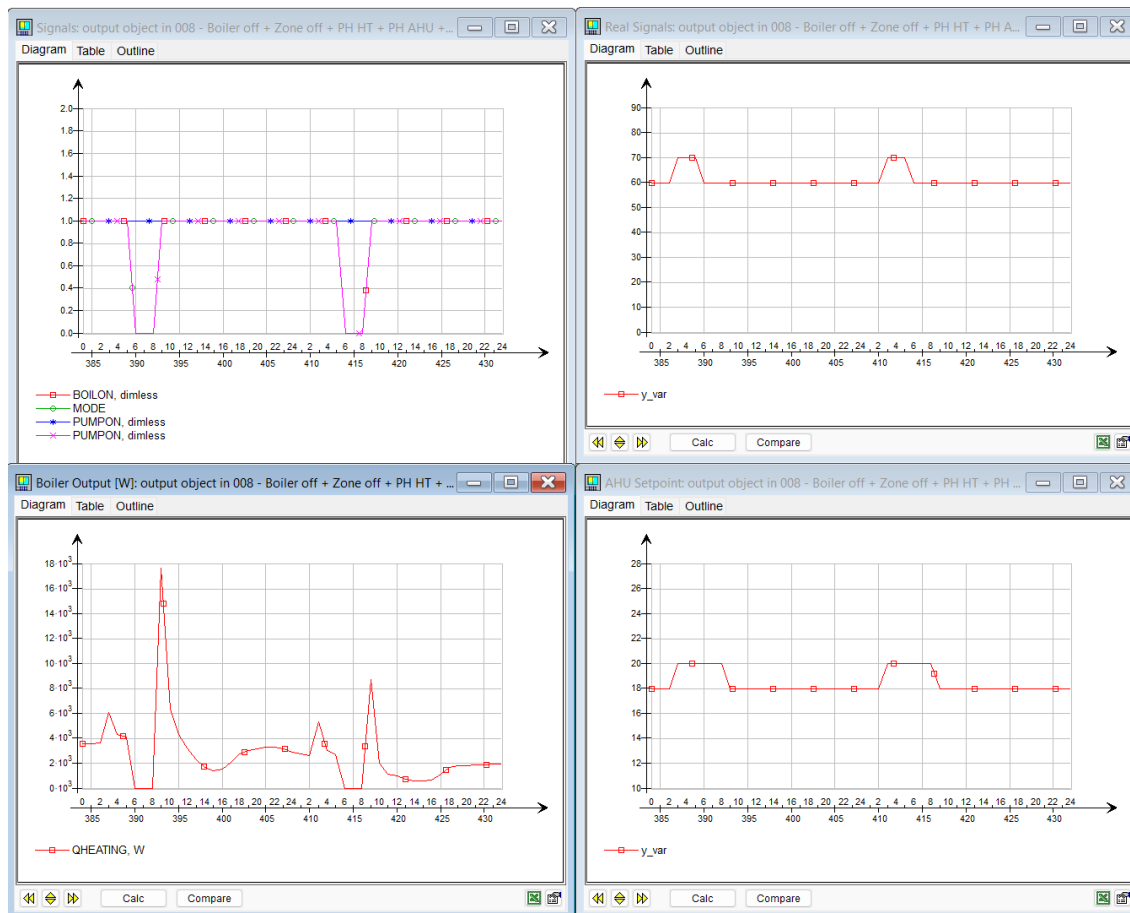


Figure 96: Signals and boiler output from Simulation 5A for TEK17 case. From left to right, top to bottom: Control signals (Boiler + AHU & zone pumps), Setpoint of boiler and PI controller [$^{\circ}\text{C}$], Boiler output [W], AHU controller SP [$^{\circ}\text{C}$] (Note that this is 1°C lower than resulting setpoint due to 1°C increase over supply fan).

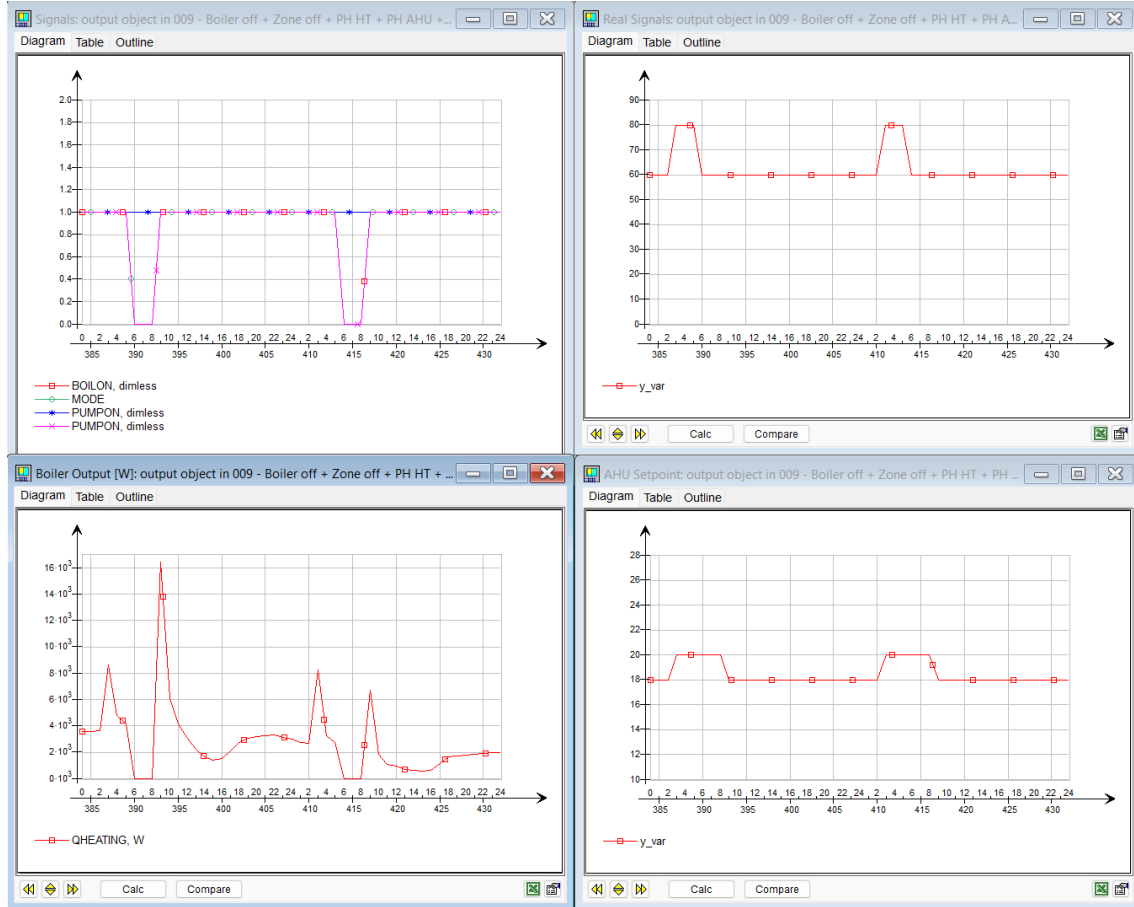


Figure 97: Signals and boiler output from Simulation 5B for TEK17 case. From left to right, top to bottom: Control signals (Boiler + AHU & zone pumps), Setpoint of boiler and PI controller [°C], Boiler output [W], AHU controller SP [°C] (Note that this is 1 °C lower than resulting setpoint due to 1 °C increase over supply fan).

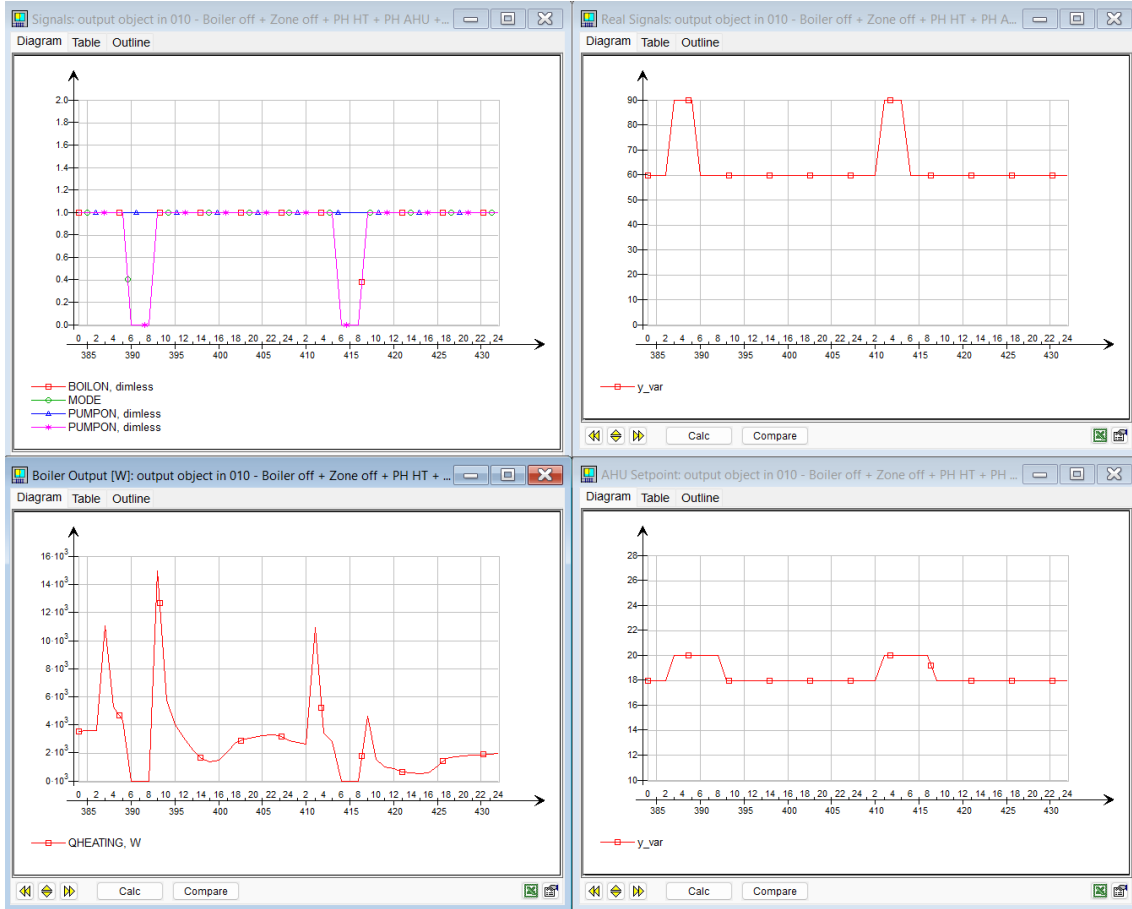


Figure 98: Signals and boiler output from Simulation 5C for TEK17 case. From left to right, top to bottom: Control signals (Boiler + AHU & zone pumps), Setpoint of boiler and PI controller [$^{\circ}\text{C}$], Boiler output [W], AHU controller SP [$^{\circ}\text{C}$] (Note that this is 1°C lower than resulting setpoint due to 1°C increase over supply fan).

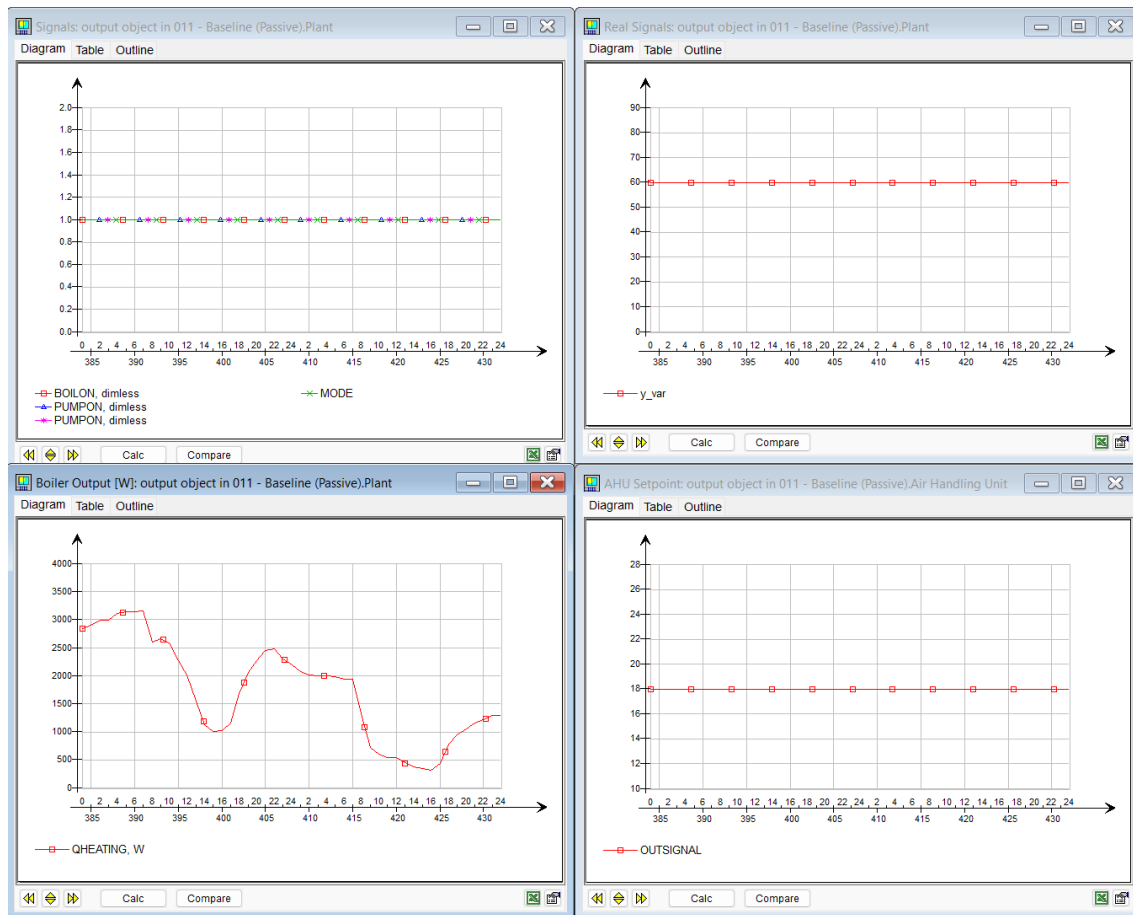


Figure 99: Signals and boiler output from Simulation 1 for Passive House case. From left to right, top to bottom: Control signals (Boiler + AHU & zone pumps), Setpoint of boiler and PI controller [$^{\circ}\text{C}$], Boiler output [W], AHU controller SP [$^{\circ}\text{C}$] (Note that this is 1°C lower than resulting setpoint due to 1°C increase over supply fan).

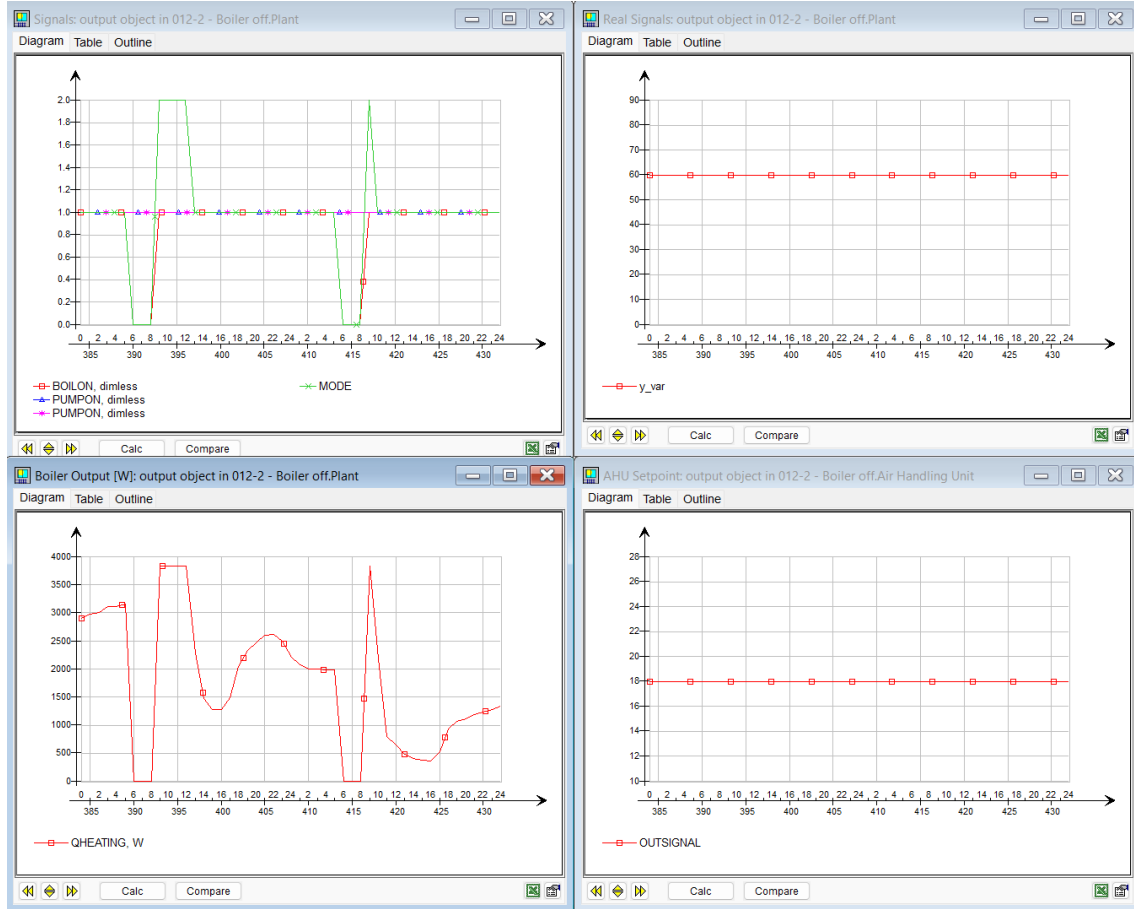


Figure 100: Signals and boiler output from Simulation 2 for Passive House case. From left to right, top to bottom: Control signals (Boiler + AHU & zone pumps), Setpoint of boiler and PI controller [°C], Boiler output [W], AHU controller SP [°C] (Note that this is 1 °C lower than resulting setpoint due to 1 °C increase over supply fan).

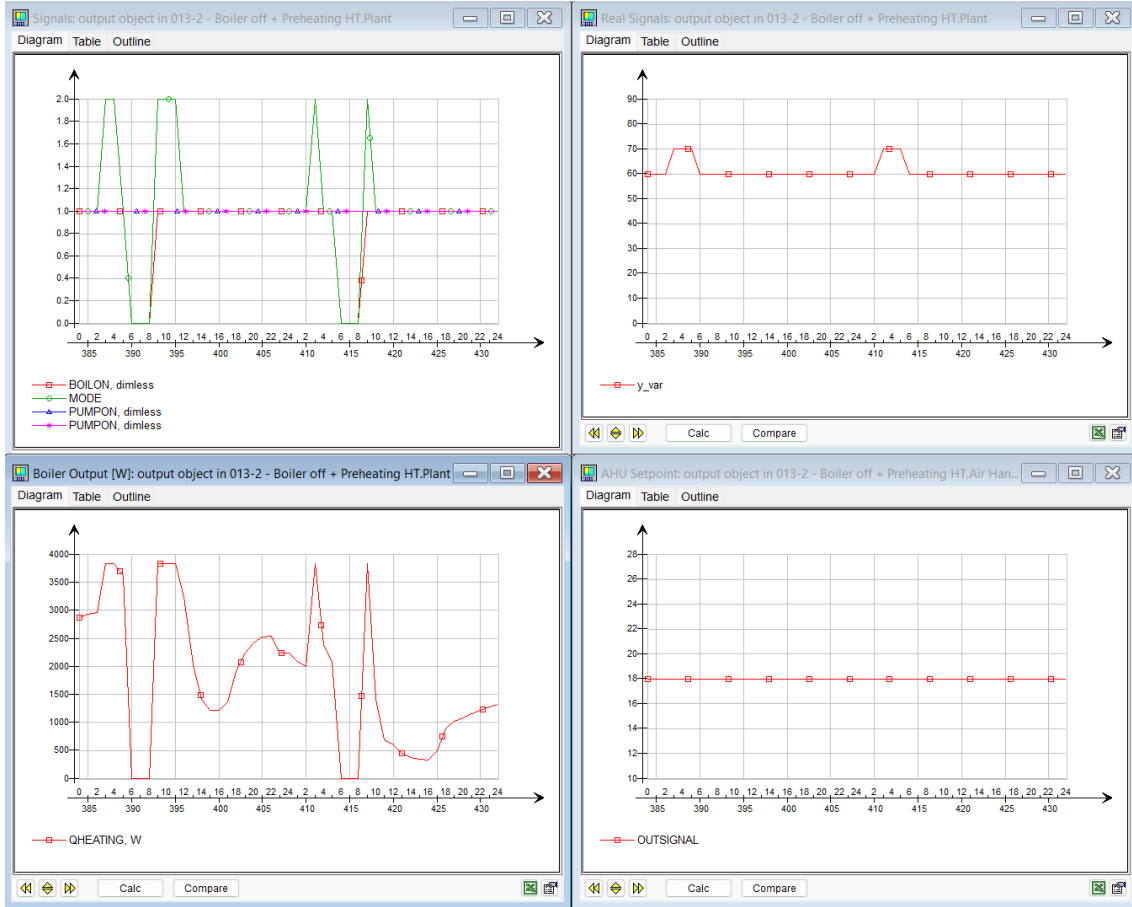


Figure 101: Signals and boiler output from Simulation 3 for Passive House case. From left to right, top to bottom: Control signals (Boiler + AHU & zone pumps), Setpoint of boiler and PI controller [$^{\circ}\text{C}$], Boiler output [W], AHU controller SP [$^{\circ}\text{C}$] (Note that this is 1°C lower than resulting setpoint due to 1°C increase over supply fan).

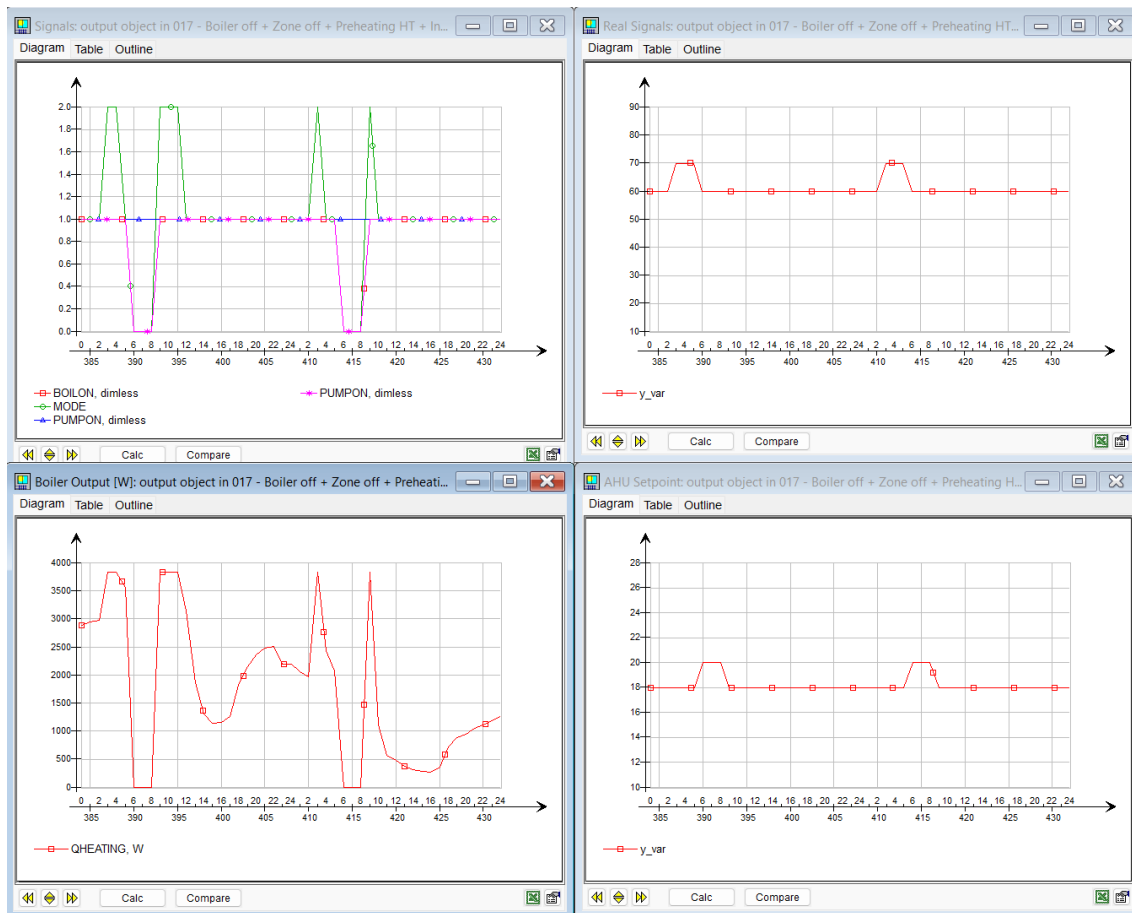


Figure 102: Signals and boiler output from Simulation 4 for Passive House case. From left to right, top to bottom: Control signals (Boiler + AHU & zone pumps), Setpoint of boiler and PI controller [$^{\circ}\text{C}$], Boiler output [W], AHU controller SP [$^{\circ}\text{C}$] (Note that this is 1°C lower than resulting setpoint due to 1°C increase over supply fan).

Q Supply & Return + HotTank Temperatures (16.-20. January)



Figure 103: TEK17 case - Simulation 5B. From left to right, top to bottom: Supply/Return temperatures for boiler circuit, Temperature of top and bottom layer of HotTank, Supply/Return temperatures for AHU circuit, Supply/Return temperatures for Zone heating circuit

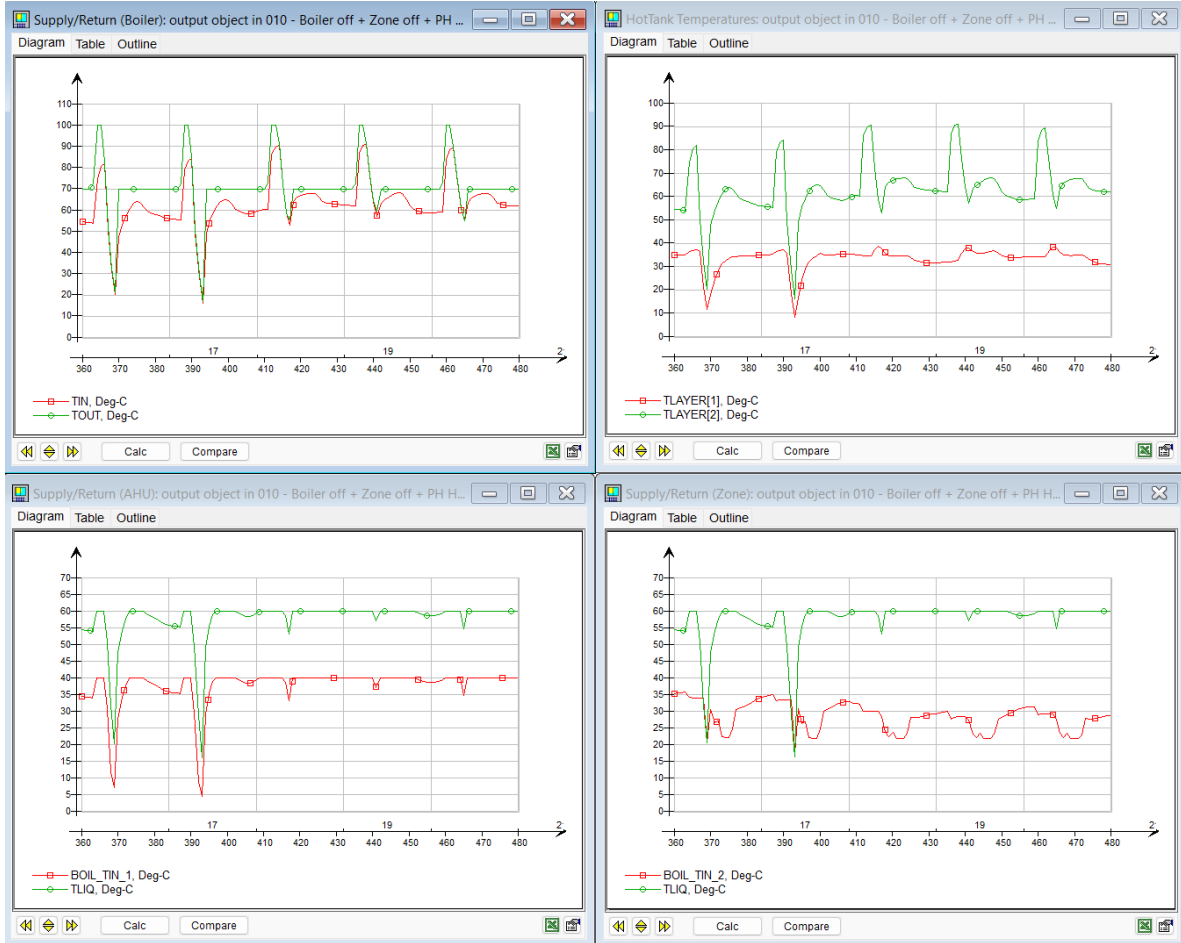


Figure 104: TEK17 case - Simulation 5C. From left to right, top to bottom: Supply/Return temperatures for boiler circuit, Temperature of top and bottom layer of HotTank, Supply/Return temperatures for AHU circuit, Supply/Return temperatures for Zone heating circuit

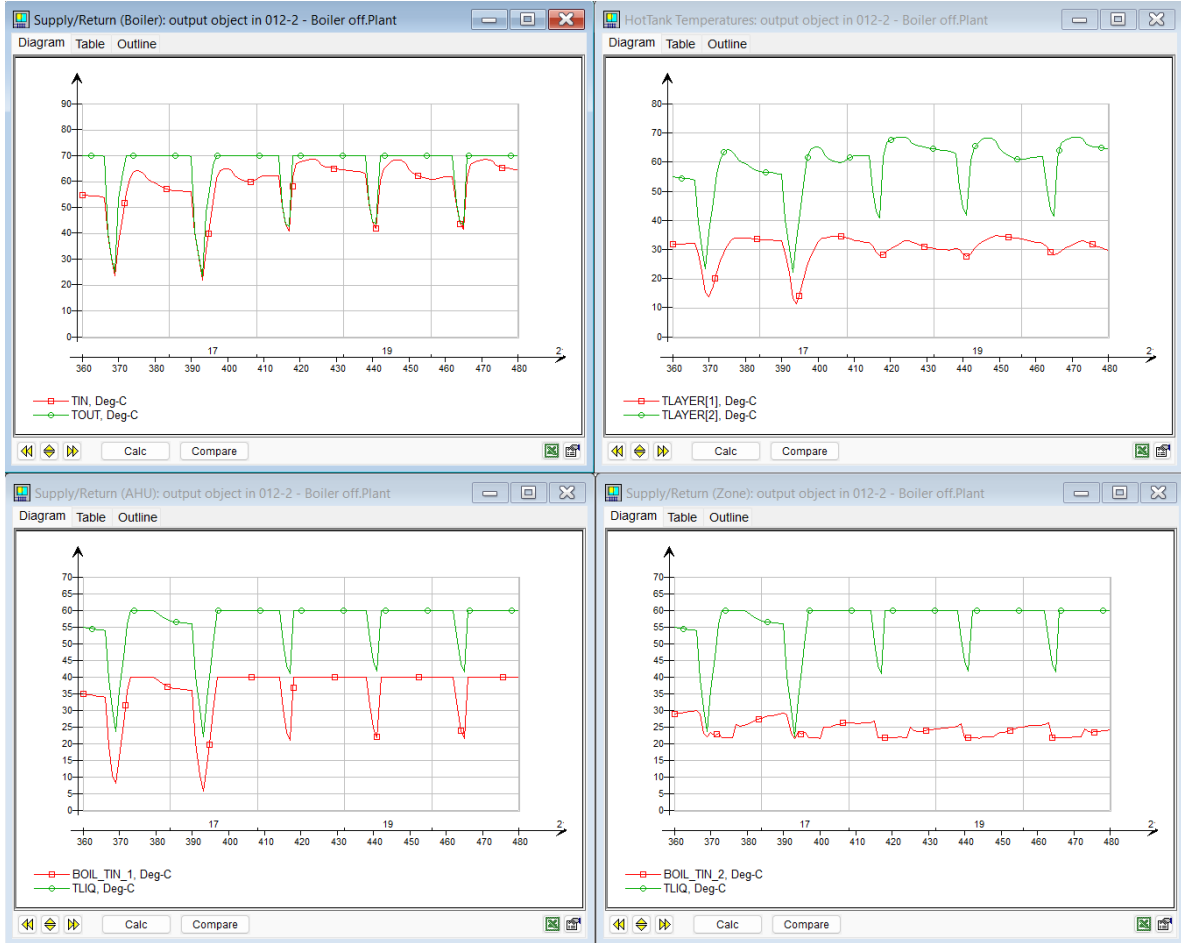


Figure 105: Passive House case - Simulation 2. From left to right, top to bottom: Supply/Return temperatures for boiler circuit, Temperature of top and bottom layer of HotTank, Supply/Return temperatures for AHU circuit, Supply/Return temperatures for Zone heating circuit

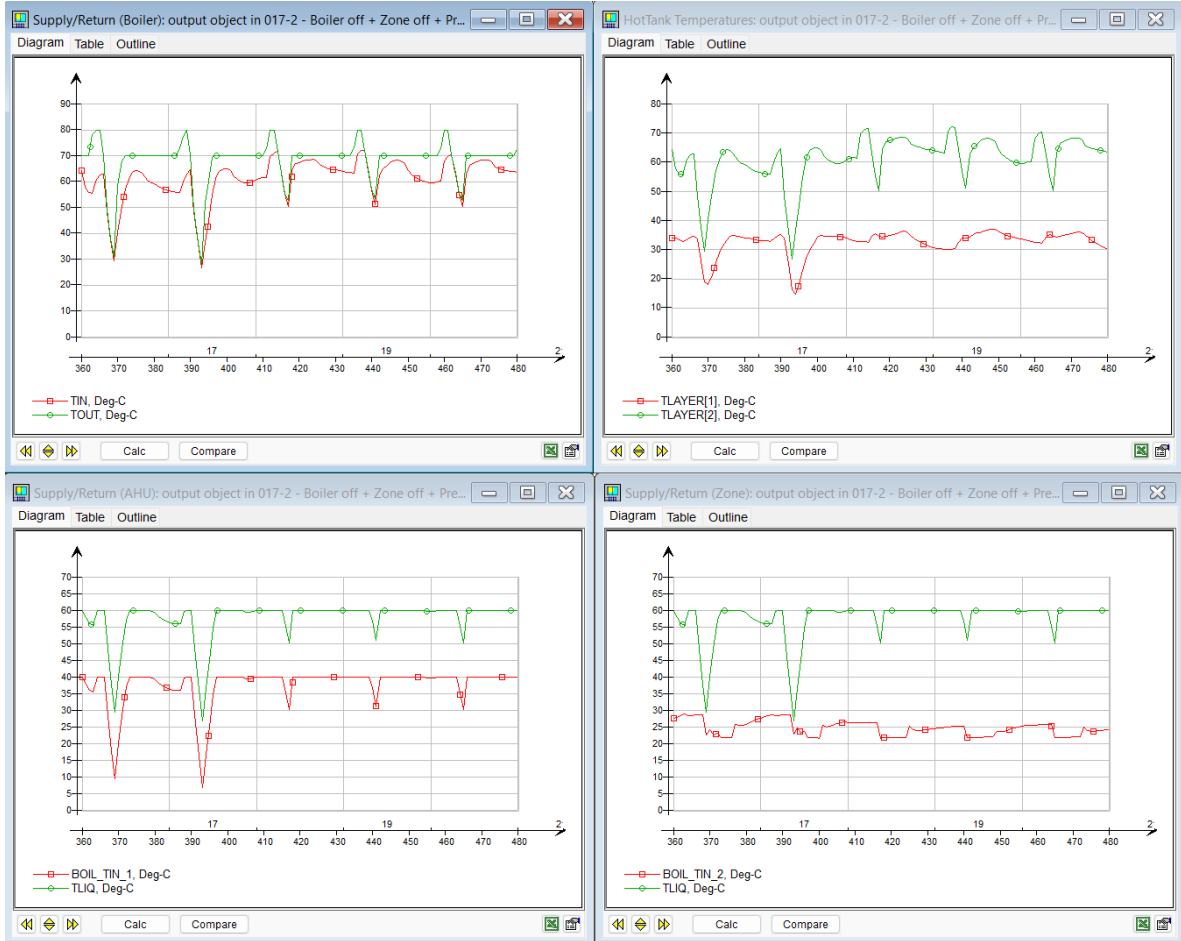


Figure 106: Passive House case - Simulation 4. From left to right, top to bottom: Supply/Return temperatures for boiler circuit, Temperature of top and bottom layer of HotTank, Supply/Return temperatures for AHU circuit, Supply/Return temperatures for Zone heating circuit

R Mass Flow Rates (16.-22. January)

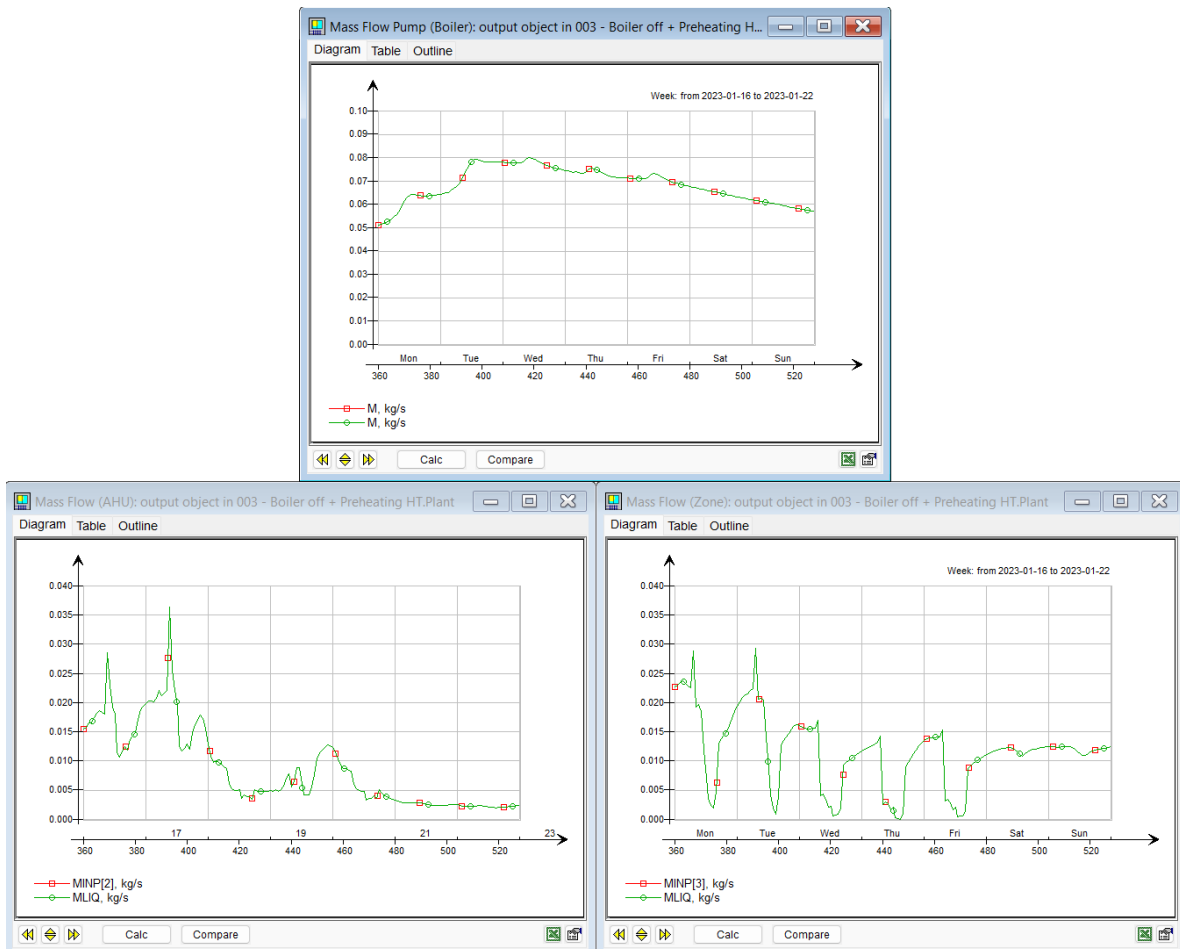


Figure 107: Mass flow rates for TEK17 case - Simulation 3. From top to bottom, left to right: Mass flow of main pump, mass flow of AHU pump, mass flow of zone pump

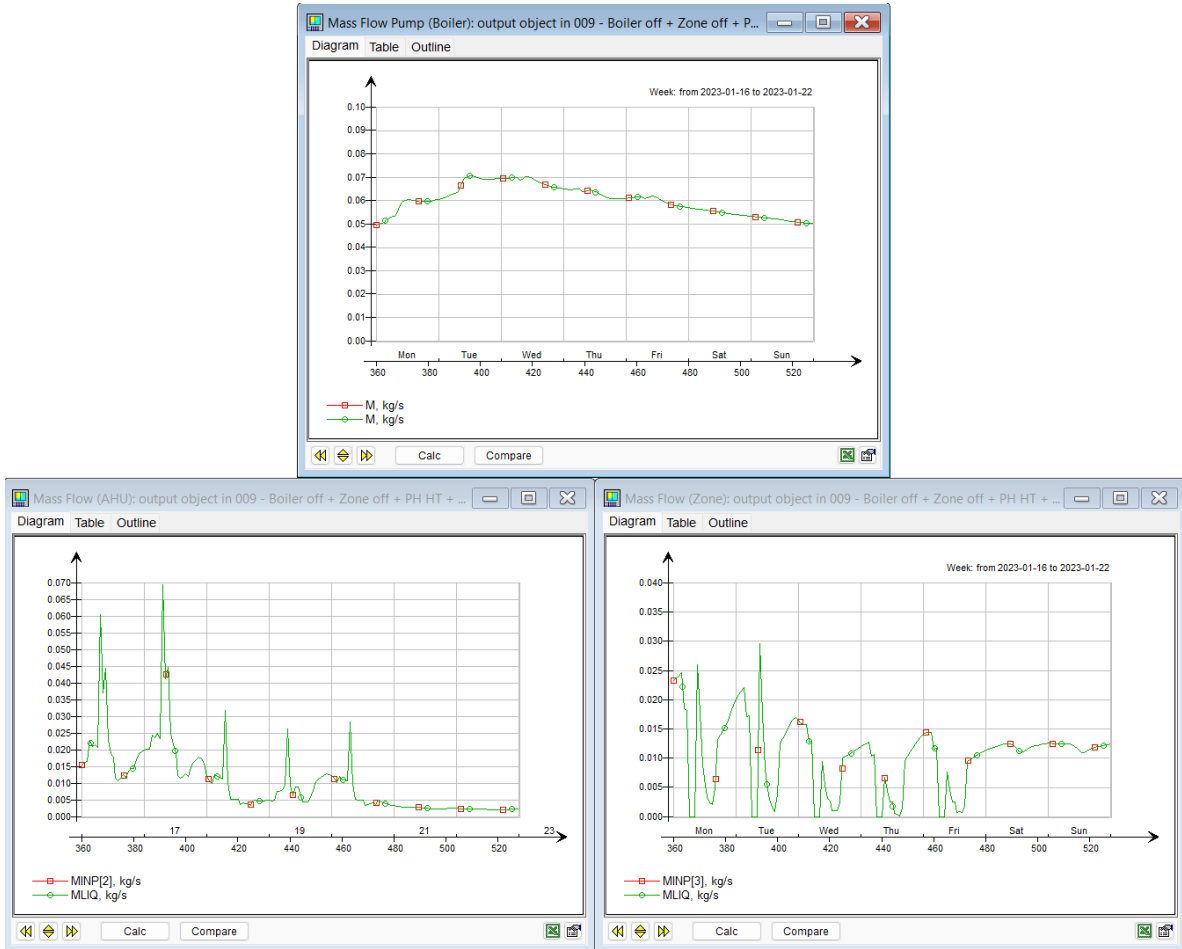


Figure 108: Mass flow rates for TEK17 case - Simulation 5B. From top to bottom, left to right: Mass flow of main pump, mass flow of AHU pump, mass flow of zone pump

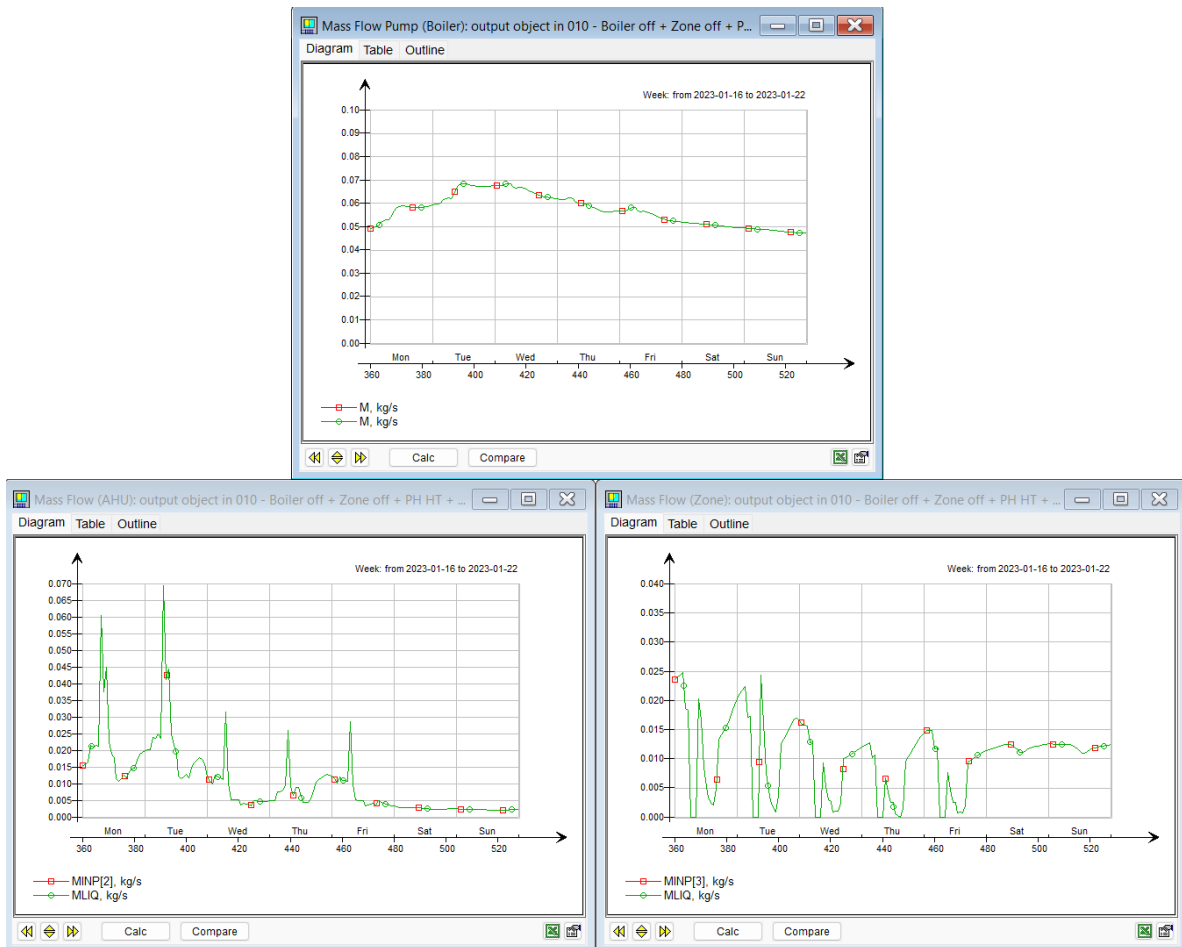


Figure 109: Mass flow rates for TEK17 case - Simulation 5C. From top to bottom, left to right: Mass flow of main pump, mass flow of AHU pump, mass flow of zone pump